C.P. No. 517
(22,103)
A.R.C. Technical Report

BEDFORD.

C.P. No. 517
(22,103)
A.R.C. Technical Report

MINISTRY OF AVIATION

AERONAUTICAL RESEARCH COUNCIL

CURRENT PAPERS

Wind Tunnel Experiments on a Model of a Tandem Rotor Helicopter

By

A.S. Halliday, Ph.D., B.Sc., D.I.C., and Miss D.K. Cox, B.Sc.,
of the Aerodynamics Division, N.P.L.

LONDON: HER MAJESTY'S STATIONERY OFFICE

1961

PRICE 10s 6d NET

Wind Tunnel Experiments on a Model of a Tandem Rotor Helicopter

- By -
A. S. Halliday, Ph.D., B.Sc., D.I.C., and Miss D. H. Cox, B.Sc.
of the Aerodynamics Division, N.P.L.

July, 1960

1. Introduction

At the time of the initiation of the present tests little or no research had been done in this country on helicopter models, other than on single rotors at the R.A.E. A programme of research on a twin rotor helicopter was therefore suggested to be carried out at the N.P.L.

The main feature of the research was to be the investigation of mutual interference; the front rotor to be fixed in position relative to the body whilst the rear one could be varied in height as well as in distance from the front one. The angle of the axis of the rear rotor could also be varied in a fore and aft direction.

The present report gives the results of the experiments described in A.R.C.19,829[1] after the effect of flapping hinge offset has been taken into account using the method given in report A.R.C.20,561[2].

2.1 Description of model and measuring equipment

The tests on a model of a twin-rotor helicopter were made in one of the 9' × 7' wind tunnels at the N.P.L.; a photograph of the model viewed from the rear is shown in Fig.1.

The rotors were driven by two squirrel-cage induction motors, coupled together in tandem and each capable of developing about 3 h.p. The motors were fed from a variable frequency set and the motor speed was controlled by varying the frequency of the supply current. Fig.2 shows the arrangement for driving the rotors through bevel gears. Rotational speed was measured by means of a Maxwell Bridge circuit operated by a contact breaker driven by the main motor shaft. The bridge circuit was calibrated by timing a flashing lamp also operated by a contact from the motor shaft via a 50:1 worm reduction gear.

The rotors were driven in opposite directions at three-fifths of the motor speed and provision was made in the coupling of the two motors to alter the relative angular positions of the rotor shafts so that there was accurate intermeshing of the rotor blades. As the primary object of the experiments was to determine the interaction of one rotor on the other it was essential that their relative positions could be altered. The front rotor was fixed in position but the rear rotor position could be varied to give three different distances from the front rotor L_1 = 3'-2", L_2 = 3'-7" and L_3 = 4'-3$\frac{1}{8}$". The height, H, could also be varied to give the same height as the front one (H_1) and also increased by 5" or 8", H_2 and H_3 respectively. The shaft angle, A, of the rear rotor could be altered by approximately 4° and 8° in a fore and aft direction. All these variations are indicated in Fig.3.

2.2 Rotors

The three-bladed rotors were 4'-3" diameter and identical in construction. The blades were untwisted, 1.5" constant chord of NACA 0012 section and effective length 19". Due to the high stresses

involved/

involved the hub was relatively large compared to full scale. Details can be seen in the photograph, Fig.4.

During the early part of the tests the rotors were run at 1,800 r.p.m., at which speed the radial acceleration was approximately 2,350 g, resulting in very high forces at the hub. The blades were provided with both flapping and drag hinges, the former being freely mounted on ball races and the latter having adjustable cork friction dampers. The blades were found to vary slightly in weight so provision was made for final balancing by means of small adjustable weights on screwed rods radiating from the hubs between the blades. These can be seen in the photograph, Fig.4.

In order to avoid the possibility of resonance it was at first thought advisable to run the rotors with drag hinges locked. Eventually however fatigue cracks were noticed in the roots of two of the blades and it was suspected that the lack of freedom in the drag hinges was the possible cause. Later, after new blades had been fitted, it was thought better to run with drag hinges free and so reduce root stresses, experience having shown that the possibility of resonance was small. As a further precaution, to eliminate fatigue failure, the new blades of a modified design were run at a reduced top speed of 1200 r.p.m. This question of blade fatigue is more fully discussed in the Appendix.

2.3 Equipment for m.asuring tracking of blades and flapping angle

The front rotor carried a commutator with a single brass segment contacting four carbon brushes mounted on a ring attached to the front rotor spindle housing. Three of these brushes were approximately 120° apart and the fourth diametrically opposite to one of the three. The brush contacts were used to trigger off a stroboscope lamp illuminating the blades whilst rotating. The three contacts at approximately 120° spacings were set so that, with all three in circuit together, they were successively out of phase by about one chord length when the ends of the rotor blades were observed. By this method it could be seen if the blades were tracking correctly.

The two diametrically opposed contacts were used to facilitate the observation of flapping angles. Each contact had a switch in circuit and the timing adjusted so that the stroboscope flashed when a particular blade was parallel to the longitudinal body axis either in a fore or aft direction. The height of the blade tips in each position was measured by means of a travelling periscope projecting vertically downwards into the tunnel. The difference in height of the blade tips in these two positions gave a measure of flapping angle. The periscope was of the type used on midget submarines. The stroboscope lamp was mounted on gimbals and the direction of the light, shining through a thick perspex window, could be adjusted by the observer to illuminate the particular blade tip under observation. It was estimated that the accuracy of the measurements was of the order of one tenth of a degree. A photograph of the head of the periscope is shown in Fig.6 from which can be seen one of the two vertical slides behind which is the measuring scale.

As the periscope weighed about 60 lb it had to be counter-weighted and the wires carrying these weights, passing over pulleys, can be seen in the photograph.

3. Safety Precautions

Due to the high value of centrifugal force on the rotors and the possibility of instability, resonance, or fatigue, it was

thought/

thought expedient to protect the personnel by reinforcing the tunnel inside with sheet steel and outside with shutters. These shutters were of sandwich construction comprised of blocks of paper between ¼" thick plywood, totalling about two inches in thickness.

To minimise the possibility of stopping the rotors before the tunnel and thereby losing the stabilising effect of centrifugal force on the blades, an interlock was incorporated in the electrical circuits, with a time delay of about a quarter of a minute, to ensure that the rotors attained a reasonable speed before starting the tunnel and also that the tunnel speed had dropped sufficiently on shutting down. As the electrical supplies to the 'unnel and rotors were separate there remained the danger arising from a failure of the current to the rotors but as that was thought to be very improbable, no attempt was made to cover that eventuality.

4. Method and Scope of Experiments

The model was suspended from the main roof balance by two struts spaced 22½" apart. These struts carried at their ends a spindle mounted on ball races, passing through and fixed to the helicopter body 29½" from the nose. This spindle being freely mounted acted as a pitching axis. A further support was provided towards the rear of the body, using a pair of V-wires attached to an overhead split-beam balance, see Fig. 2. These wires were adjustable by means of a windlass carried on the balance, so that the attitude of the model could be varied.

The earlier tests were made at 1800 r.p.m. giving a tip speed of about 400 ft/sec. Later the speed was reduced to 1200 r.p.m. and a tip speed of 267 ft/sec. Lift, drag, and pitching moments were measured at wind speeds of 40, 80, 120, 160 and 180 ft/sec for the tests at a rotor speed of 1800 r.p.m. giving approximate values of tip-speed ratio, μ, of 0.1, 0.2, 0.3, 0.4 and 0.45. When the rotor speed was reduced to 1200 r.p.m. the wind speeds used were 25, 55, 80, 100 and 120 ft/sec giving values of μ = 0.094, 0.206, 0.300, 0.374 and 0.449 respectively.

Measurements were made for blade angles, θ_o, of 4°, 8° and 12°. The angles were set by a worm and wheel at the blade roots using a surface table and scribing blocks to measure the difference in heights at leading and trailing edges.

Flapping angles were also measured by the method described in para. 2.3.

Although it would have been desirable to make measurements at very low values of μ, less than 0.1, difficulty was experienced due to the flow induced by the rotors themselves, especially at the higher body angles. For example, without the tunnel motor running, a vane anemometer indicated a wind speed of about 15 ft/sec at $\theta_o = 8°$ and $\theta = 20°$. As the flow was unreliable these tests were abandoned.

Table 1 gives a summary of all the tests on the various rotor combinations together with references to the tables giving the results.

5. Corrections

The tunnel measurements were converted to the coefficients C_T and C_m where C_T is the coefficient of the force normal to the longitudinal axis of the helicopter and C_m is the pitching moment coefficient about the axis shown in Fig. 3. A further correction was made for the forces and moments on the body and rig, etc., by making the appropriate measurements with rotors removed and substracting from the total. No account is therefore taken of forces due to the interference between rotors and body.

As the final results were to be presented for constant values of tip speed ratio, μ, and the wind speeds chosen did not give exact values and also as $\mu = V \cos\theta/\Omega R$, where θ is the body angle, the correction varied with attitude of the model and so all the results had first to be plotted against μ and then the values for $\mu = 0.1$, 0.2, 0.3, 0.4 and 0.45 taken from the curves. Corrections had also to be made to θ due to tunnel interference and therefore the values corrected for μ had then to be plotted against θ and values read off at the chosen values of θ viz., 0°, 5°, 10°, 15°, 20° and 25°. For convenience θ has been taken to be positive with the nose of the model downwards which is opposite to the normal convention.

For the 9' × 7' wind tunnel the correction to body angle (θ) has been taken to be

$$\Delta\theta = 0.111 \frac{A}{C} C_L \text{ (rad)}$$

where A is the total rotor disc area C is the cross-sectional area of the wind tunnel, C_L is the overall lift coefficient based on total disc area. The correction is such that the effective inclination is less than the geometric inclination. It is felt that the above correction is not entirely satisfactory as it is based on fixed wing theory. I' is hoped that at some future time a systematic series of experiments will be made to establish the order of wind tunnel corrections to be applied to helicopter model testing.

The corrections to pitching moment due to flapping hinge offset are included in para. 6.

6. Results

6.1 Effect of flapping hinge offset

In addition to the corrections mentioned in para. 5 account had also to be taken of the effect of flapping hinge offset which, due to design difficulties, was of necessity rather large, about 6.275%.

The effect of flapping hinge offset on the characteristics of a rotor is dealt with in a report by Meyer and Falabella3 and the analysis given in that report has been used to estimate the theoretical values of rotor thrust and flapping angles and also the effect on overall pitching moment.

6.2 Thrust coefficient

Assuming uniform distribution of induced velocity and neglecting blade tip losses the theoretical value of C_T is given by equation (38) of Ref. 3.

$$C_T = \frac{\sigma a}{2}\left\{\frac{A_o}{3}\left[(1-\xi^3) + \frac{3}{2}\mu^2(1-\xi)\right] - \frac{\mu B_1}{2}(1-\xi^2) + \frac{\lambda}{2}(1-\xi^2) + \frac{\mu a_1}{2}(\xi-\xi^2)\right\}. \quad \ldots(1)$$

As there is no cyclic pitch $B_1 = 0$ and the term involving a_1 is small and may be neglected and therefore approximately

$$C_T = \frac{\sigma a}{2}\left\{\frac{A_o}{3}\left[(1-\xi^3) + \frac{3}{2}\mu^2(1-\xi)\right] + \frac{\lambda}{2}(1-\xi^2)\right\}. \quad \ldots(1a)$$

For zero forward speed where $\mu = 0$

$$C_T = \frac{\sigma a}{2}\left\{\frac{A_o}{3}(1-\xi^3) + \frac{\lambda}{2}(1-\xi^2)\right\}. \quad \ldots(2)$$

Also/

Also

$$\lambda = -\sqrt{\frac{C_T}{2}}. \qquad \ldots(3)$$

In order to determine "a" the slope of the lift curve of the blade section C_T was required for zero wind speed. As the tunnel was of the return flow type itwas difficult to obtain a true zero wind speed due to the flow induced by the rotors. This was cut down to a minimum by closing the tunnel with a screen, but even so there was a circulation of air in the neighbourhood of the model, particularly at the larger blade angles. It was assumed that at zero tunnel speed the induced circulation at $\theta_o = 4^\circ$ would be very small and the measured value of $C_T = 0.00142$ was inserted in the equations (2) and (3). This gave a value of $a = 5.0$ (per rad) which was subsequently used in equation (1a). A curve of static thrust coefficient using the above value of "a" is given in Fig.7. The theoretical values of C_T using equation (1a) for $\theta_o = 4^\circ$, 8° and 12° are included in Figs.9, 13 and 19. It is of interest to note that the effect of flapping hinge offset on C_T is negligible, particularly at the lower values of μ.

6.3 Division of thrust

From a knowledge of the total thrust and the pitching moment about a defined axis the contribution of thrust due to each rotor has been calculated. It was assumed that the thrust of each rotor acted at the disc centre and normal to the body axis and also that the rotor drag force, parallel to the longitudinal axis, acted at the mean height of the two rotors.

The pitching moments as measured in the experiments included a contribution due to the effect of the offset flapping hinges and therefore before the thrust due to each rotor could be calculated the pitching moments had to be corrected for offset.

In the report by Meyer and Falabella[3] an expression is given for pitching moment due to hinge offset (M_y). This expression is

$$M_y = [\mu a_o P - b_1 N]\,\Omega^2 + \frac{bI_1}{2}\,\zeta\Omega^2 a_1 \qquad \ldots(4)$$

where

$$\frac{P}{I_1} = \frac{by}{8}\,[\xi - \xi^3]$$

$$\frac{N}{I_1} = \frac{by}{4}\left[\frac{\xi}{3} - \frac{\xi^2}{2} + \frac{\xi^4}{6}\right].$$

Values of a_o, b_1, and a_1 are obtained by solving three simultaneous equations; these solutions are given in equations (27), (28) and (29) in the report. As there is no cyclic pitch, i.e., $B_1 = 0$ in the case of the model, these solutions become

$$a_1 = \frac{2\mu A_o C + \lambda\mu E + \dfrac{\zeta\mu C}{1+\zeta}\left[\dfrac{A_o\left(B + \dfrac{\mu^2}{2}E\right) + \lambda C}{A + \dfrac{\mu^2}{4}E}\right]}{A - \dfrac{\mu^2}{4}E + \dfrac{\zeta^2 - \dfrac{\zeta\mu^2 C\frac{D}{2}}{1+\zeta}}{A + \dfrac{\mu^2}{4}E}} \qquad \ldots(5)$$

$$a_o = \frac{A_o\left(B+\frac{\mu^2}{2}E\right) + \lambda C + \mu a_1 \frac{D}{2}}{1 + \zeta} \qquad \ldots(6)$$

$$b_1 = \frac{\mu a_o C - \zeta a_1}{A + \frac{\mu^2}{4} E}. \qquad \ldots(7)$$

The value of λ is given by the expression

$$\lambda = \frac{-\frac{\sigma a}{2}\left\{\frac{A_Q}{3}\left[(1-\xi^3) + \frac{3}{2}\mu^2(1-\xi)\right] + \frac{\mu a_1}{2}(\xi-\xi^2)\right\} + 2\mu^2 \tan\alpha}{2\mu + \frac{\sigma a}{4}(1-\xi^2)} \qquad \text{(see footnote)} \quad \ldots(8)$$

and

$$\tan\alpha = \frac{C_T + 2\mu\lambda}{2\mu^2}. \qquad \ldots(9)$$

$$A = \frac{\gamma}{2}\left[\frac{1}{4} - \frac{2}{3}\xi + \frac{\xi^2}{2} - \frac{\xi^4}{12}\right].$$

$$B = \frac{\gamma}{2}\left[\frac{1}{4} - \frac{\xi}{3} + \frac{\xi^4}{12}\right].$$

$$C = \frac{\gamma}{2}\left[\frac{1}{3} - \frac{\xi}{2} + \frac{\xi^3}{6}\right].$$

$$D = \frac{\gamma}{2}\left[\frac{\xi}{2} - \xi^2 + \frac{\xi^3}{2}\right].$$

$$E = \frac{\gamma}{2}\left[\frac{1}{2} - \xi + \frac{\xi^2}{2}\right].$$

Using the wind tunnel values of C_T, in equation (9) M_y has been calculated for various cases and it was found that the terms involving a_o and b_1 were quite small compared with the a_1 term. Typical results are shown in Fig. 8 for a blade angle θ_o of 8°, and a rotational speed, Ω, of 1200 r.p.m. The first set of curves shows M_y in lb/ft varying with μ for zero pitch angle, whilst the second set refers to a change in body angle at a constant value of $\mu = 0.3$. The contributions of the a_o and b_1 terms together are given by the curves marked A whilst the a_1 term is given by curves B and the total by curves C.

On examination of these curves it will be seen that, for all values of μ of the one curve and all values of θ of the other, the magnitude of all points on the C curve are very nearly 1.09 times the corresponding values on the B curves. It was therefore decided, in order to avoid much laborious computation, to use the third term only in the expression (equation (4)), for M_y, that is the one involving a_1, and add 9%. In the above calculations the observed

values/

- -

Note In the expression for λ (equation (41)) given in Ref. 3 the sign of the last term in the numerator, $2\mu^2 \tan\alpha$, is given as negative, this should be positive.

values of flapping angles, rather than the theoretical ones, have been used. The pitching moment due to offset may therefore be expressed as

$$M_y = 1.09\, b \frac{I_1}{2} \zeta\Omega^2 (a_{1_F} + a_{1_R})$$

which has to be subtracted from the total measured pitching moment, a_{1_F} and a_{1_R} being the observed values of flapping angle for front and rear rotors respectively.

Figs. 9-19 and Tables 18-43 show the thrust distribution taking into account blade offset.

It was considered that the configuration $L_2H_2A_0$ was the closest approach to a helicopter of the type Bristol 173 and therefore fuller experimental work was done for that arrangement.

For $L_2H_2A_0$ and blade angles $\theta_0 = 4°$ Fig. 9 gives the curves C_T against θ, the body angle, for values of $\mu = 0.1$, 0.2, 0.3, 0.4 and 0.45. For each value of μ five curves are given, two showing the contribution of thrust due to each rotor of the twin rotor combination, two the thrust of each rotor acting singly, the fifth curve the theoretical value of C_T.

It will be seen from further examination of the curves that the front rotor contributes considerably more thrust than the rear. There is an increase in thrust from the front rotor compared to the single front rotor, but this increase is less than the loss on the rear one. The result is that the twin rotor configuration gives less thrust than the sum of the thrusts of the two rotors separately; this is as one would expect.

The theoretical curves show quite good agreement with the mean values of the two separate rotor curves.

In order to compensate for the loss of lift on the rear rotor its blade angles were increased to 6° leaving those for the front one at 4°. Fig. 10 shows the results of these experiments. For values of μ up to 0.3 it will be seen from the curves that the compensation is more than adequate, that is the rear rotor contributes more thrust than the front one. For values of μ of 0.4 and 0.45 a differential blade setting of 2° is roughly the best compromise.

Although the presence of the rear rotor causes an increase of thrust from the forward rotor, the increment of thrust by increasing θ_0 from 4° to 6° of the rear rotor blades reflects little increase from the front one.

Figs. 11 to 18 all apply to blade angles $\theta_0 = 8°$, the curves again, as for $\theta_0 = 4°$, refer to twin rotors, single rotors and theoretical cases.

If one compares Figs. 11, 13 and 14, which refer to L_1H_2, L_2H_2 and L_3H_2 the effect will be seen of altering the distance between the rotor axes. The total thrust appears almost independent of distance between the rotors but at the higher values of μ and θ there is a small shedding of thrust from the rear rotor to the front one on reduction of distance apart.

There is a small effect on thrust from varying the height of the rear rotor relative to the front one (Figs. 12, 13 and 15). This effect, which is a slight increase with height, is on the rear rotor only and confined to values of μ below 0.2.

Experience/

Experience with full-scale tandem rotor helicopters has shown that there is little alteration in thrust due to changing the distance apart of the rotors but that there is a definite effect from height change of the rear rotor for very low values of μ.

With a view to compensating for loss of thrust from the rear rotor, experiments were made with the rear rotor axis tilted at 7.7° and 4.4° backwards and also 4° forwards. The results of these measurements for $\theta_o = 8°$ are given in Figs.16-18. Again the change of attitude of the rear rotor has little effect on the thrust from the front one as has already been noted when the angles of the rear rotor blades were made greater than the front ones. There is however a gain in thrust from the rear rotor when it is given a backwards tilt.

Fig.20 shows the results of tilting the axis of the rear rotor when acting alone; C_T has been plotted against $\theta + A$, A being the angle of tilt, forwards being positive. For each value of μ it will be noted that all the values of C_T, for the various angles of tilt, lie substantially on a single curve. This shows that for a single rotor, axis tilt produces the same effect as an equal change in body angle, that is body interference is independent of angle between rotor and body. In the case of the twin rotor model there is more scatter of the points when plotting C_T of the rear rotor against $\theta + A$ but these curves are not reproduced.

Fig.19 gives curves for L_2H_2 with blade angle $\theta_o = 12°$ and, as before, there is wide spacing of the two thrust curves for front and rear rotors. Except for low values of μ the values of C_T for the individual rotors differ considerably and this deviation increases with body angle. The theoretical curves, however, agree well with the mean value of C_T for the separate rotors except for values of μ below 0.3.

6.4 Centre of rotor thrust

From the curves of division of thrust it is easy to calculate the position of the centre of thrust, examples of which are given in Fig.21. The distance of the centre of thrust from the centre of the front rotor divided by the distance between the rotor centres is plotted against body angle for the various values of μ.

It is normal practice in twin rotor helicopter design to make the two rotors identical. As there is a loss of thrust from the rear rotor, trim can only be maintained by applying a suitable blade angle mixing ratio. An example showing the effect of differential blade setting is given in Fig.21d where the front rotor has a blade angle setting of 4° and the rear 6°. This results in more satisfactory curves of centre of thrust position.

The effect on position of centre of thrust due to tilting the rear rotor axis is shown in Fig.22 and it will be noticed that a backwards tilt of about 7.7° has roughly the same effect on the shapes of the curves as a differential blade setting of 2°, shown in Fig.21a.

It will also be seen that when the axis of the rear rotor is tilted backwards 4.4°, the position of the centre of thrust varies little with either a change in μ or in θ, Fig.22b.

6.5 Equivalent downwash

Fig.23 gives curves of equivalent downwash for the rotor configuration $L_2H_2A_o$. These curves have been estimated by comparing the curves of thrust coefficient of each rotor of the twin-rotor combination with the thrust of each as a single rotor. In other words the equivalent downwash is taken to be the angle change on the single rotor to give the same thrust as the corresponding rotor in the twin-rotor condition i.e., downwash angle $= \theta_{S.R.} - \theta_{T.R.}$ where $\theta_{S.R.}$ and $\theta_{T.R.}$ apply to single rotor and the same rotor of the twin rotors respectively when C_T is same value for both cases.

6.6 Longitudinal flapping angle

The longitudinal flapping angle is given by equation (5) and the relationship between shaft angle i_s, rotor disc angle, i_d, and flapping angle is given by $i_s = i_d + a_1$. Figs.24-30 give longitudinal flapping angles for a limited number of cases and for each blade angle. They are plotted against body angle for each value of μ. The theoretical curves are given in Figs.24 and 25; the observed values for each rotor of the arrangement $L_2H_2A_0$ in Fig.26 and single rotors in Fig.27. Figs.26-27 are shown in a different form in Figs.31-34 where the flapping angle, a_1, is plotted against μ for various body angles.

On examination of the curves it will be seen that the experimental values are less in magnitude than the corresponding theoretical ones except for low values of μ. There are two possible explanations for this deviation; firstly the close proximity of the body and secondly tunnel constraint as the tunnel height was only 1.65 times the rotor diameter.

Results of experiments at the R.A.E. on a 12 ft diameter rotor[4] and on a 6 ft diameter rotor[5] differ from the present ones. In the R.A.E. experiments the flapping angles increased more rapidly than indicated by theory both with increase of tip speed ratio and reduction of shaft inclination. Their experiments were made without a body being present and the tunnels concerned were the 24 ft open jet for the 12 ft rotor and the $11\frac{1}{2}$ ft tunnel as well as the 24 ft one for the 6 ft rotors.

The discrepancy between the observed and theoretical values of flapping angles could be explained by a non-uniform distribution of downwash across the disc; theory assumes uniformity of downwash.

6.7 Longitudinal forces

The forces parallel to the body axis were estimated but were not regarded with any great significance, due to the relatively large size of hub, and have, therefore, been omitted in the present report.

7. Conclusions

(a) The curves of thrust distribution show that the front rotor contributes more thrust than does the rear one and a little more than it does as a single rotor, that is without the presence of the rear rotor.

(b) Fig.10 shows the results of the contribution to C_T by the individual rotors when the blade angle of the rear rotor is increased to 6° leaving the front one at 4°. It will be seen that for the lower values of μ the compensation for loss of thrust from the rear rotor is more than sufficient.

(c) At values of μ above 0.1 a backward tilt of the rear rotor of 7.7° (Fig.16) gives a considerable degree of compensation (c.f. Fig.13).

(d) The increase of thrust brought about by increasing the blade angle of the rear rotor or by giving a backward tilt is borne almost entirely by the rear rotor there being a negligible effect by the front rotor.

(e)/

(e) The effect of varying the height of the rear rotor above the front one (Figs. 12, 13 and 15) is small and confined to the rear rotor and to values of μ below 0.2 there being a slight increase of thrust with height.

(f) There appears to be no apparent effect on total thrust due to a change of longitudinal spacing of the rotors (Figs. 11, 13 and 14).

(g) When the axis of the rear rotor is tilted backwards by 4.4° (Fig. 22b) the position of the centre of thrust varies little with either a change in μ or in θ.

(h) The calculated flapping angles are greater than the measured ones, particularly at the smaller values of θ.

8. Acknowledgments

The authors wish to express their thanks to Mr. C. A. Culverhouse who was responsible for the design of the model and ancillary equipment and also to Mr. A. R. S. Bramwell of R.A.E., Bedford for his helpful suggestions in the analysis of the results.

References

No.	Author(s)	Title, etc.
1	A. S. Halliday and Miss D. K. Cox	Wind-tunnel experiments on a model of a tandem rotor helicopter. A.R.C.19,829 - H.342. 10th January, 1958
2	A. S. Halliday and Miss D. K. Cox	Analysis of results from wind-tunnel experiments on a model of a tandem rotor helicopter allowing for flapping hinge offset. A.R.C.20,561 - H.360. 18th November, 1958.
3	J. R. Meyer and G. Falabella Jr.	The effect of blade mass constant and flapping hinge offset on maximum blade angles of attack at high advance ratios. Massachusettes Institute of Technology.
4	H. B. Squire, R. A. Fail and R. C. W. Eyre	Wind-tunnel tests on a 12 ft diameter helicopter rotor. A.R.C. R. & M. 2695. April, 1949.
5	T. B. Owen, R. Fail and R. C. W. Eyre	Wind-tunnel tests on a 6 ft diameter helicopter rotor. A.R.C. C.P.216. (Also published as A.R.C. R. & M.3022) May, 1955.

List of Symbols/

List of Symbols

R	radius of rotor = 2.125 ft
c	chord of blades = 1.5 in.
b	number of blades per rotor = 3
σ	solidity = $bc/\pi R$ = 0.0562
θ_o	blade section pitch angle
θ	body angle, positive nose down
A	total rotor disc area = $2\pi R^2$
A_{deg}	rear rotor shaft inclination relative to body axis (see Fig.3)
$L_1, L_2, L_3, H_1, H_2, H_3$	see Fig. 3.
l	distance of centre of thrust from front rotor axis
i_d	incidence of tip path plane
a_o	coning angle
a_1	longitudinal flapping angle
b_1	lateral flapping angle
Ω	angular velocity of rotor (rads per sec)
V	tunnel speed (ft/sec)
Q_D	fluctuating drag torque lb/ft
T	total thrust in lb normal to body axis
C_T	thrust coefficient = $T/\rho(\Omega R)^2 A$
C_{T_F}	thrust coefficient contribution by front rotor
C_{T_R}	thrust coefficient contribution by rear rotor
M	pitching moment (lb/ft)
C_m	pitching moment coefficient = $M/\frac{1}{2}\rho AV^2R$
μ	tip speed ratio = $V\cos\theta/\Omega R$
u	component by V parallel to rotor shaft
λ	$u/\Omega R$
a	slope of lift curve of blade section = 5.0

Symbols used in Ref.3 not appearing above

A_o	blade section pitch angle corresponding to θ_o above
α	rotor angle of attack
m_b	mass of each blade $=0.5/g$ slug
L	distance of blade tip from flapping hinge
I_1	mass moment of inertia of blade about flapping hinge
γ	blade mass constant = $\rho acR^4/I_1$
e	distance of flapping hinge to rotor centre
ξ	flapping hinge offset = e/R = 0.06275
ζ	$\xi m_b R\frac{L}{2}/I_1$

APPENDIX/

APPENDIX

Blade Fatigue Failure

At the outset of the tests it was decided to run the rotors with drag hinges locked, as it was thought that resonance would then be less likely to occur, particularly as the natural frequency of the model and rig was low and of the order of 6 to 7 per sec. When the rotors were being run up a small vibration was noticed at low speed, but this region was soon run through and no violent disturbance was ever experienced.

During the experiments two sets of blades have been in use, see Fig.5. In order to avoid blade twist it was essential to design the blades so that the position of the section centre of gravity was on the quarter chord line, necessitating composite construction. The first set had the front part made of brass and the rear part hollow magnesium alloy, tongued, riveted and resin bonded together.

After a considerable time of running the first set of blades at 1800 r.p.m., perhaps 30-40 hours, it was noticed that one blade on each rotor had cracked through the magnesium at the root. These cracks were examined by H. L. Cox of N.P.L. who suggested that the failures were caused by fretting fatigue starting at the inner rivets. The remaining blades were carefully examined under a stereo-microscope for incipient cracks and indications were observed on one other blade.

The hubs were then stripped down and several features indicated that they had suffered from severe hammering. The flapping thrust races were badly indented, two of the drag hinge pin keys were sheared and the remainder had their corners rounded off. All these factors indicated that the forces in the direction of the blade drag were more serious than envisaged.

The fluctuating drag torque due to the combined action of flapping and coning and neglecting flapping hinge offset is given by the equation

$$Q_D = -2I_1\omega^2\left[a_0\left(a_1\sin\psi - b_1\cos\psi\right) - \tfrac{1}{2}\left(a_1^2 - b_1^2\right)\sin 2\psi + a_1 b_1\cos 2\psi\right].$$

A similar equation has been developed including offset from which the maximum drag torque has been estimated to be about 8.8 lb/ft. With a torque of this value the local force on the balls in the flapping thrust races could be as high as 140 lb. With a reversal of load of this magnitude at a frequency of 30 per sec it is fairly certain that indenting of the ball races could take place.

The shearing force on the drag hinge keys due to the fluctuating drag torque was estimated to be a little over 480 lb which, no doubt, was the cause of the ultimate failure of the keys.

It is reasonable to assume that with a drag torque of the above magnitude on the blades and no freedom in the drag direction, and with the presence of ball indents in the flapping thrust races, there would be a considerable flapping friction hinge moment. This was probably the primary cause of the blade fatigue failures.

It was therefore decided to have new blades made to a modified design. They were made of spherodised steel for the front portion tongued and grooved into a boxwood rear portion and resin bonded, but not riveted, see Fig.5. Again the centre of gravity of the section was at the quarter chord.

As a precaution the top speed was reduced from 1800 r.p.m. to 1200 r.p.m., the drag hinges were unlocked but had friction damping. After a considerable period of running with the modified blades there have been no indications of blade failure or bearing trouble.

Table 1/

TABLE 1

SUMMARY OF TESTS

θ_o		A_o°			$A_{+4^{\circ}}$	$A_{-4.4^{\circ}}$	$A_{7.9^{\circ}}$	$A_{-7.7^{\circ}}$
		L_1	L_2	L_3	L_2	L_3	L_2	L_2
4°	H_1	F(2,3), F + R(18)	F + R(19)	F + R(20)				
	H_2		R(4), F + R(22)		F + R(25)	F + R(24)	R(6), F + R(26)	R(5), F + R(23)
	H_3		F + R(21)					
Front 4° Rear 6°	H_1							
	H_2		R(7), F + R(27)					
	H_3							
8°	H_1		F + R(32)					
	H_2	F + R(34)	F(8), R(9), F + R(28)	F + R(35)	F + R(31)	R(10), F + R(30)		R(11), F + R(29)
	H_3		F + R(33)					
12°	H_1		R(16), F + R(41)					
	H_2	F + R(43)	F(13), R(12) F + R(39)	F + R(36)	F + R(40)	R(15), F + R(38)		R(14), F + R(37)
	H_3		R(17), F + R(42)					

<u>Note</u>: Figs. in brackets refer to Table numbers. F = Front Rotor only R = Rear Rotor only F + R = Both Rotors.

TABLE 2/

TABLE 2

$C_T \times 10^3$ for Single Rotor Cases

θ_o	Arrangement	$\theta°$	μ=0.1	μ=0.2	μ=0.3	μ=0.4	μ=0.45
4°	$L_1H_1A_o$	0	2.21	3.43	3.89	4.30	4.62
	Forward Rotor	5	2.30	2.46	2.34	2.30	2.20
	1,200 r.p.m.	10	1.78	1.36	0.54	-0.29	-0.63
		15	1.33	0.12	-1.27		
		20	0.76	-1.18			
		25	0.09				

TABLE 3

4°	$L_1H_1A_o$	0	2.62		3.84		4.58
	Forward Rotor	5	2.17		2.32		2.32
	1,800 r.p.m.	10	1.64		0.53		-0.42
		15	1.16		-1.11		
		20	0.64				
		25					

TABLE 4

4°	$L_2H_2A_o$	0	2.50	3.05	3.26	3.51	3.65
	Rear Rotor	5	2.02	2.00	1.82	1.55	1.57
	1,200 r.p.m.	10	1.49	0.77	-0.19	-0.97	-1.36
		15	0.94	-0.60			
		20	0.33				
		25	-0.29				

TABLE 5/

TABLE 5

$C_T \times 10^3$ for Single Rotor Cases

θ_0	Arrangement	θ°	μ=0.1	μ=0.2	μ=0.3	μ=0.4	μ=0.45
4°	$L_2H_2A_{-7.7^\circ}$	0	3.21	4.32	5.27	6.27	6.57
	Rear Rotor	5	2.77	3.46	4.02	4.48	4.70
	1,200 r.p.m.	10	2.29	2.55	2.67	2.62	2.56
		15	1.76	1.48	0.80		
		20	1.26	0.06			
		25	0.76				

TABLE 6

4°	$L_2H_2A_{7.9^\circ}$	0	1.66	1.12	0.35	-0.35	-0.58
	Rear Rotor	5	1.16	-0.19	-1.54	-2.50	-3.10
	1,200 r.p.m.	10	0.62	-1.51	-3.17		
		15	0.09				
		20	-0.45				
		25	-1.07				

TABLE 7

6°	$L_2H_2A_0$	0	3.71	4.10	4.54	4.93	5.12
	Rear Rotor	5	3.35	3.34	3.28	3.08	3.03
	1,200 r.p.m.	10	2.86	2.32	1.52	0.76	0.34
		15	2.35	1.14	-0.50		
		20	1.84	-0.27			
		25	1.35				

TABLE 8/

TABLE 8

$C_T \times 10^3$ for Single Rotor Cases

θ_o	Arrangement	θ^o	μ=0.1	μ=0.2	μ=0.3	μ=0.4	μ=0.45
8°	$L_2H_2A_O$	0	4.59	5.62	6.06	6.64	7.11
	Forward Rotor	5	4.29	4.76	4.95	5.02	5.05
	1,200 r.p.m.	10	4.04	4.07	3.88	3.53	3.33
		15	3.69	3.14	2.24	1.29	0.80
		20	3.27	2.11			
		25	2.81	0.64			

TABLE 9

8°	$L_2H_2A_O$	0	4.54	5.20	5.62	6.13	6.37
	Rear Rotor	5	4.30	4.62	4.72	4.68	4.64
	1,200 r.p.m.	10	4.02	3.82	3.25	2.70	2.40
		15	3.66	2.79	1.48	-0.01	-0.75
		20	3.27	1.52			
		25	2.85				

TABLE 10

8°	$L_2H_2A_{-4.4}$	0	4.90	5.91	6.40	7.04	7.49
	Rear Rotor	5	4.53	5.29	5.65	5.98	6.20
	1,200 r.p.m.	10	4.23	4.49	4.37	4.29	4.31
		15	4.00	3.62	2.83	2.12	1.85
		20	3.66	2.58	0.77		
		25	3.23	0.99			

TABLE 11/

TABLE 11

$C_T \times 10^3$ for Single Rotor Cases

θ_o	Arrangement	θ^o	μ=0.1	μ=0.2	μ=0.3	μ=0.4	μ=0.45
8°	$L_2H_2A_{-7.7}$	0	5.19	6.28	7.02	8.00	8.48
	Rear Rotor	5	4.80	5.72	6.25	6.80	7.20
	1,200 r.p.m.	10	4.44	5.10	5.26	5.45	5.72
		15	4.16	4.28	4.05	3.64	3.90
		20	3.90	3.33	2.36		
		25	3.41	1.97			

TABLE 12

12°	$L_2H_2A_0$	0	6.14	6.67			
	Rear Rotor	5	5.90	6.30	6.65		
	1,200 r.p.m.	10	5.82	5.87	5.72	5.56	5.49
		15	5.78	5.39	4.38	3.44	3.22
		20	5.48	4.44	2.55	0.73	0.15
		25	5.05	3.26	0.66		

TABLE 13

12°	$L_2H_2A_0$	0	6.36	7.24			
	Forward Rotor	5	6.10	6.70	7.19		
	1,200 r.p.m.	10	5.96	6.26	6.53	6.82	6.98
		15	5.88	5.80	5.43	4.99	4.85
		20	5.72	5.21	4.05	3.26	2.58
		25	5.12	4.06	2.48	1.04	

TABLE 14/

TABLE 14

$C_T \times 10^3$ for Single Rotor Cases

θ_o	Arrangement	θ	μ=0.1	μ=0.2	μ=0.3	μ=0.4	μ=0.45
12°	$L_2H_2A_{-7.7^\circ}$	0	6.63	7.37			
	Rear Rotor	5	6.24	6.94	7.35		
	1,200 r.p.m.	10	5.91	6.50	6.71	7.18	7.36
		15	5.69	6.01	6.12	6.17	6.40
		20	5.62	5.47	5.05	4.56	4.26
		25	5.68	4.75	3.55	2.42	

TABLE 15

12°	$L_2H_2A_{-4.4}$	0	6.31	7.07			
	Rear Rotor	5	6.00	6.55	7.00		
	1,200 r.p.m.	10	5.83	6.17	6.25	6.57	6.65
		15	5.76	5.73	5.40	5.14	5.03
		20	5.64	5.20	4.22	3.19	2.71
		25	5.18	4.14	2.47	0.68	

TABLE 16

12°	$L_2H_1A_0$	0	6.04	6.67			
	Rear Rotor	5	5.87	6.33	6.50		
	1,200 r.p.m.	10	5.80	5.94	5.79	5.60	5.57
		15	5.74	5.36	4.55	3.74	3.43
		20	5.52	4.57	2.99	1.51	0.73
		25	5.12	3.58	1.25	-1.11	

TABLE 17

$C_T \times 10^3$ for Single Rotor Cases

θ_o	Arrangement	$0°$	μ=0.1	μ=0.2	μ=0.3	μ=0.4	μ=0.45
$12°$	$L_2H_3A_o$	0	6.02	6.57			
	Rear Rotor	5	5.82	6.04	6.30		
	1,200 r.p.m.	10	5.74	5.77	5.65	5.60	5.30
		15	5.66	5.22	4.47	3.54	3.07
		20	5.44	4.48	2.83	1.23	-0.27
		25	4.78	3.34	0.88	-1.88	

TABLE 18

C_{T_F} and C_{T_R} for Twin Rotors

θ_o	Arrangement	θ	Coeff $\times 10^3$	μ=0.1	μ=0.2	μ=0.3	μ=0.4	μ=0.45
$4°$	$L_1H_1A_o$	0	C_{T_F}	1.30	1.69	2.04	2.45	2.52
			C_{T_R}	0.68	1.02	1.33	1.37	1.56
	1,800 r.p.m.	5	C_{T_F}	1.05	1.17	1.23	1.33	1.27
			C_{T_R}	0.63	0.76	0.75	0.62	0.64
		10	C_{T_F}	0.79	0.61	0.25	0.02	-0.35
			C_{T_R}	0.57	0.35	0.03	-0.39	-0.32
		15	C_{T_F}	0.55	-0.03	-0.64		
			C_{T_R}	0.47	-0.05	-0.67		
		20	C_{T_F}	0.30	-0.44			
			C_{T_R}	0.31	-0.53			
		25	C_{T_F}	-0.01				
			C_{T_R}	0.06				

TABLE 19/

TABLE 19

C_{T_F} and C_{T_R} for Twin Rotors

θ_o	Arrangement	θ	Coeff $\times 10^3$	μ=0.1	μ=0.2	μ=0.3	μ=0.4	μ=0.45
4°	$L_2H_1A_o$	0	C_{T_F}	1.33	1.74	2.01	2.32	2.56
			C_{T_R}	0.67	0.98	1.26	1.46	1.48
	1,800 r.p.m.	5	C_{T_F}	1.05	1.20	1.17	1.29	1.31
			C_{T_R}	0.66	0.72	0.63	0.62	0.50
		10	C_{T_F}	0.81	0.59	0.17	-0.06	-0.18
			C_{T_R}	0.58	0.36	0.04	-0.49	-0.69
		15	C_{T_F}	0.58	-0.08			
			C_{T_R}	0.44	0.02			
		20	C_{T_F}	0.30				
			C_{T_R}	0.28				
		25	C_{T_F}	0.02				
			C_{T_R}	0.08				

TABLE 20

4°	$L_3H_1A_o$	0	C_{T_F}	1.30	1.75	2.02	2.22	2.46
			C_{T_R}	0.71	1.06	1.26	1.51	1.59
	1,800 r.p.m.	5	C_{T_F}	1.08	1.23	1.27	1.35	1.27
			C_{T_R}	0.69	0.75	0.71	0.69	0.45
		10	C_{T_F}	0.80	0.59	0.25	-0.14	-0.23
			C_{T_R}	0.61	0.32	-0.06	-0.49	-0.69
		15	C_{T_F}	0.56	-0.01	-0.65		
			C_{T_R}	0.45	-0.12	-0.79		
		20	C_{T_F}	0.29				
			C_{T_R}	0.27				
		25	C_{T_F}	0				
			C_{T_R}	0.06				

TABLE 21/

TABLE 21

C_{T_F} and C_{T_R} for Twin Rotors

θ_o	Arrangement	θ	Coeff × 10^3	μ=0.1	μ=0.2	μ=0.3	μ=0.4	μ=0.45
4°	$L_2H_3A_o$	0	C_{T_F}	1.28	1.75	2.12	2.49	2.64
			C_{T_R}	0.93	1.24	1.40	1.47	1.53
	1,800 r.p.m.	5	C_{T_F}	1.05	1.20	1.24	1.31	1.37
			C_{T_R}	0.80	0.85	0.73	0.54	0.44
		10	C_{T_F}	0.82	0.62	0.28	-0.02	-0.20
			C_{T_R}	0.66	0.36	-0.05	-0.51	-0.68
		15	C_{T_F}	0.59	0.03			
			C_{T_R}	0.47	-0.14			
		20	C_{T_F}	0.31				
			C_{T_R}	0.27				
		25	C_{T_F}	0				
			C_{T_R}	0.08				

TABLE 22

4°	$L_2H_2A_o$	0	C_{T_F}	1.31	1.75	2.07	2.37	2.55
			C_{T_R}	0.85	1.15	1.31	1.44	1.46
	1,800 r.p.m.	5	C_{T_F}	1.09	1.23	1.23	1.31	1.27
			C_{T_R}	0.80	0.84	0.78	0.57	0.51
		10	C_{T_F}	0.82	0.60	0.27	-0.04	-0.22
			C_{T_R}	0.65	0.40	-0.03	-0.49	-0.68
		15	C_{T_F}	0.57	0.05	-0.65		
			C_{T_R}	0.46	-0.15	-0.80		
		20	C_{T_F}	0.31	-0.58			
			C_{T_R}	0.28	-0.64			
		25	C_{T_F}	0.07				
			C_{T_R}	0.08				

TABLE 23/

TABLE 23

C_{T_F} and C_{T_R} for Twin Rotors

θ_o	Arrangement	θ	Coeff × 10^3	μ=0.1	μ=0.2	μ=0.3	μ=0.4	μ=0.45
4°	$L_2H_2A_{-7.7°}$	0	C_{T_F}	1.35	1.80	2.18	2.39	2.66
			C_{T_R}	1.08	1.82	2.17	2.63	2.84
	1,200 r.p.m.	5	C_{T_F}	1.14	1.31	1.27	1.39	1.34
			C_{T_R}	1.01	1.50	1.77	1.89	2.07
		10	C_{T_F}	0.91	0.70	0.38	0.15	-0.36
			C_{T_R}	0.91	1.18	1.25	1.13	1.44
		15	C_{T_F}	0.68	0.10	-0.51		
			C_{T_R}	0.76	0.75	0.38		
		20	C_{T_F}	0.42	-0.49			
			C_{T_R}	0.58	0.14			
		25	C_{T_F}	0.12				
			C_{T_R}	0.35				

TABLE 24

4°	$L_2H_2A_{-4.4°}$	0	C_{T_F}	1.37	1.76	2.12	2.49	2.52
			C_{T_R}	0.99	1.49	1.82	2.09	2.15
	1,800 r.p.m.	5	C_{T_F}	1.13	1.28	1.29	1.38	1.33
			C_{T_R}	0.91	1.21	1.29	1.26	1.27
		10	C_{T_F}	0.86	0.64	0.35	0.02	-0.09
			C_{T_R}	0.77	0.81	0.61	0.44	0.26
		15	C_{T_F}	0.61	0.07	-0.61		
			C_{T_R}	0.61	0.27	-0.21		
		20	C_{T_F}	0.37	-0.50			
			C_{T_R}	0.43	-0.27			
		25	C_{T_F}	0.16				
			C_{T_R}	0.25				

TABLE 25/

TABLE 25

C_{T_F} and C_{T_R} for Twin Rotors

θ_o	Arrangement	θ	Coeff × 10^3	μ=0.1	μ=0.2	μ=0.3	μ=0.4	μ=0.45
4°	$L_2H_2A_{+4°}$	0	C_{T_F}	1.32	1.75	2.04	2.32	2.52
			C_{T_R}	0.61	0.63	0.56	0.49	0.40
	1,800 r.p.m.	5	C_{T_F}	1.08	1.18	1.16	1.24	1.23
			C_{T_R}	0.53	0.28	-0.08	-0.48	-0.67
		10	C_{T_F}	0.85	0.59	0.32	-0.06	-0.20
			C_{T_R}	0.40	-0.15	-0.83	-1.44	-1.66
		15	C_{T_F}	0.61	0.01			
			C_{T_R}	0.24	-0.63			
		20	C_{T_F}	0.31	-0.64			
			C_{T_R}	0.06	-1.07			
		25	C_{T_F}	0.02				
			C_{T_R}	-0.12				

TABLE 26

C_{T_F} and C_{T_R} for Twin Rotors

4°	$L_2H_2A_{7.9°}$	0	C_{T_F}	1.36	1.79	2.05	2.37	2.59
			C_{T_R}	0.30	0.06	-0.24	-0.60	-0.69
	1,200 r.p.m.	5	C_{T_F}	1.14	1.28	1.21	1.25	1.18
			C_{T_R}	0.22	-0.31	-0.92	-1.59	-1.80
		10	C_{T_F}	0.89	0.70	0.32	-0.07	
			C_{T_R}	0.12	-0.70	-1.52	-2.37	
		15	C_{T_F}	0.64	-0.01			
			C_{T_R}	-0.04	-1.13			
		20	C_{T_F}	0.33				
			C_{T_R}	-0.23				
		25	C_{T_F}	-0.03				
			C_{T_R}	-0.39				

TABLE 27/

TABLE 27

C_{T_F} and C_{T_R} for Twin Rotors

θ_o	Arrangement	θ	Coeff × 10^3	μ=0.1	μ=0.2	μ=0.3	μ=0.4	μ=0.45
(F) =4°	$L_2H_2A_o$	0	C_{T_F}	1.33	1.81	2.08	2.40	2.53
			C_{T_R}	1.46	1.80	1.97	2.12	2.19
(R) =6°	1,200 r.p.m.	5	C_{T_F}	1.12	1.30	1.34	1.33	1.29
			C_{T_R}	1.42	1.53	1.47	1.30	1.35
		10	C_{T_F}	0.88	0.71	0.38	0.09	-0.04
			C_{T_R}	1.31	1.13	0.81	0.38	0.26
		15	C_{T_F}	0.64	0.07	-0.57		
			C_{T_R}	1.13	0.64	-0.11		
		20	C_{T_F}	0.39	-0.58			
			C_{T_R}	0.92	-0.01			
		25	C_{T_F}	0.13				
			C_{T_R}	0.68				

TABLE 28

8°	$L_2H_2A_o$	0	C_{T_F}	2.39	2.94	3.26	3.63	3.84
			C_{T_R}	1.78	2.12	2.24	2.42	2.62
	1,200 r.p.m.	5	C_{T_F}	2.21	2.55	2.65	2.92	2.92
			C_{T_R}	1.76	1.92	1.90	1.75	1.83
		10	C_{T_F}	2.07	2.14	2.00	1.91	1.83
			C_{T_R}	1.71	1.60	1.33	0.99	0.89
		15	C_{T_F}	1.88	1.66	1.14	0.67	0.48
			C_{T_R}	1.58	1.21	0.61	-0.01	-0.36
		20	C_{T_F}	1.66	1.04	0.05		
			C_{T_R}	1.43	0.68	-0.20		
		25	C_{T_F}	1.41	0.28			
			C_{T_R}	1.24	0.04			

TABLE 29/

TABLE 29

C_{T_F} and C_{T_R} for Twin Rotors

θ_o	Arrangement	θ	Coeff × 10^3	μ=0.1	μ=0.2	μ=0.3	μ=0.4	μ=0.45
8°	$L_2H_2A_{-7.7°}$	0	C_{T_F}	2.43	2.97	3.30	3.65	3.88
			C_{T_R}	2.00	2.58	2.91	3.36	3.49
	1,200 r.p.m.	5	C_{T_F}	2.27	2.61	2.73	2.88	2.95
			C_{T_R}	1.98	2.33	2.64	2.79	3.03
		10	C_{T_F}	2.11	2.19	2.07	1.95	1.95
			C_{T_R}	1.89	2.13	2.29	2.31	2.46
		15	C_{T_F}	1.91	1.66	1.27	0.87	0.67
			C_{T_R}	1.79	1.88	1.70	1.56	1.46
		20	C_{T_F}	1.68	1.11	0.25		
			C_{T_R}	1.66	1.50	0.99		
		25	C_{T_F}	1.48	0.41			
			C_{T_R}	1.49	0.91			

TABLE 30

8°	$L_2H_2A_{-4.4°}$	0	C_{T_F}	2.43	3.02	3.19	3.71	3.99
			C_{T_R}	1.89	2.31	2.73	2.88	3.03
	1,200 r.p.m.	5	C_{T_F}	2.26	2.64	2.70	2.89	3.05
			C_{T_R}	1.84	2.13	2.37	2.40	2.54
		10	C_{T_F}	2.10	2.18	2.05	1.94	1.85
			C_{T_R}	1.77	1.88	1.86	1.71	1.76
		15	C_{T_F}	1.94	1.73	1.23	0.80	0.62
			C_{T_R}	1.67	1.53	1.16	0.85	0.65
		20	C_{T_F}	1.73	1.17	0.28		
			C_{T_R}	1.52	1.07	0.30		
		25	C_{T_F}	1.38	0.42			
			C_{T_R}	1.28	0.43			

TABLE 31

C_{T_F} and C_{T_R} for Twin Rotors

θ_o	Arrangement	θ	Coeff × 10^3	μ=0.1	μ=0.2	μ=0.3	μ=0.4	μ=0.45
8°	$L_2H_2A_{+4°}$	0	C_{T_F}	2.39	2.93	3.24	3.60	3.79
			C_{T_R}	1.65	1.75	1.77	1.80	1.81
	1,200 r.p.m.	5	C_{T_F}	2.24	2.52	2.66	2.87	2.99
			C_{T_R}	1.61	1.58	1.30	0.94	0.88
		10	C_{T_F}	2.08	2.10	1.96	1.84	1.90
			C_{T_R}	1.51	1.20	0.58	0.08	-0.26
		15	C_{T_F}	1.88	1.62	1.18		
			C_{T_R}	1.39	0.69	-0.24		
		20	C_{T_F}	1.66	1.03			
			C_{T_R}	1.24	0.12			
		25	C_{T_F}	1.41	0.47			
			C_{T_R}	1.09	-0.30			

TABLE 32

8°	$L_2H_1A_0$	0	C_{T_F}	2.37	2.96	3.34	3.62	3.79
			C_{T_R}	1.55	2.01	2.31	2.50	2.60
	1,200 r.p.m.	5	C_{T_F}	2.21	2.54	2.74	2.92	3.04
			C_{T_R}	1.62	1.81	1.77	1.83	1.83
		10	C_{T_F}	2.06	2.15	2.05	1.96	1.89
			C_{T_R}	1.61	1.52	1.28	1.03	0.94
		15	C_{T_F}	1.88	1.65	1.23	0.72	0.50
			C_{T_R}	1.54	1.12	0.56	-0.08	-0.32
		20	C_{T_F}	1.68	1.06	-0.04		
			C_{T_R}	1.40	0.65	-0.31		
		25	C_{T_F}	1.44	0.28			
			C_{T_R}	1.23	0.03			

TABLE 33/

TABLE 33

C_{T_F} and C_{T_R} for Twin Rotors

θ_o	Arrangement	θ	Coeff × 10^3	μ=0.1	μ=0.2	μ=0.3	μ=0.4	μ=0.45
8°	$L_2H_3A_o$	0	C_{T_F}	2.42	2.95	3.33	3.72	3.94
			C_{T_R}	1.90	2.15	2.30	2.41	2.57
	1,200 r.p.m.	5	C_{T_F}	2.23	2.54	2.74	2.87	2.94
			C_{T_R}	1.84	1.93	1.97	1.90	1.87
		10	C_{T_F}	2.05	2.12	2.02	1.92	1.83
			C_{T_R}	1.74	1.63	1.36	1.10	0.90
		15	C_{T_F}	1.85	1.67	1.15	0.61	0.40
			C_{T_R}	1.59	1.20	0.55	-0.11	-0.30
		20	C_{T_F}	1.62	1.05	0.04		
			C_{T_R}	1.42	0.66	-0.37		
		25	C_{T_F}	1.30	0.24			
			C_{T_R}	1.22	0.03			

TABLE 34

8°	$L_1H_2A_o$	0	C_{T_F}	2.38	2.90	3.25	3.55	3.64
			C_{T_R}	1.80	2.15	2.36	2.73	2.89
	1,200 r.p.m.	5	C_{T_F}	2.20	2.55	2.69	2.84	3.04
			C_{T_R}	1.78	1.95	1.92	1.90	1.81
		10	C_{T_F}	2.04	2.14	2.12	1.86	2.10
			C_{T_R}	1.70	1.59	1.27	0.99	0.70
		15	C_{T_F}	1.84	1.70	1.31	0.87	0.81
			C_{T_R}	1.59	1.11	0.46	-0.25	-0.63
		20	C_{T_F}	1.63	1.18	0.45		
			C_{T_R}	1.42	0.54	-0.62		
		25	C_{T_F}	1.34	0.38			
			C_{T_R}	1.22	-0.19			

TABLE 35/

TABLE 35

C_{T_F} and C_{T_R} for Twin Rotor

θ_o	Arrangement	θ	Coeff × 10^3	μ=0.1	μ=0.2	μ=0.3	μ=0.4	μ=0.45
8°	$L_3H_2A_o$	0	C_{T_F}	2.37	2.93	3.28	3.66	3.91
			C_{T_R}	1.87	2.11	2.23	2.36	2.51
		5	C_{T_F}	2.20	2.49	2.62	2.88	2.94
	1,200 r.p.m.		C_{T_R}	1.82	1.92	1.88	1.77	1.84
		10	C_{T_F}	2.03	2.12	1.98	1.92	1.85
			C_{T_R}	1.74	1.60	1.30	0.86	0.74
		15	C_{T_F}	1.82	1.65	1.18	0.62	0.42
			C_{T_R}	1.59	1.15	0.52	-0.12	-0.45
		20	C_{T_F}	1.69	1.08	0.11		
			C_{T_R}	1.40	0.63	-0.37		
		25	C_{T_F}	1.40	0.15			
			C_{T_R}	1.20	-0.03			

TABLE 36

12°	$L_3H_2A_o$	0	C_{T_F}	3.30	3.72			
			C_{T_R}	2.73	2.87			
		5	C_{T_F}	3.15	3.52	3.78		
	1,200 r.p.m.		C_{T_R}	2.70	2.76	2.75		
		10	C_{T_F}	3.11	3.27	3.41	3.55	3.56
			C_{T_R}	2.64	2.64	2.45	2.22	2.14
		15	C_{T_F}	3.08	3.03	2.88	2.60	2.52
			C_{T_R}	2.52	2.37	1.98	1.49	1.25
		20	C_{T_F}	2.98	2.71	2.23	1.67	1.23
			C_{T_R}	2.27	2.01	1.31	0.43	0.33
		25	C_{T_F}	2.79	2.18	1.33	-0.01	
			C_{T_R}	1.96	1.55	0.55	-0.75	

TABLE 37

C_{T_F} and C_{T_R} for Twin Rotors

θ_0	Arrangement	θ	Coeff $\times 10^3$	μ=0.1	μ=0.2	μ=0.3	μ=0.4	μ=0.45
12°	$L_2H_2A_{-7.7^\circ}$	0	C_{T_F}	3.30	3.79			
			C_{T_R}	2.80	3.23			
	1,200 r.p.m.	5	C_{T_F}	3.19	3.56	3.82		
			C_{T_R}	2.79	3.02	3.23		
		10	C_{T_F}	3.12	3.33	3.50	3.67	3.71
			C_{T_R}	2.76	2.83	2.96	3.06	3.19
		15	C_{T_F}	3.10	3.11	2.99	2.86	2.81
			C_{T_R}	2.72	2.72	2.73	2.74	2.76
		20	C_{T_F}	2.96	2.80	2.33	1.83	1.60
			C_{T_R}	2.67	2.54	2.24	2.02	1.87
		25	C_{T_F}	2.69	2.33	1.43	0.59	
			C_{T_R}	2.50	1.97	1.61	1.02	

TABLE 38

12°	$L_2H_2A_{-4.4^\circ}$	0	C_{T_F}	3.30	3.74			
			C_{T_R}	2.79	3.00			
	1,200 r.p.m.	5	C_{T_F}	3.18	3.55	3.86		
			C_{T_R}	2.76	2.83	2.93		
		10	C_{T_F}	3.12	3.36	3.47	3.61	3.80
			C_{T_R}	2.68	2.71	2.76	2.80	2.72
		15	C_{T_F}	3.09	3.07	3.03	2.84	2.81
			C_{T_R}	2.61	2.60	2.34	2.23	2.22
		20	C_{T_F}	2.94	2.77	2.29	2.69	1.49
			C_{T_R}	2.50	2.34	1.87	1.41	1.17
		25	C_{T_F}	2.60	2.15	1.38	0.76	
			C_{T_R}	2.28	1.81	1.06	0.55	

TABLE 39/

TABLE 39

C_{T_F} and C_{T_R} for Twin Rotors

θ_o	Arrangement	θ	Coeff × 10^3	μ=0.1	μ=0.2	μ=0.3	μ=0.4	μ=0.45
12°	$L_2H_2A_0$	0	C_{T_F}	3.31	3.75			
			C_{T_R}	2.74	2.85			
	1,200 r.p.m.	5	C_{T_F}	3.19	3.56	3.89		
			C_{T_R}	2.73	2.79	2.79		
		10	C_{T_F}	3.10	3.29	3.50	3.57	3.62
			C_{T_R}	2.66	2.72	2.53	2.41	2.45
		15	C_{T_F}	3.03	3.04	2.91	2.64	2.69
			C_{T_R}	2.56	2.43	2.03	1.49	1.46
		20	C_{T_F}	2.89	2.66	2.14	1.55	1.29
			C_{T_R}	2.45	2.03	1.34	0.64	0.25
		25	C_{T_F}	2.62	2.16	1.24	0.24	
			C_{T_R}	2.26	1.51	0.48	-0.54	

TABLE 40

12°	$L_2H_2A_{+4°}$	0	C_{T_F}	3.25	3.71			
			C_{T_R}	2.62	2.73			
	1,200 r.p.m.	5	C_{T_F}	3.11	3.57	3.80		
			C_{T_R}	2.57	2.59	2.43		
		10	C_{T_F}	3.04	3.26	3.37	3.58	3.68
			C_{T_R}	2.51	2.43	2.05	1.74	1.62
		15	C_{T_F}	3.02	2.99	2.85	2.71	2.63
			C_{T_R}	2.45	2.07	1.46	0.78	0.41
		20	C_{T_F}	2.91	2.65	2.10	1.52	1.21
			C_{T_R}	2.36	1.68	0.74	-0.24	-0.82
		25	C_{T_F}	2.70	2.04	1.15	0.08	
			C_{T_R}	2.27	1.18	-0.12	-1.22	

TABLE 41/

TABLE 41

C_{T_F} and C_{T_R} for Twin Rotors

θ_o	Arrangement	θ	Coeff × 10^3	μ=0.1	μ=0.2	μ=0.3	μ=0.4	μ=0.45
12°	$L_2H_1A_O$	0	C_{T_F}	3.27	3.78			
			C_{T_R}	2.59	2.90			
	1,200 r.p.m.	5	C_{T_F}	3.13	3.56	3.86		
			C_{T_R}	2.64	2.75	2.84		
		10	C_{T_F}	3.05	3.32	2.55	3.75	3.79
			C_{T_R}	2.60	2.63	2.48	2.32	2.22
		15	C_{T_F}	3.00	3.06	3.00	2.76	2.67
			C_{T_R}	2.54	2.36	2.00	1.59	1.46
		20	C_{T_F}	2.88	2.71	2.22	1.58	1.40
			C_{T_R}	2.45	2.01	1.33	0.69	0.37
		25	C_{T_F}	-	2.14	1.23	0.21	
			C_{T_R}	-	1.58	0.59	-0.23	

TABLE 42

12°	$L_2H_3A_O$	0	C_{T_F}	3.22	3.68			
			C_{T_R}	2.82	2.85			
	1,200 r.p.m.	5	C_{T_F}	3.05	3.48	3.76		
			C_{T_R}	2.75	2.72	2.71		
		10	C_{T_F}	2.99	3.19	3.32	3.53	3.61
			C_{T_R}	2.68	2.63	2.46	2.24	2.24
		15	C_{T_F}	2.96	2.96	2.82	2.58	2.56
			C_{T_R}	2.59	2.42	2.02	1.59	1.46
		20	C_{T_F}	2.85	2.60	2.09	1.42	1.20
			C_{T_R}	2.49	2.06	1.36	0.58	0.29
		25	C_{T_F}	2.52	2.02	1.15	0.28	
			C_{T_R}	2.29	1.58	0.41	-0.41	

TABLE 43/

TABLE 43

C_{T_F} and C_{T_R} for Twin Rotors

θ_0	Arrangement	θ	Coeff x 10^3	μ=0.1	μ=0.2	μ=0.3	μ=0.4	μ=0.45
12°	$L_1H_2A_0$	0	C_{T_F}	3.24	3.66			
			C_{T_R}	2.68	2.78			
		5	C_{T_F}	3.09	3.46	3.77		
	1,200 r.p.m.		C_{T_R}	2.67	2.76	2.69		
		10	C_{T_F}	3.03	3.24	3.30	3.47	3.61
			C_{T_R}	2.61	2.67	2.50	2.25	2.25
		15	C_{T_F}	2.92	2.98	2.77	2.47	2.54
			C_{T_R}	2.53	2.39	2.01	1.60	1.53
		20	C_{T_F}	2.76	2.54	1.99	0.96	1.13
			C_{T_R}	2.45	2.03	1.39	0.35	0.22
		25	C_{T_F}	2.51	2.01	0.98	-0.27	
			C_{T_R}	2.39	1.58	0.47	-0.69	

FIG. 1.

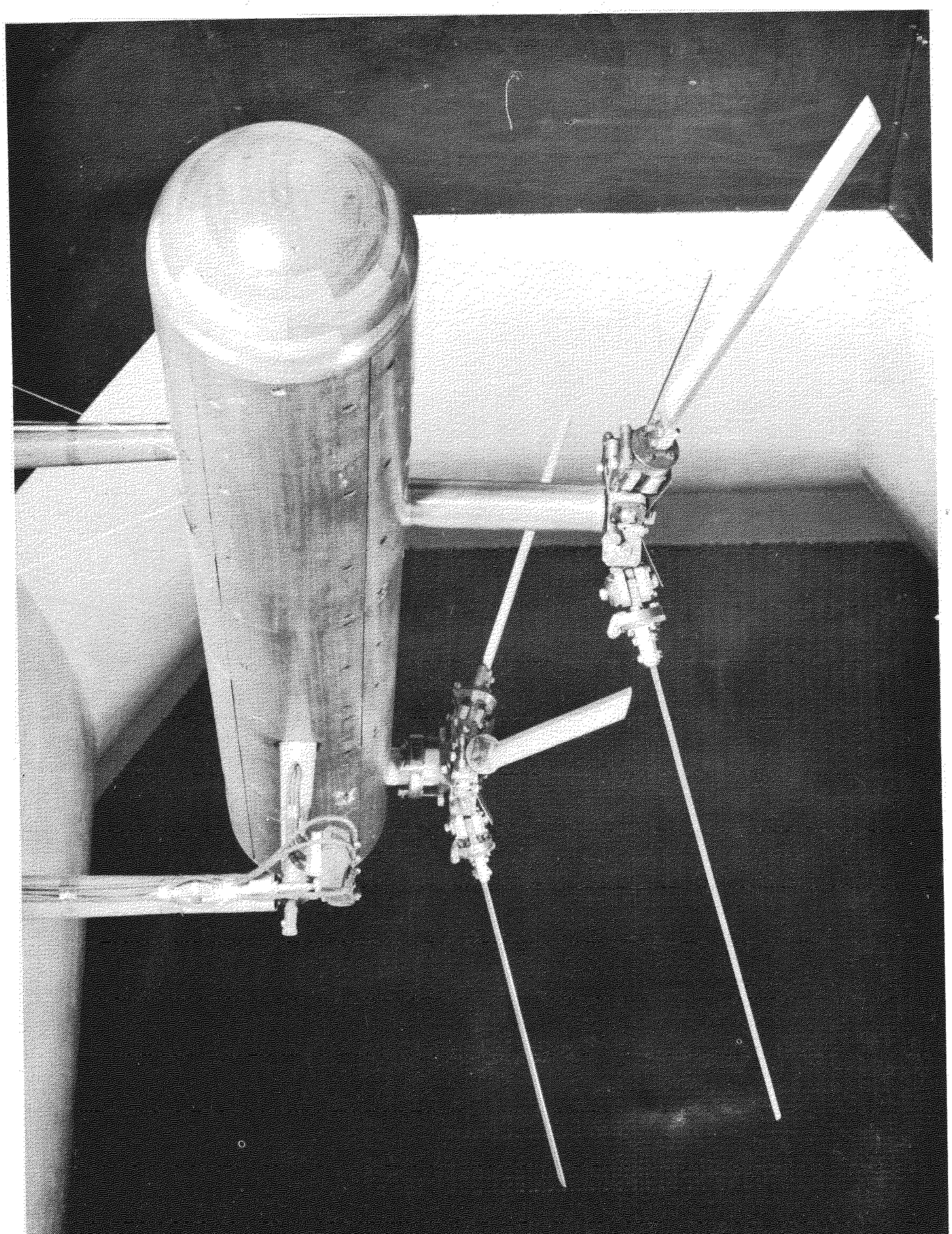

Model in wind tunnel.

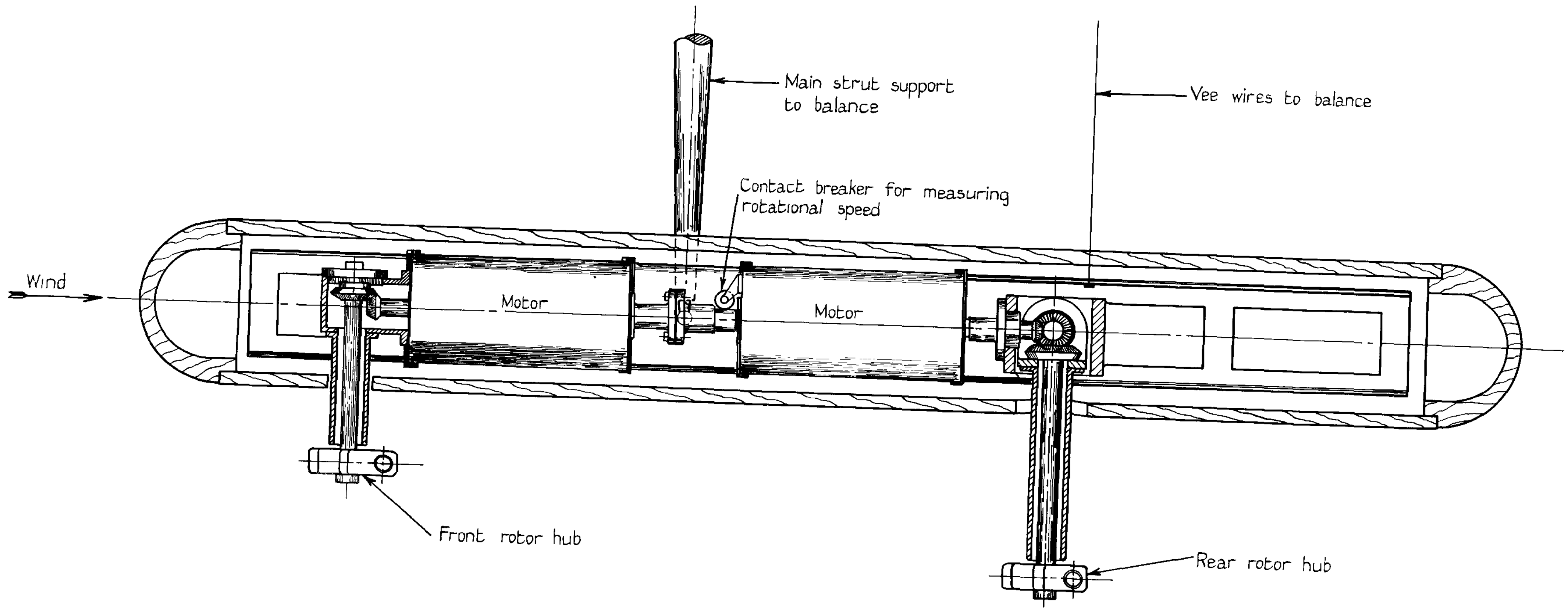

Arrangement of Helicopter Drive.

FIG 2.

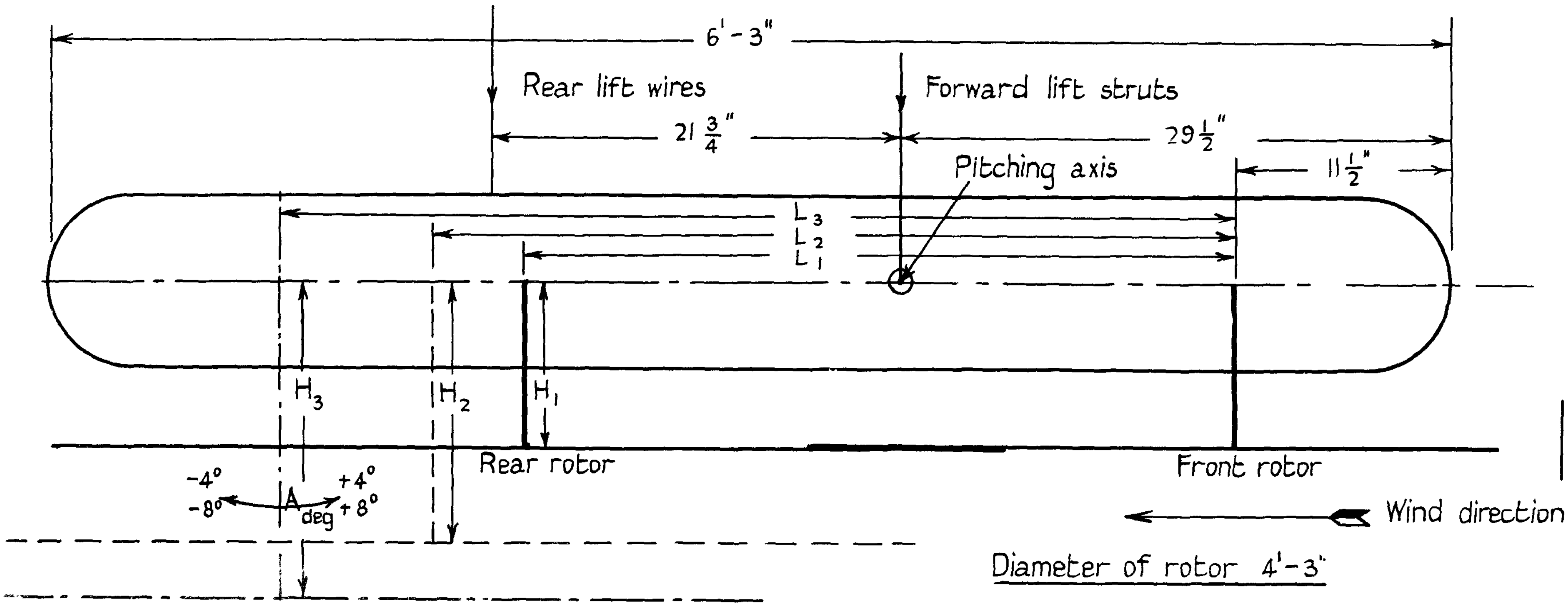

FIG. 3.

Alternative positions for rear rotor

$L_1 = 3'\text{-}2''$
$L_2 = 3'\text{-}7''$
$L_3 = 4'\text{-}3\frac{1}{8}''$
$H_1 = 8\frac{1}{2}''$
$H_2 = 13\frac{1}{2}''$
$H_3 = 16\frac{1}{2}''$

Diagram of rotor positions.

FIG. 4.

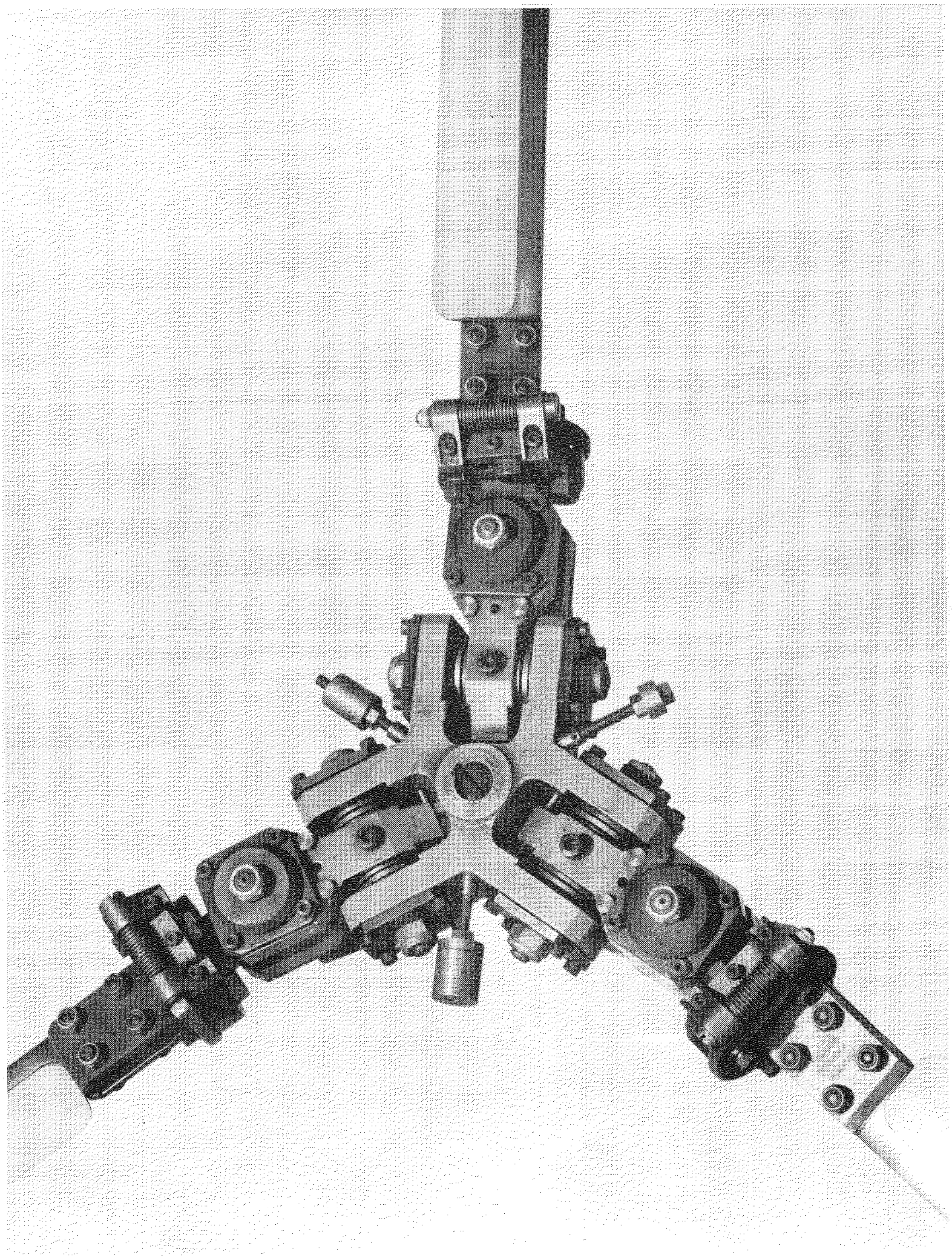

Details of hub.

Fig. 5.

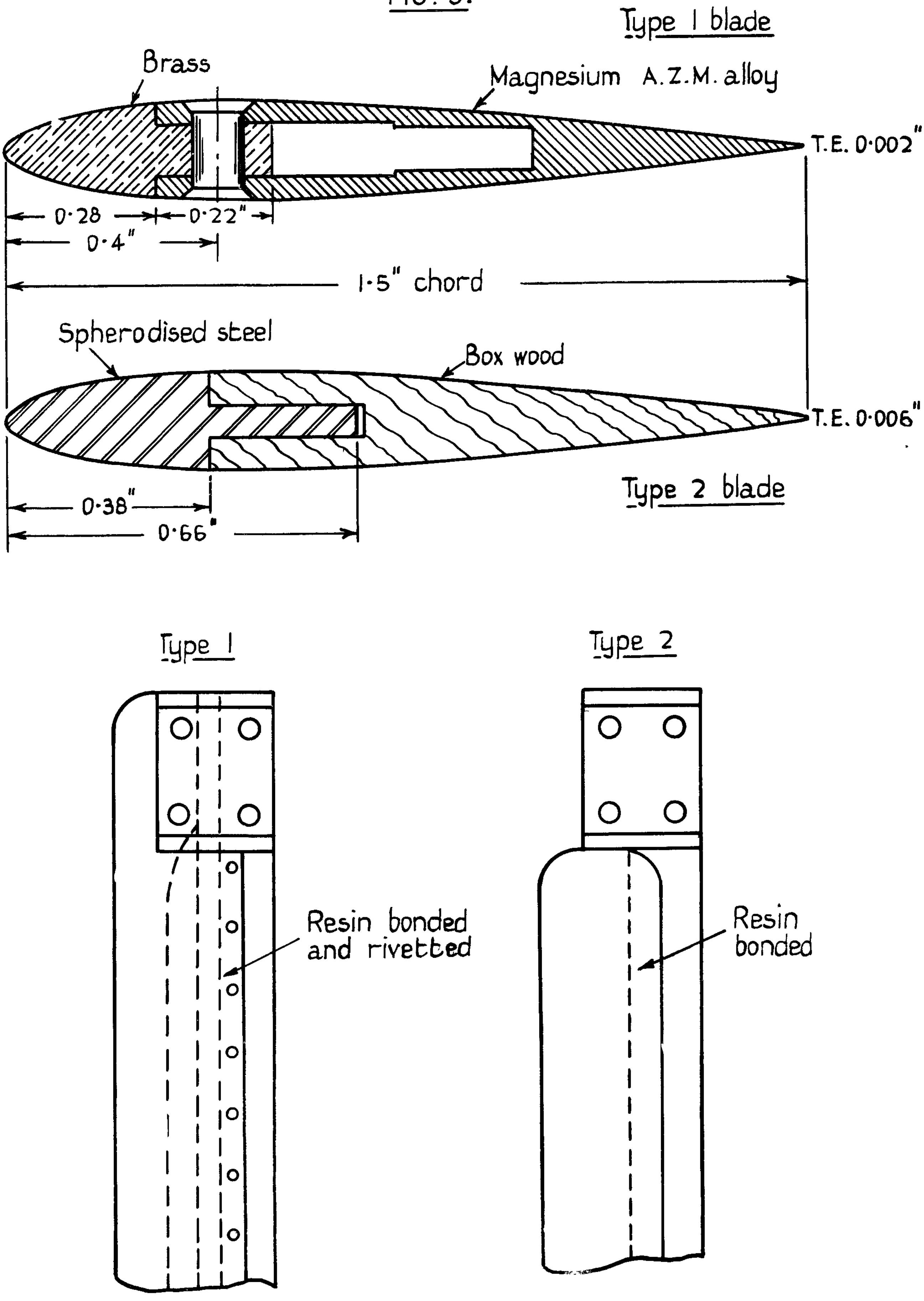

Details of blade construction

FIG. 6.

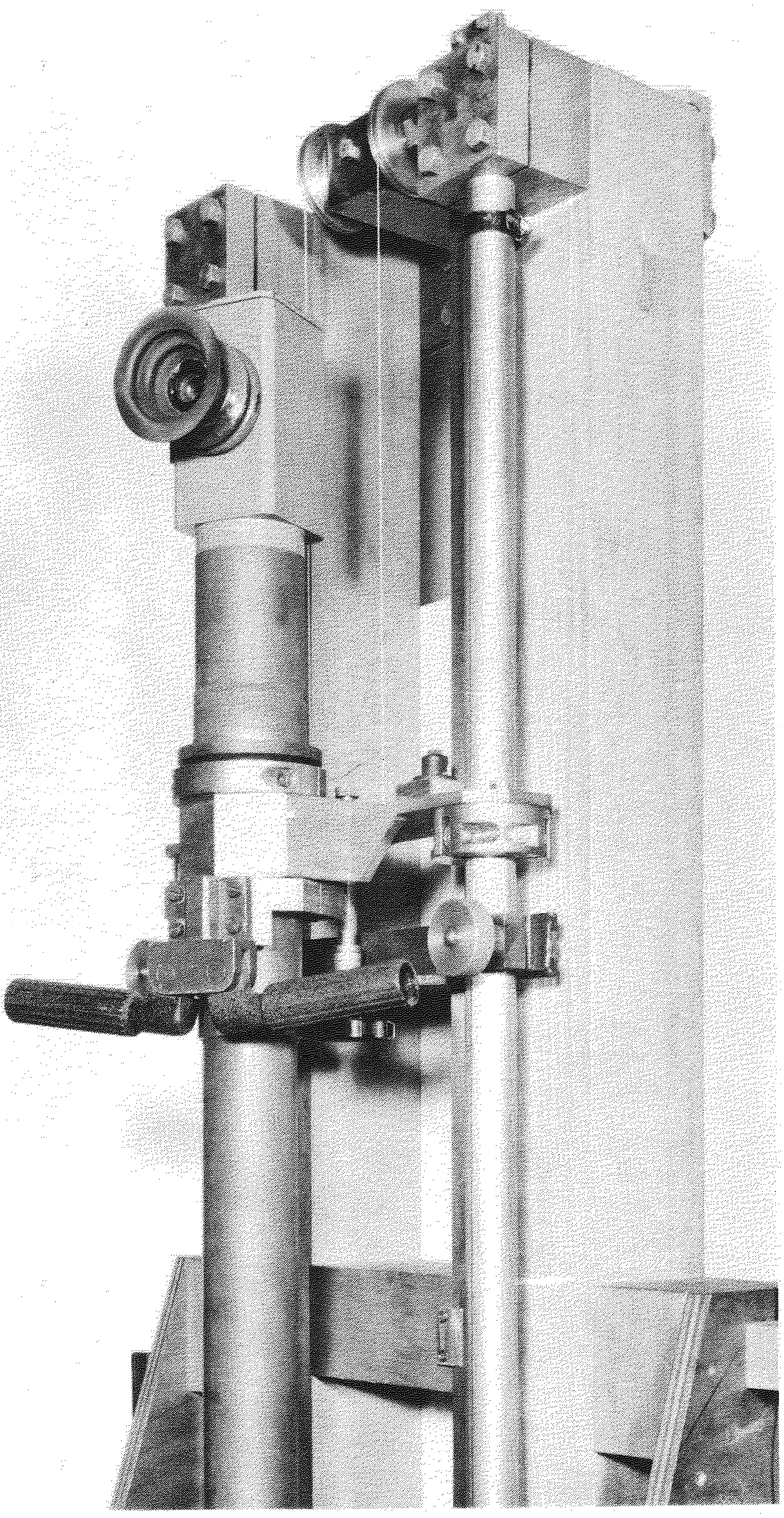

Head of periscope.

FIG. 7.

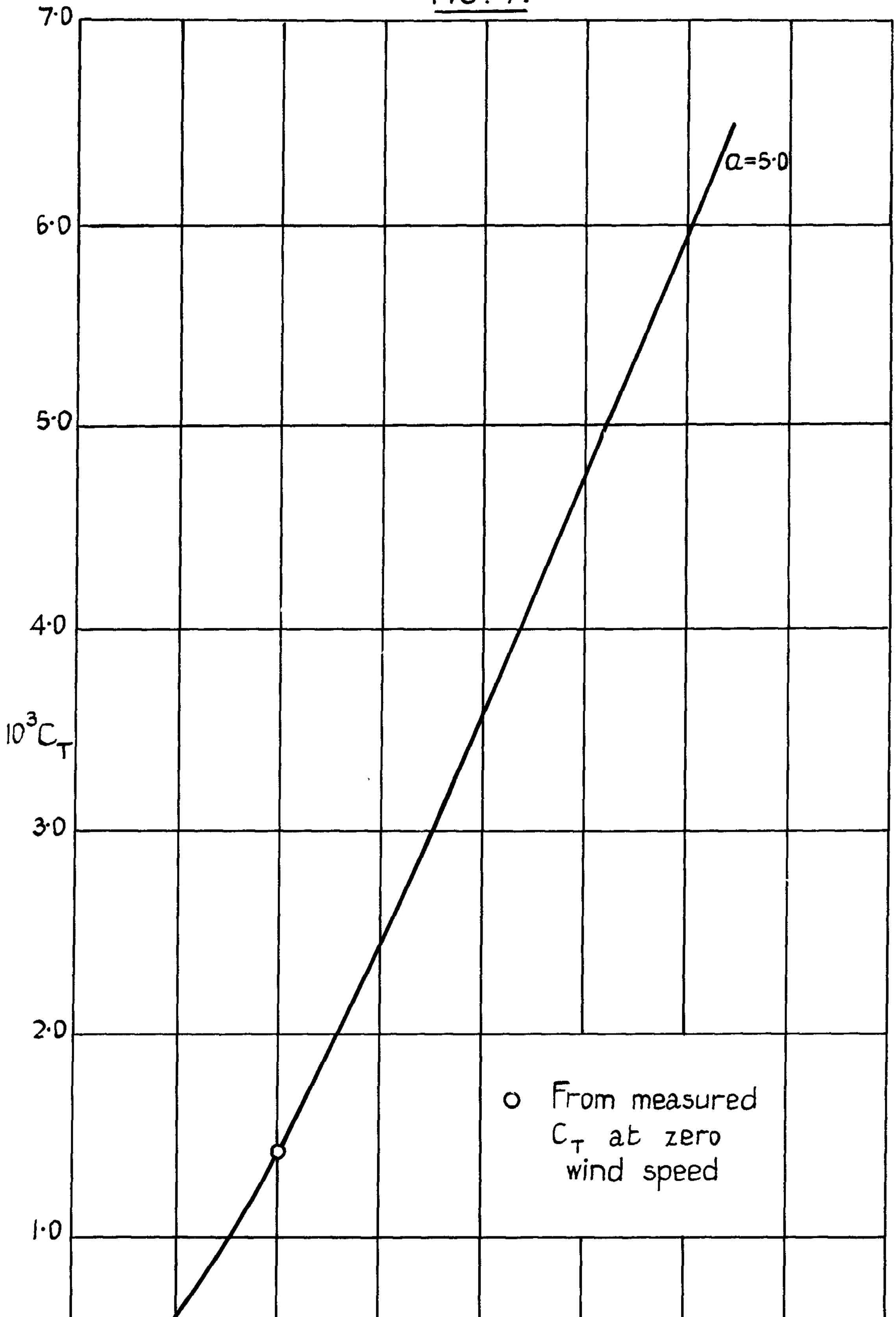

Calculated static thrust coefficient.

FIG. 8

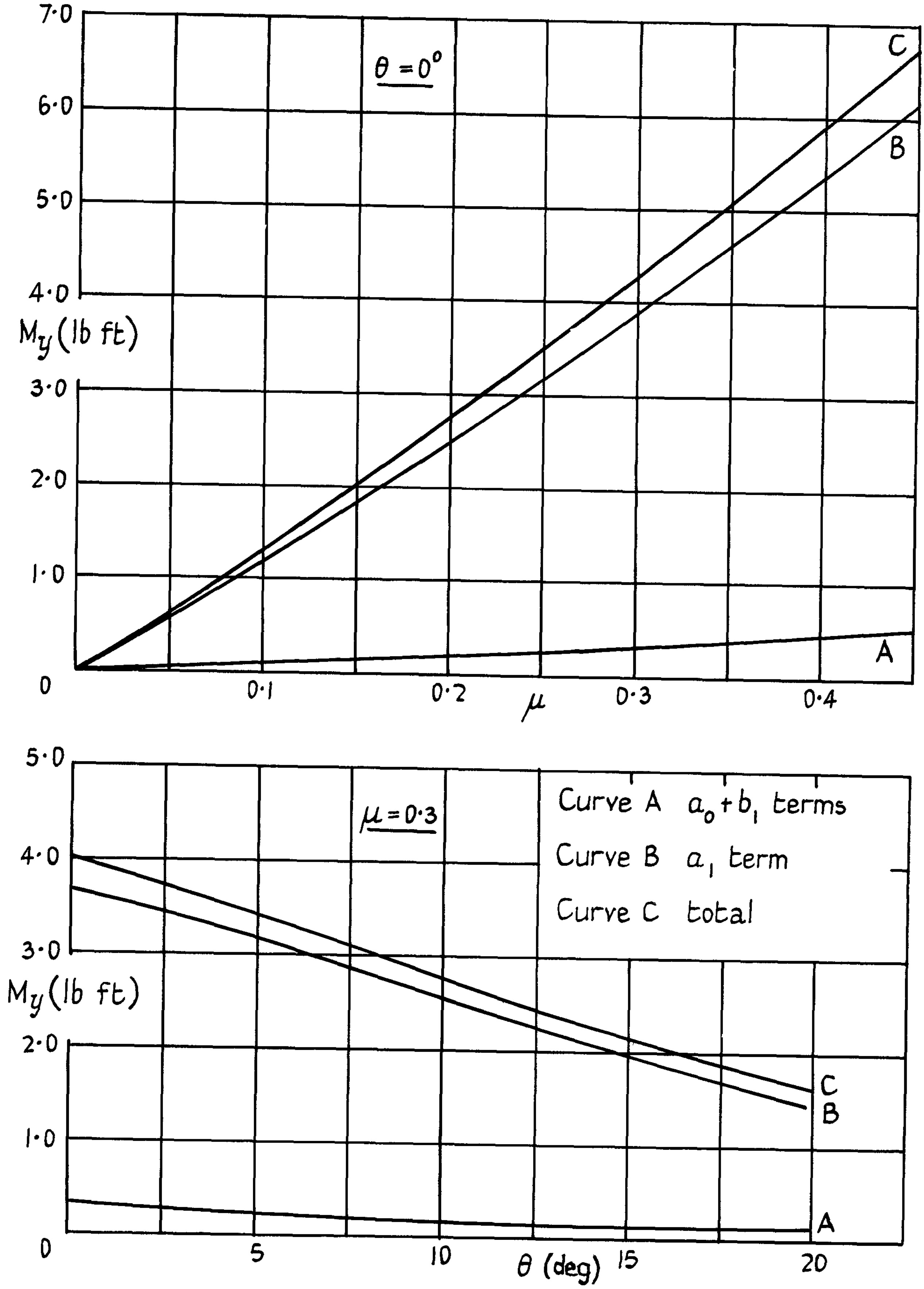

Values of M_y, $\theta_0 = 8^\circ$, 1200 rpm

FIG. 9a.

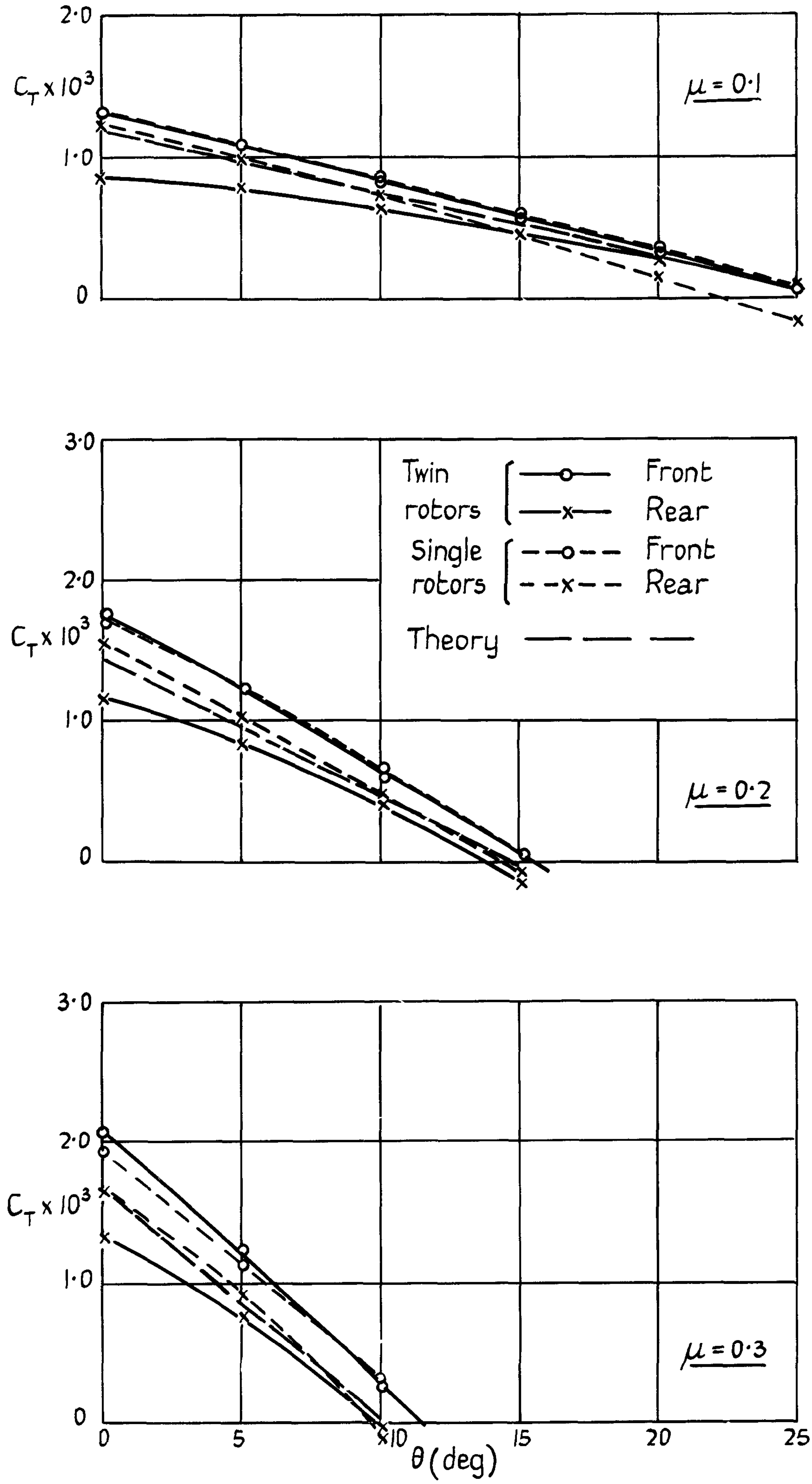

Division of thrust between rotors

$L_2H_2A_0$ $\theta_0 = 4°$

FIG. 9b.

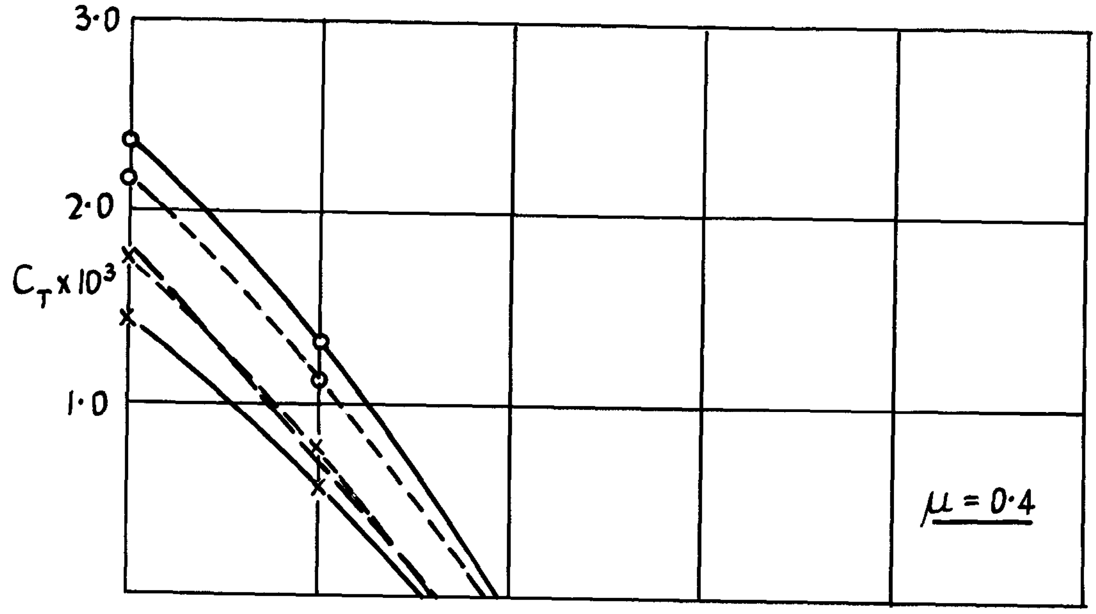

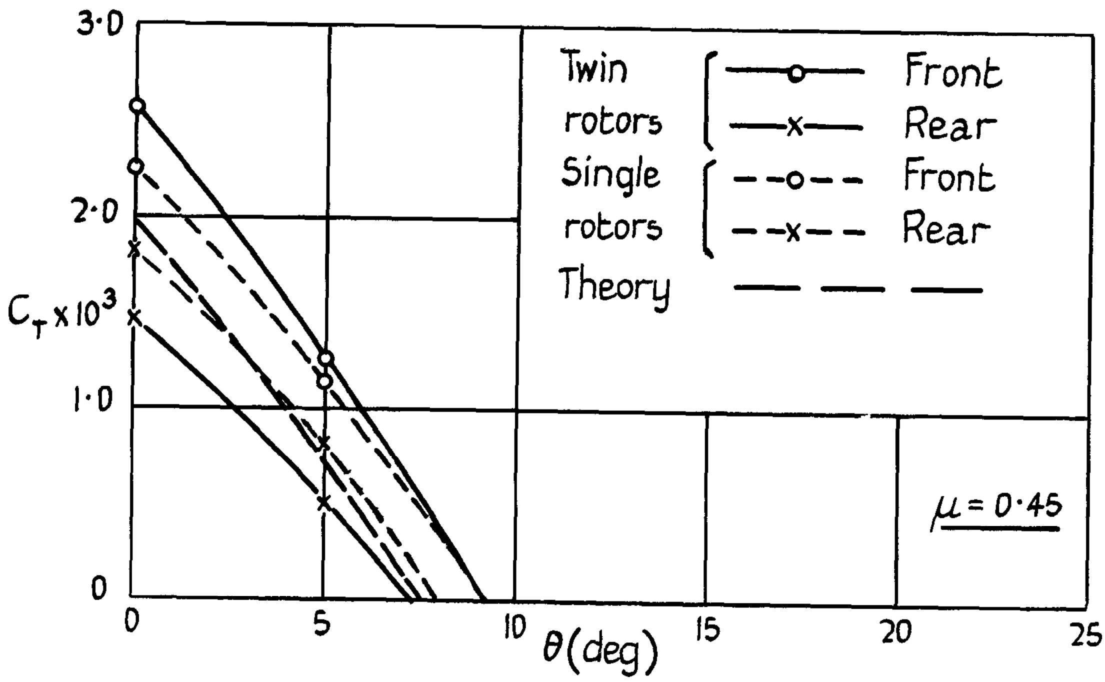

Division of thrust between rotors

$L_2 H_2 A_0$ $\theta_0 = 4°$

FIG. 10a.

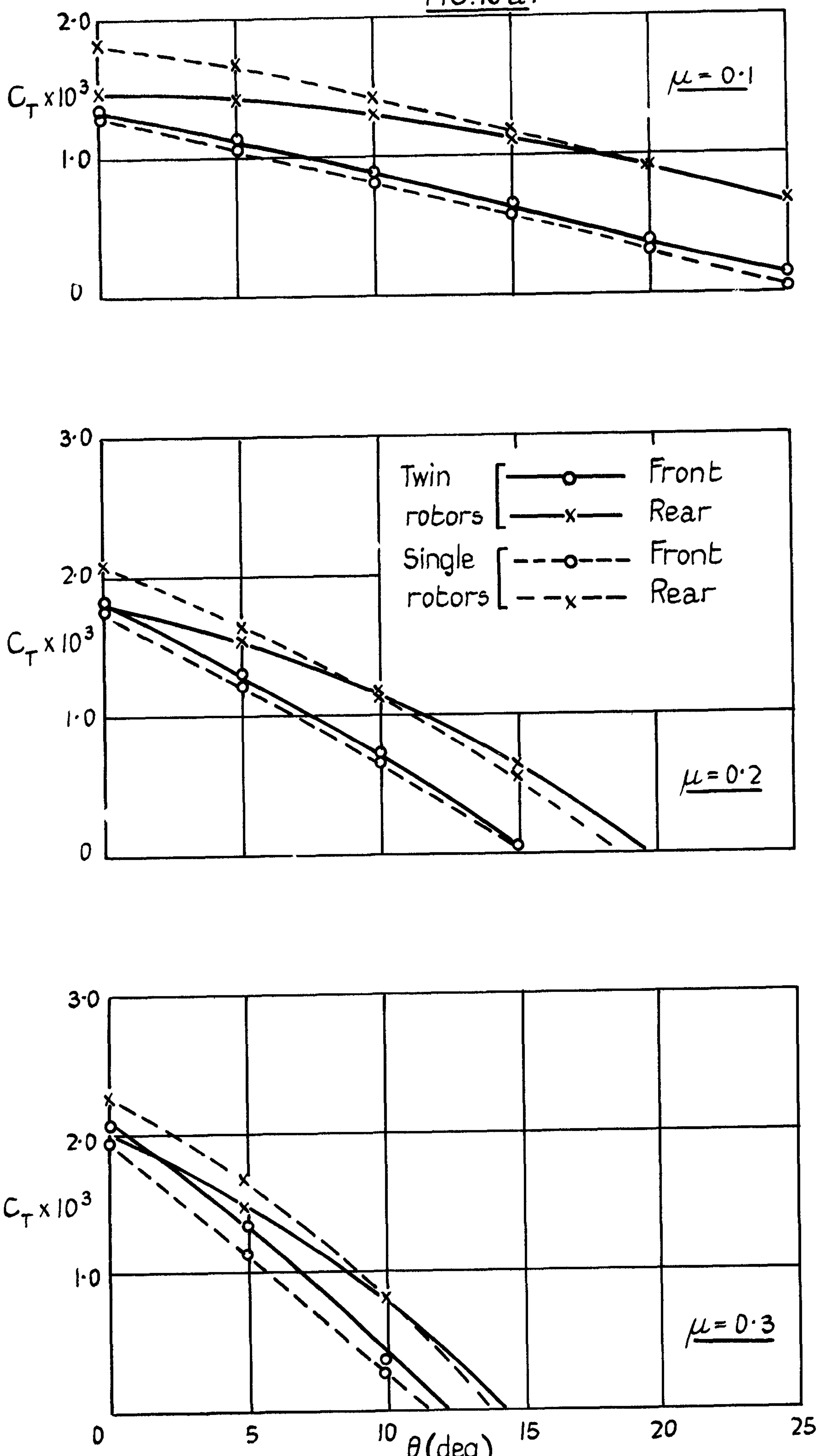

Division of thrust between rotors

$L_2 H_2 A_0$ $\quad \theta_{o_F} = 4^\circ \quad \theta_{o_R} = 6^\circ$

FIG. 10b.

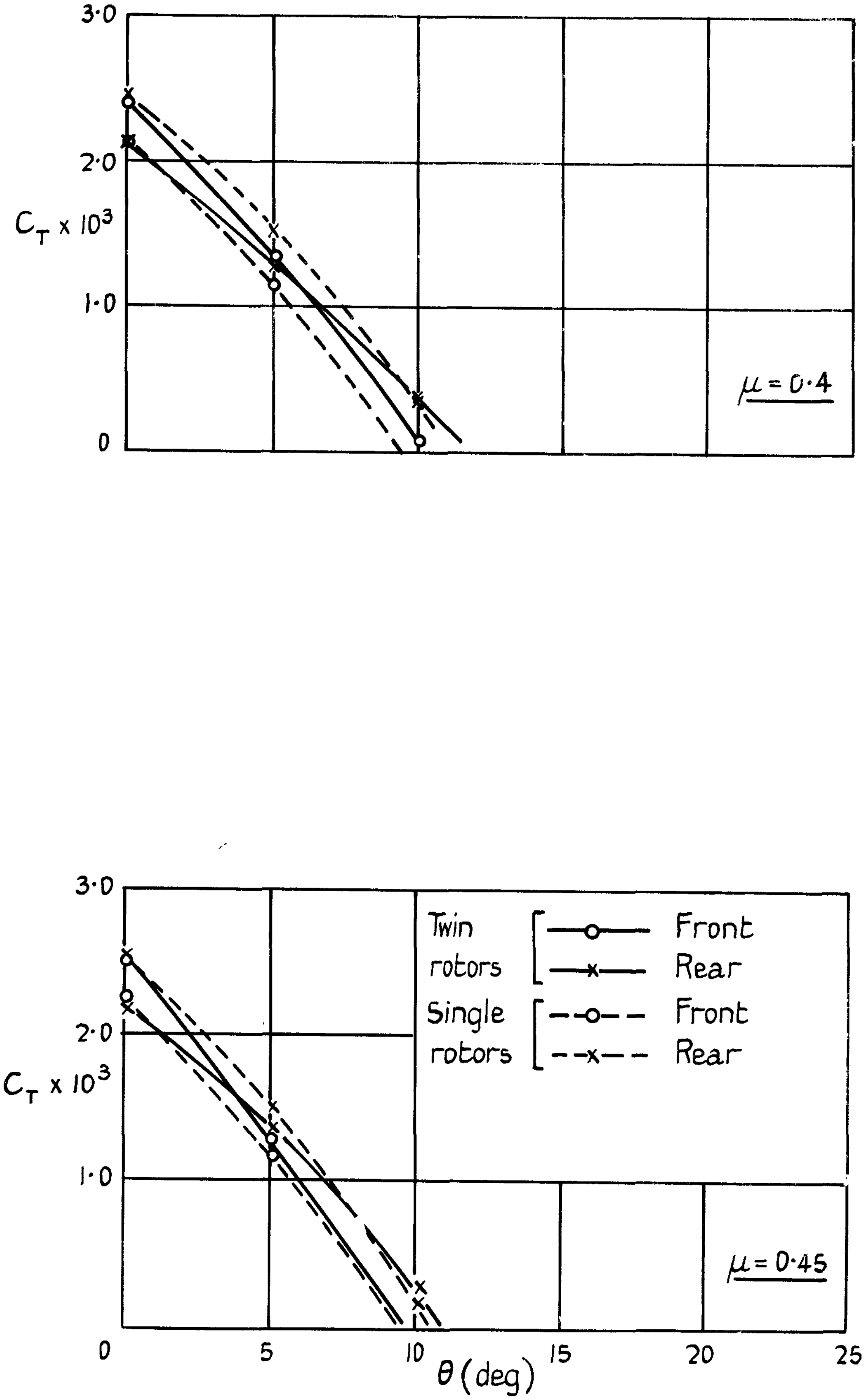

Division of thrust between rotors.

$L_2 H_2 A_0$ $\theta_{0_F} = 4°$ $\theta_{0_R} = 6°$

FIG. 11 a

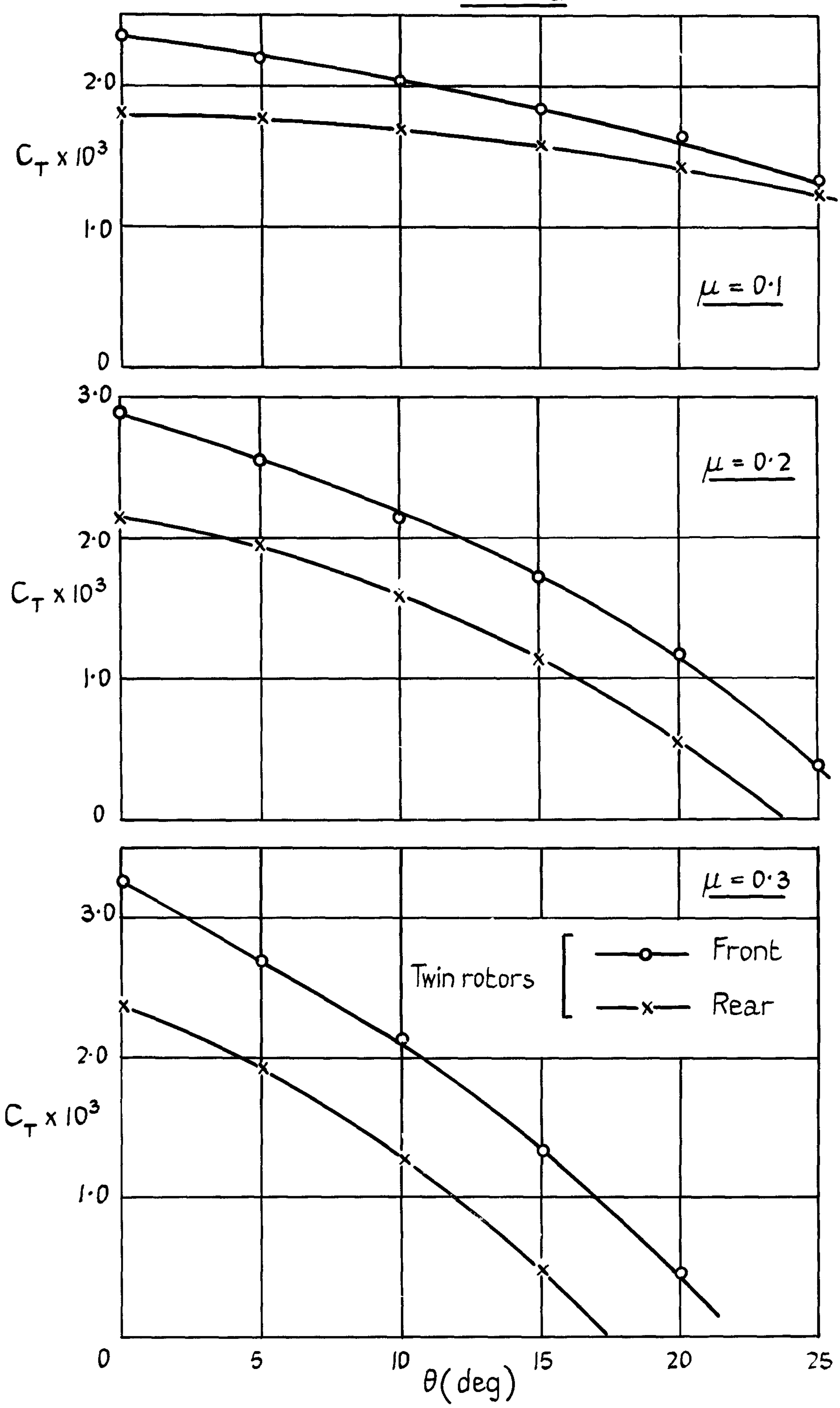

Division of thrust between rotors

$L_1 H_2 A_0$ $\theta_0 = 8°$

FIG. 11 b.

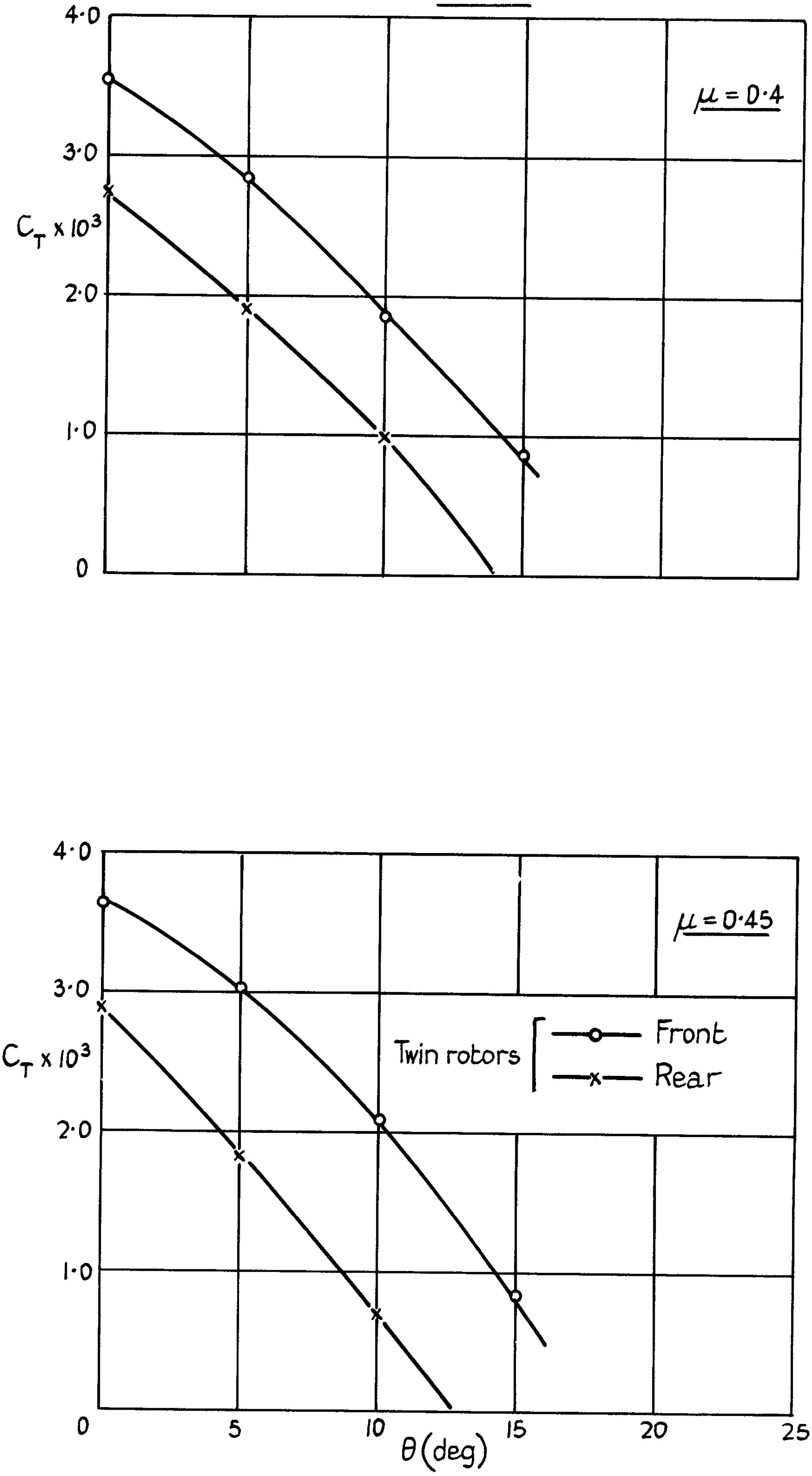

Division of thrust between rotors

$L_1 H_2 A_0$ $\theta_0 = 8^0$

FIG. 12a

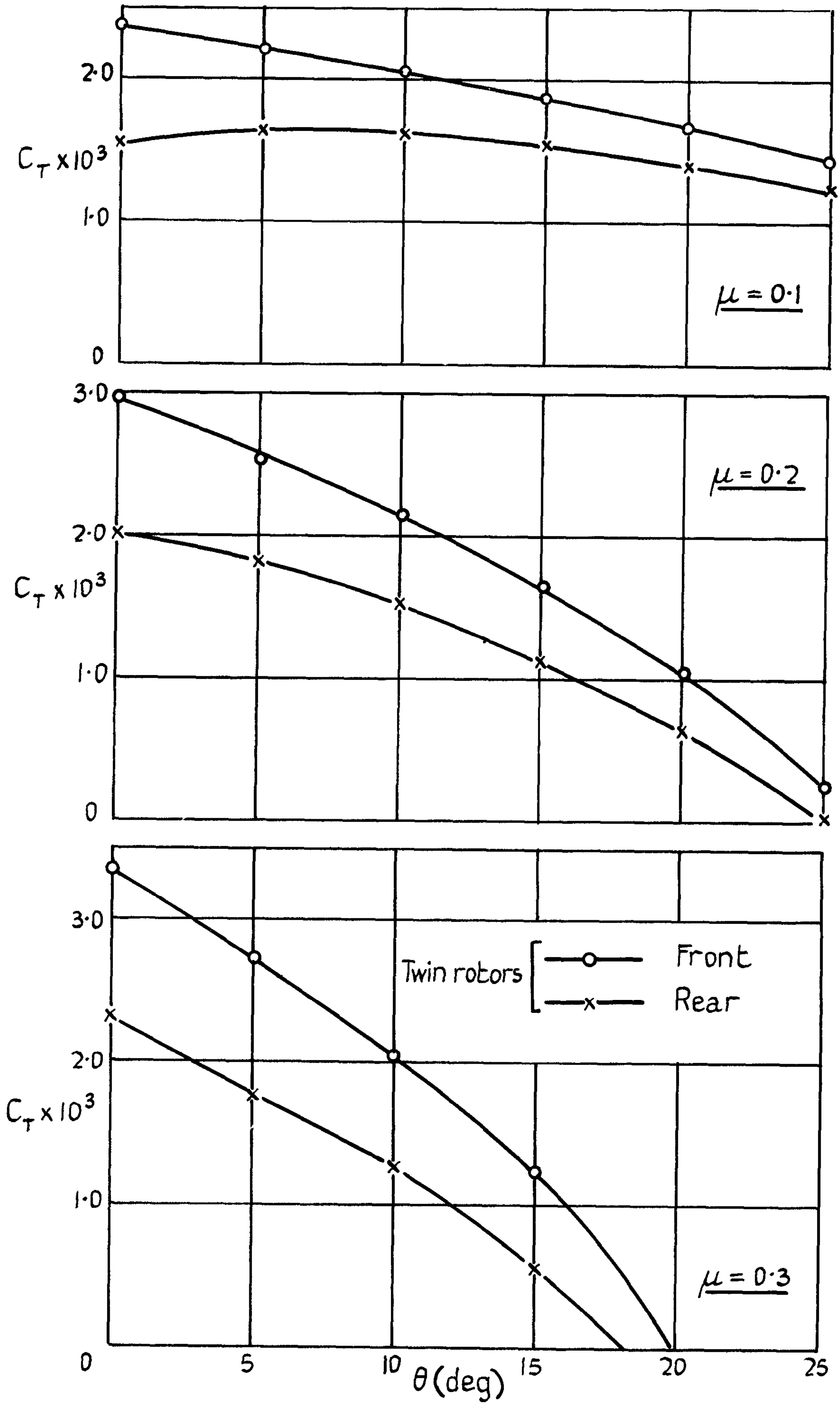

Division of thrust between rotors

$L_2 \, H_1 \, A_0$ $\qquad$ $\theta_0 = 8°$

FIG. 12b

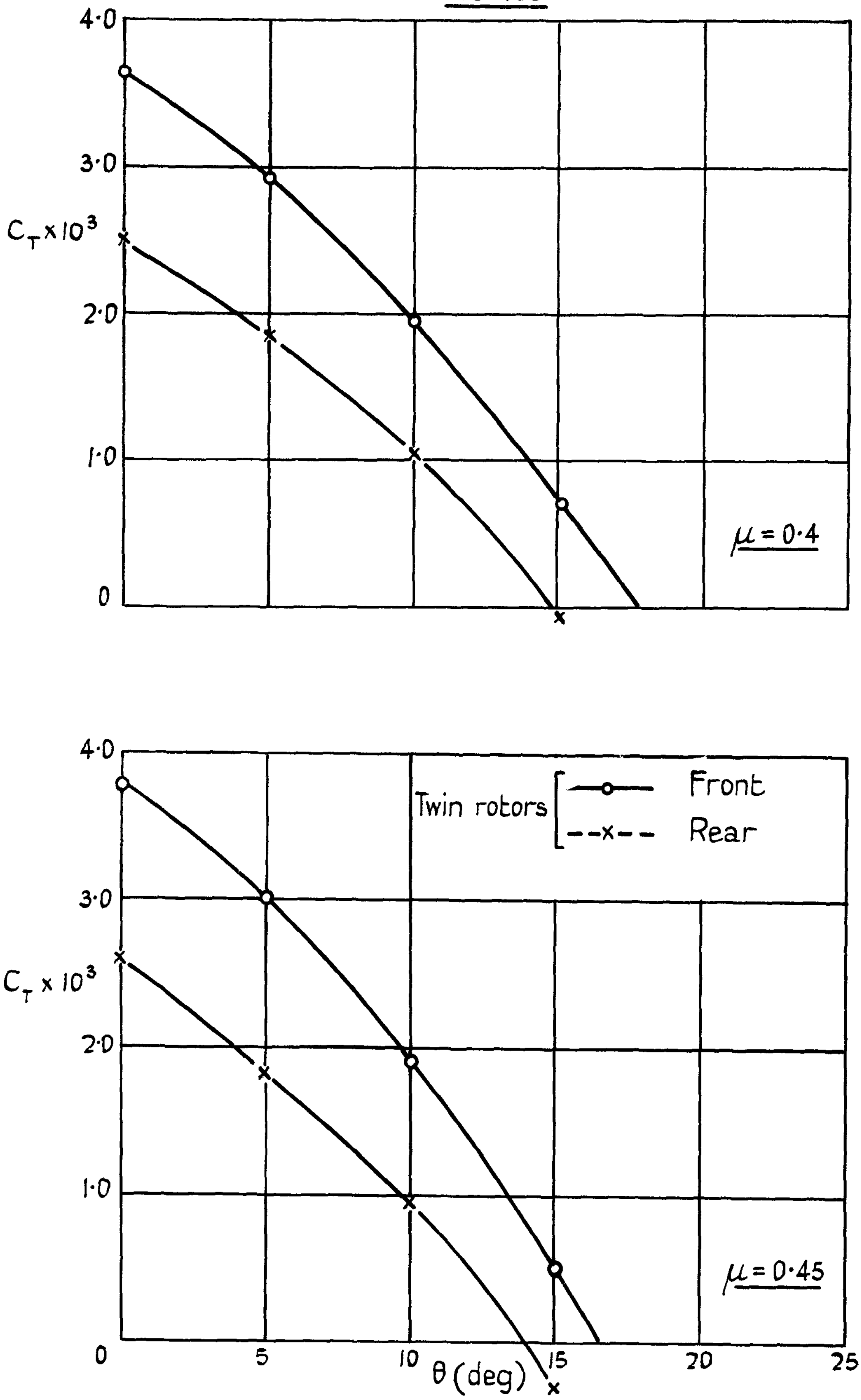

Division of thrust between rotors

$L_2 H_1 A_0$ $\theta_0 = 8°$

FIG. 13a

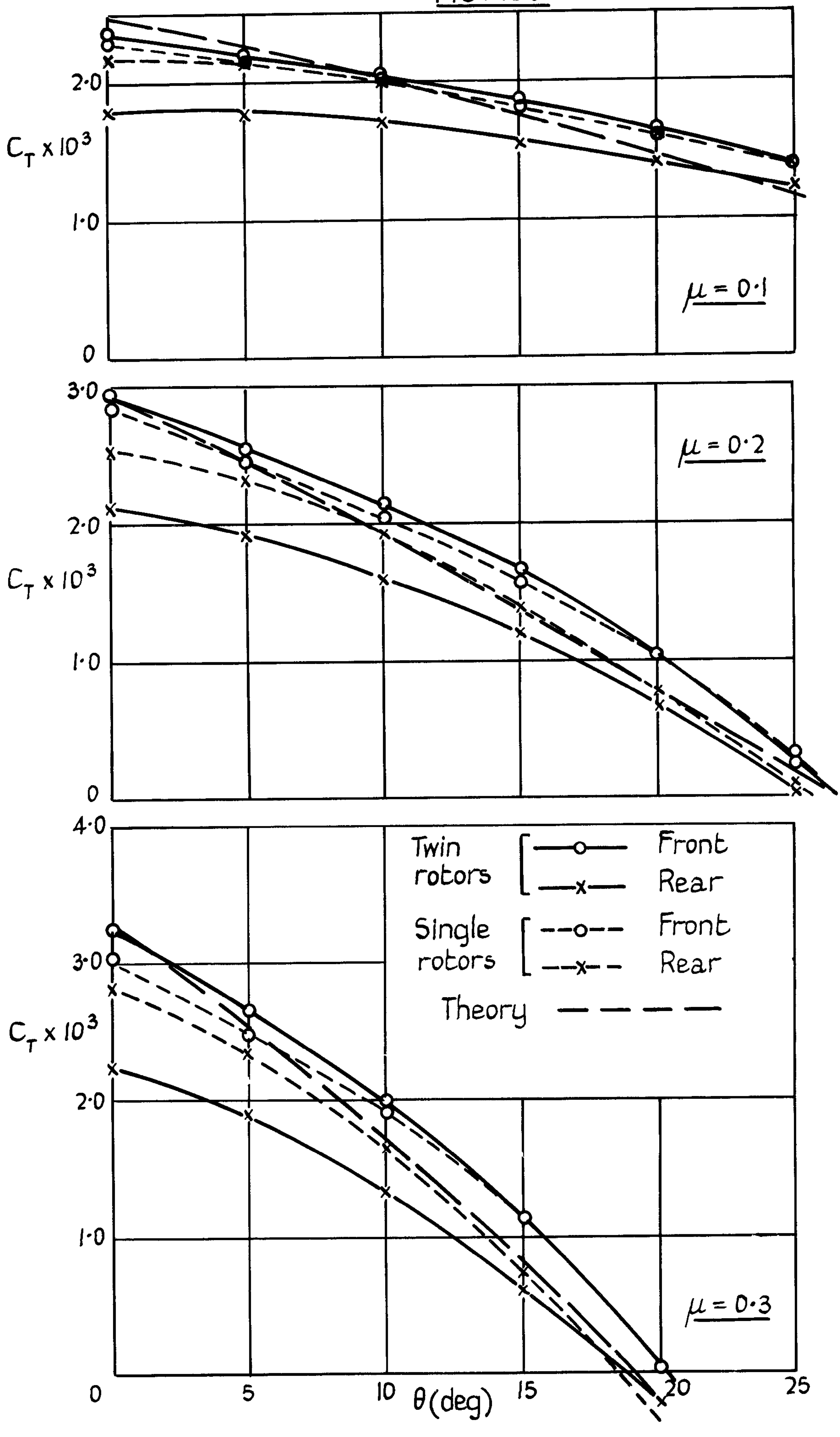

Division of thrust between rotors

$L_2 H_2 A_0$ $\theta_0 = 8°$

FIG. 13b

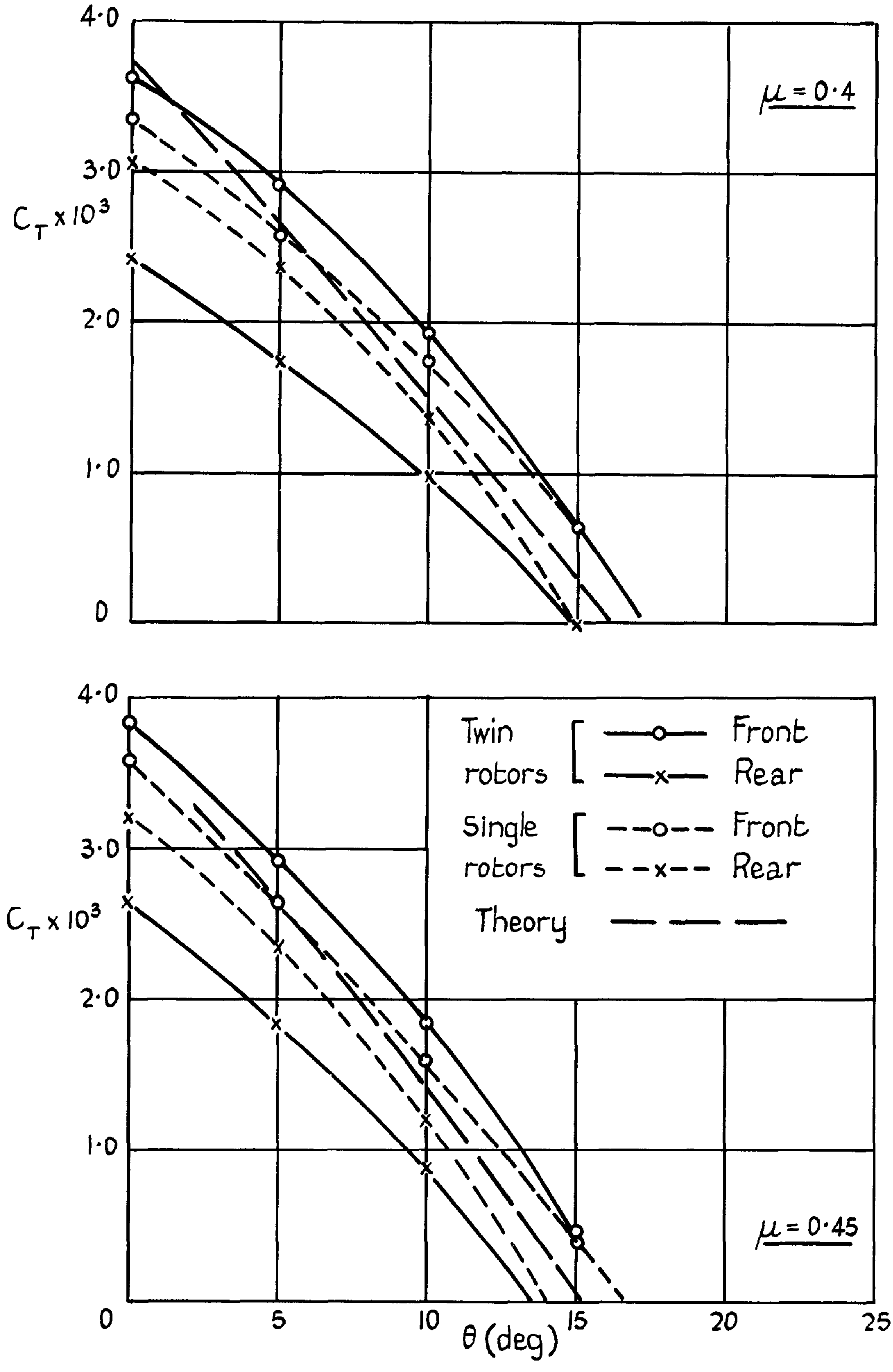

Division of thrust between rotors

$L_2 H_2 A_0$ $\theta_0 = 8°$

FIG. 14a.

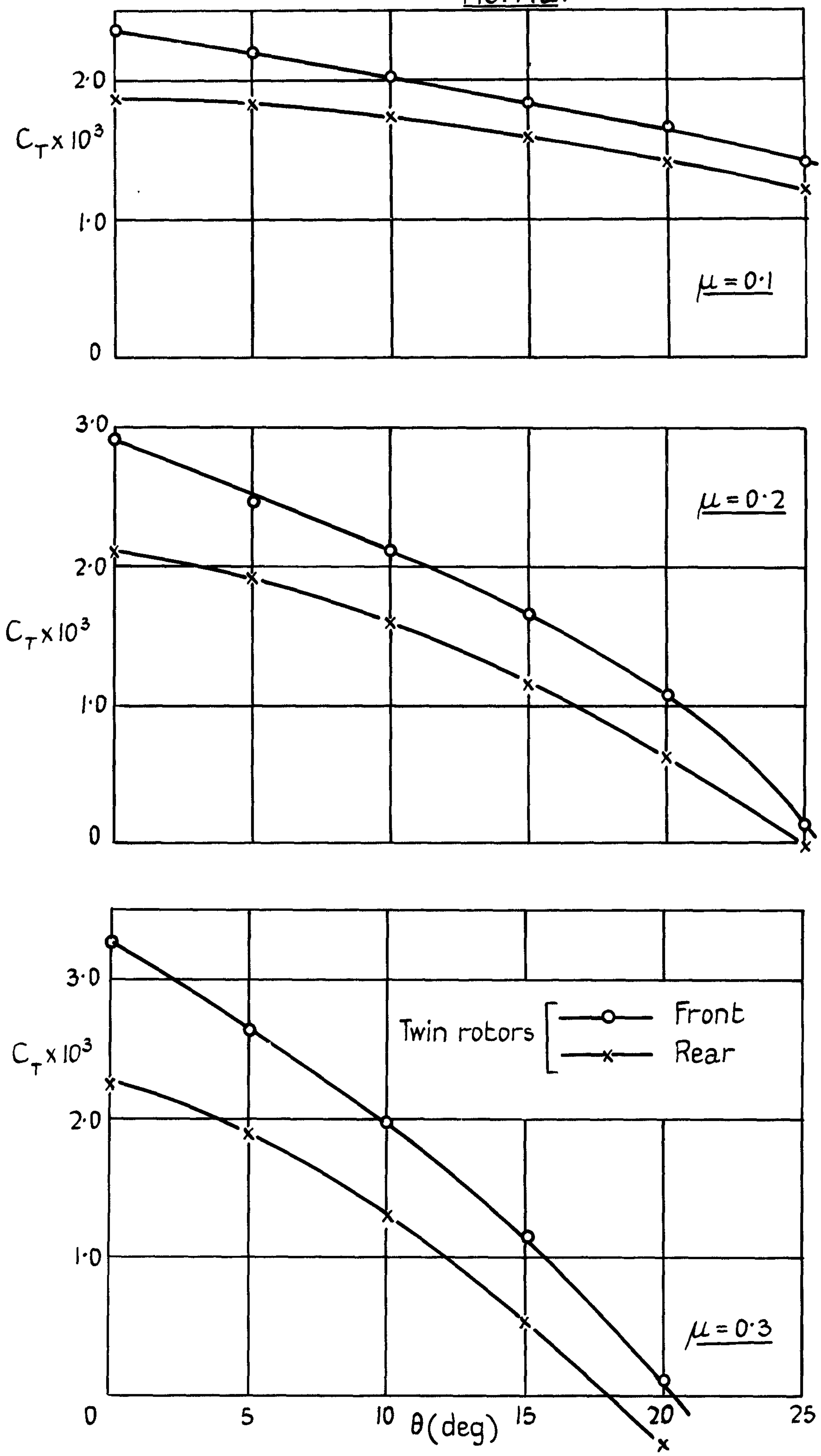

Division of thrust between rotors

$L_3 H_2 A_0$ $\theta_0 = 8^\circ$

FIG. 14b.

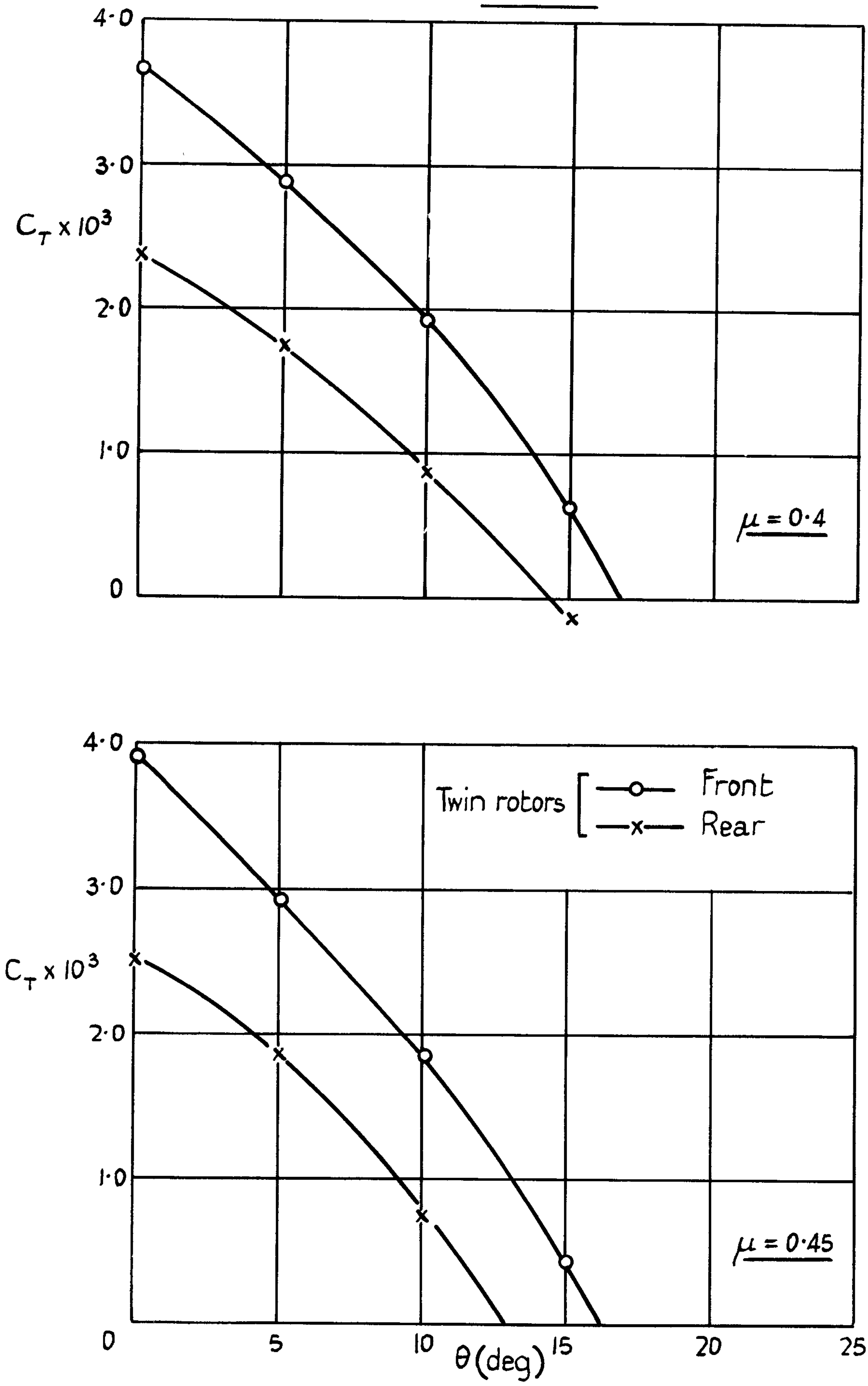

Division of thrust between rotors

$L_3 H_2 A_0$ $\theta_0 = 8°$

FIG. 15 a.

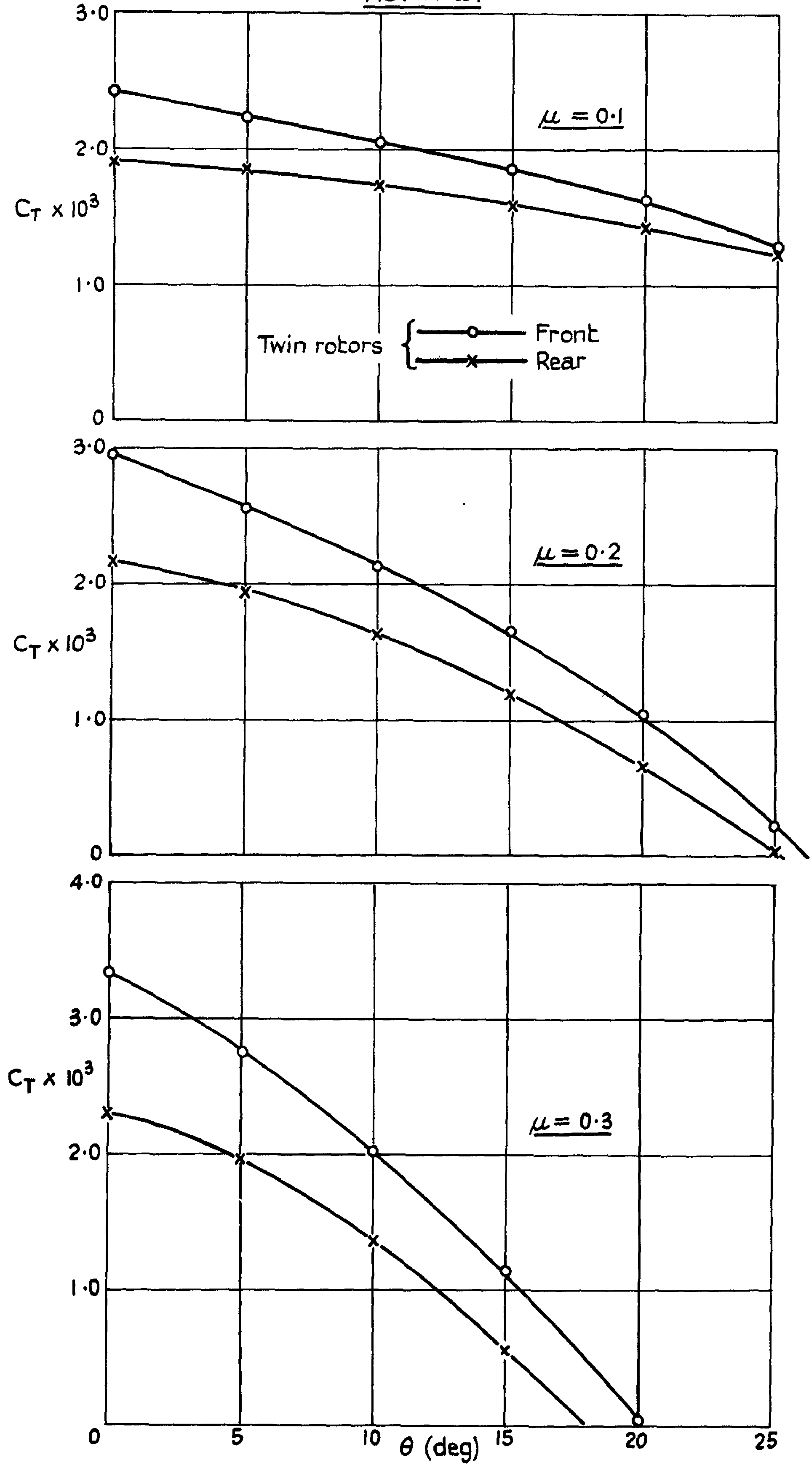

Division of thrust between rotors

$L_2\ H_3\ A_0 \qquad \theta_0 = 8°$

FIG. 15 b.

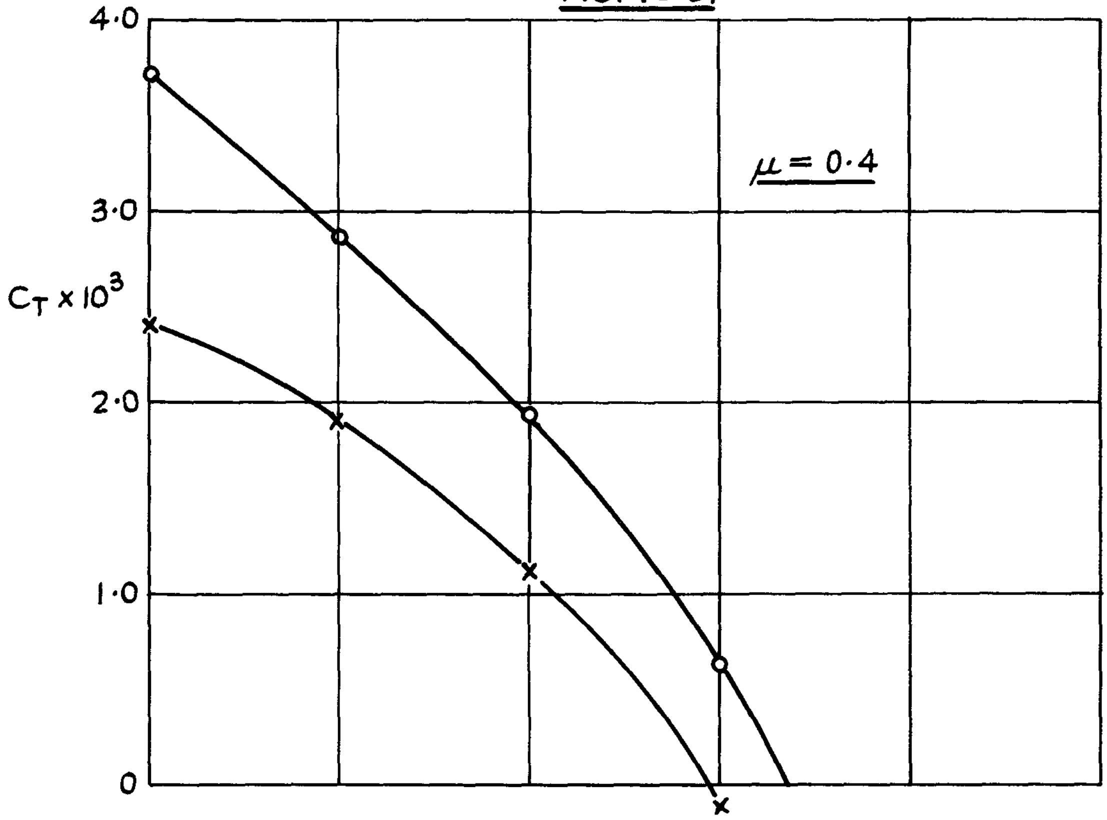

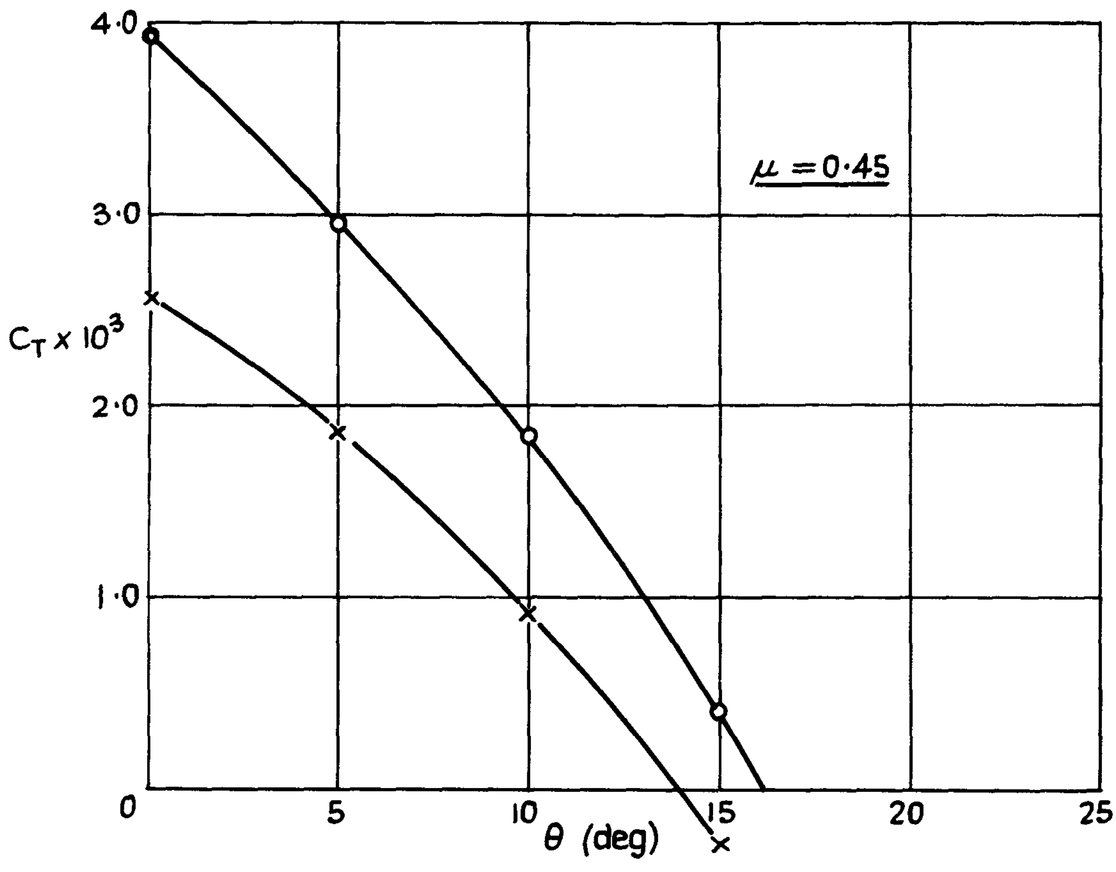

Division of thrust between rotors.

$L_2\ H_3\ A_0 \quad \theta_0 = 8^\circ$

FIG. 16 a.

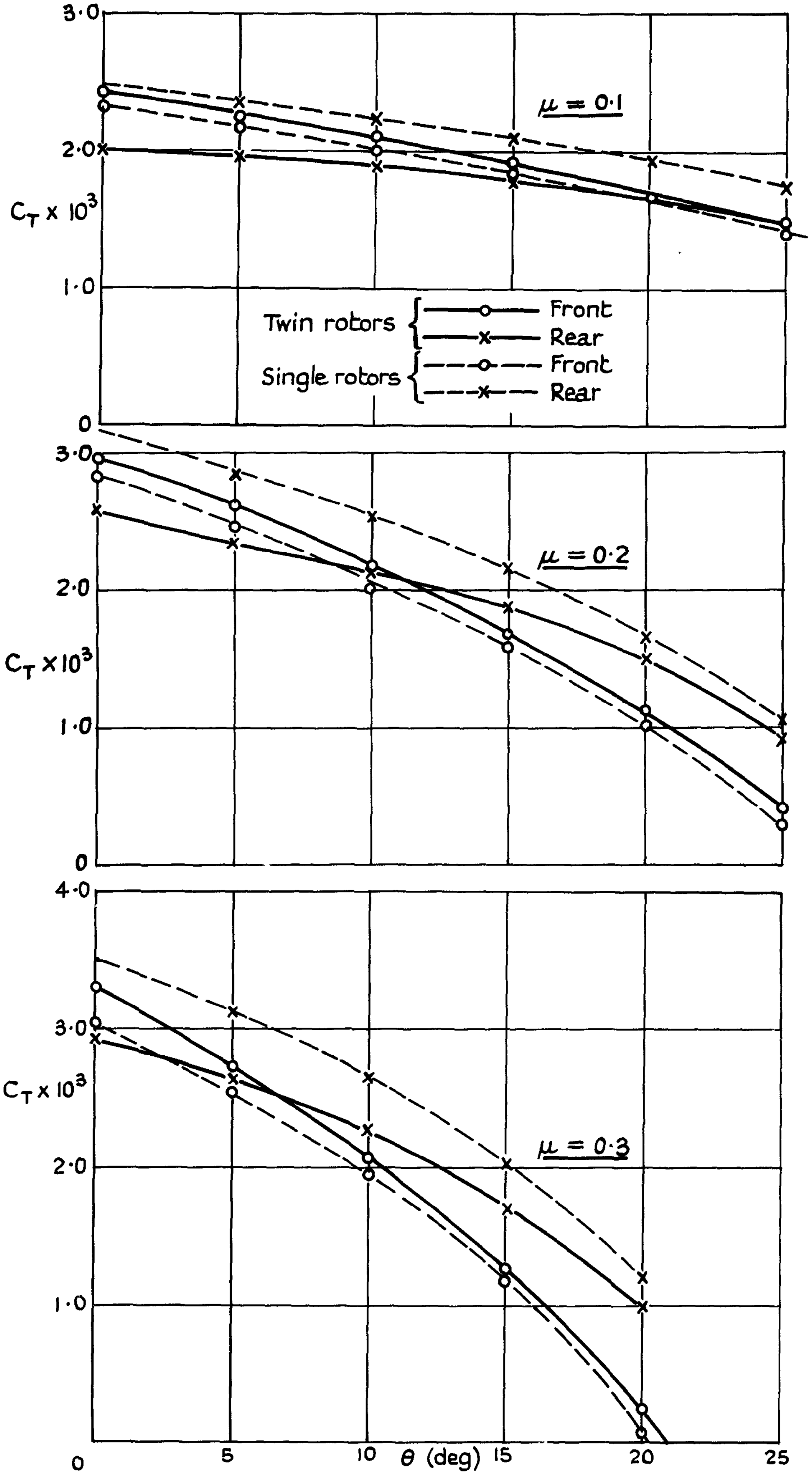

Division of thrust between rotors

L_2 H_2 $A_{-7{\cdot}7^\circ}$ $\theta_0 = 8^\circ$

FIG. 16b.

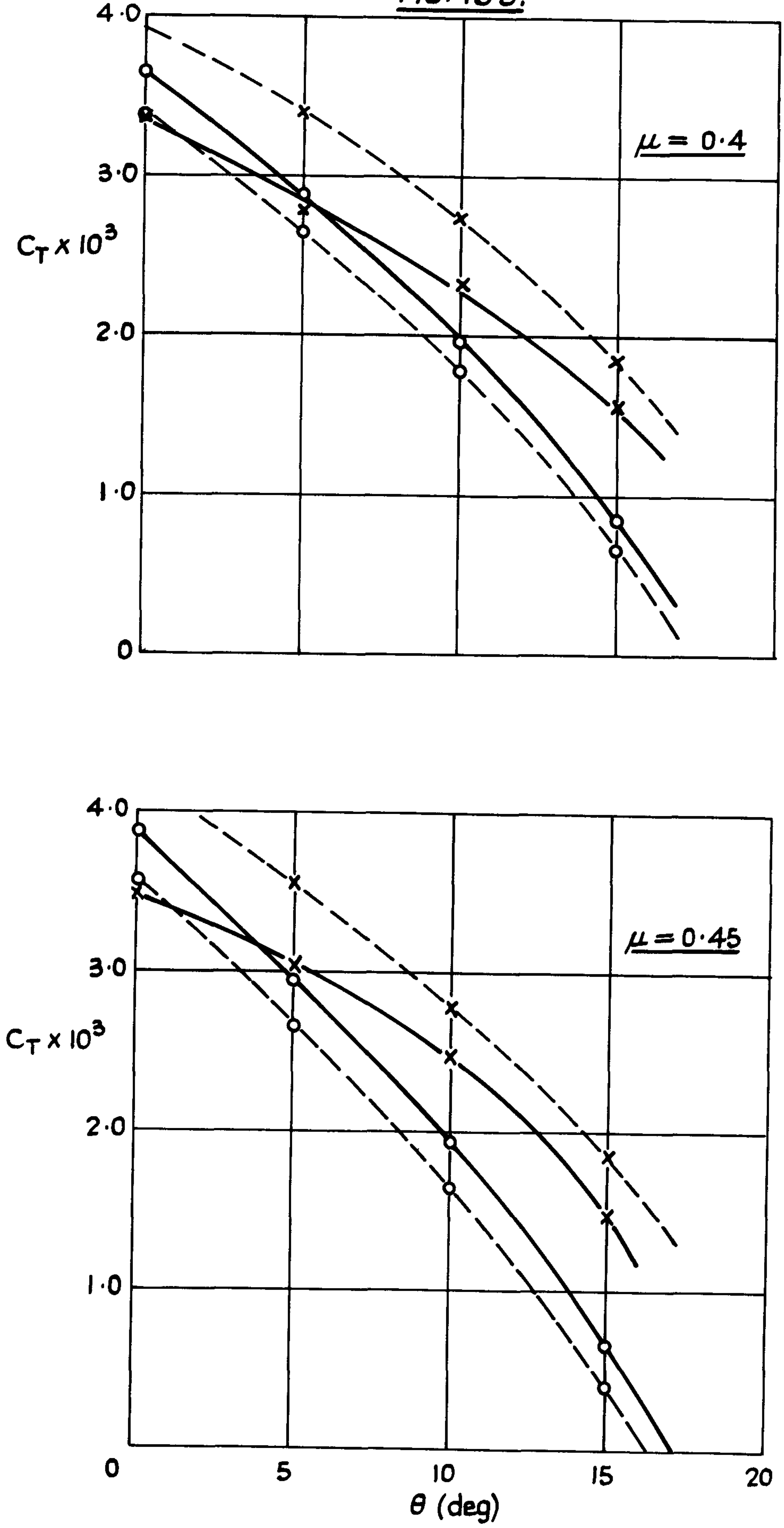

Division of thrust between rotors

$L_2 \ H_2 \ A_{-7\cdot7°} \quad \theta_0 = 8°$

FIG. 17a

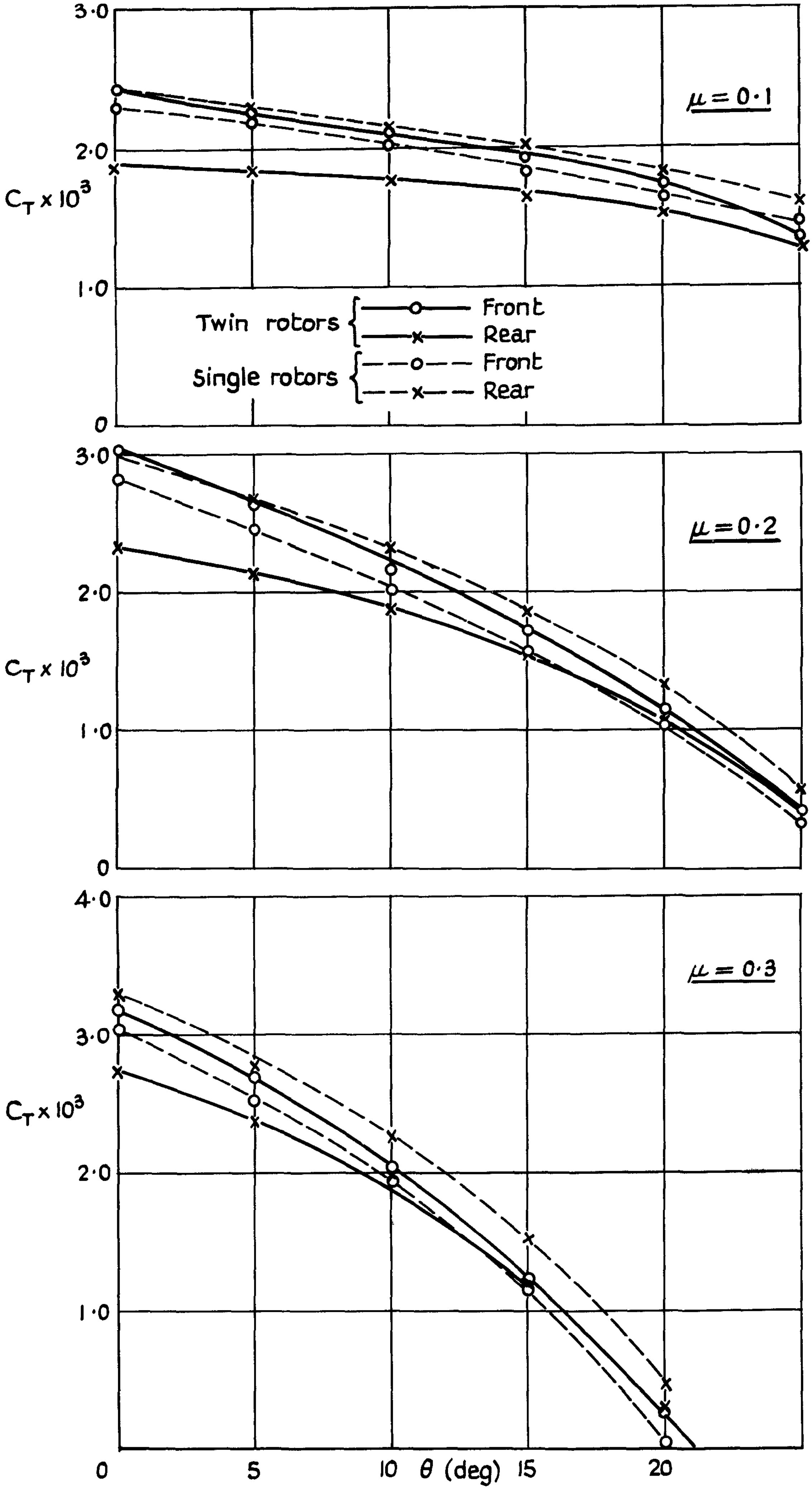

Division of thrust between rotors

$L_2\ H_2\ A_{-4.4°}$ $\theta_0 = 8°$

FIG. 17b.

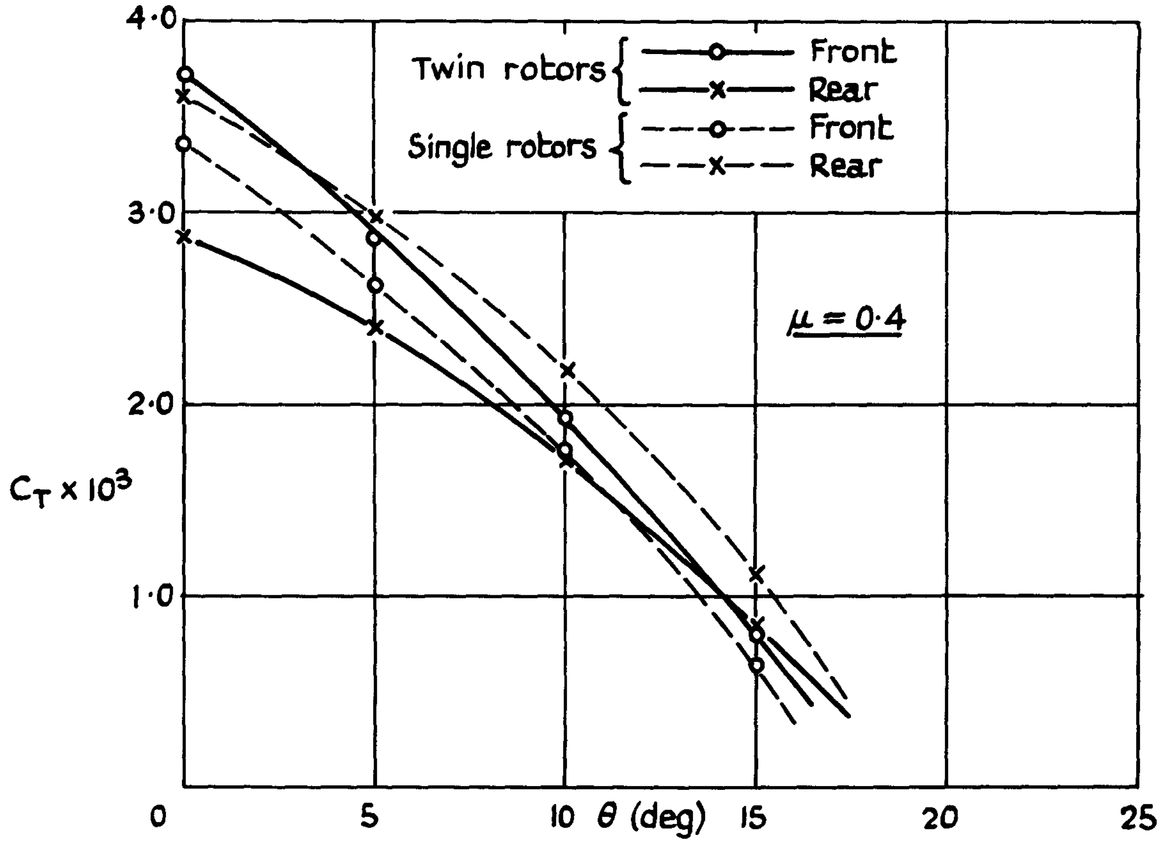

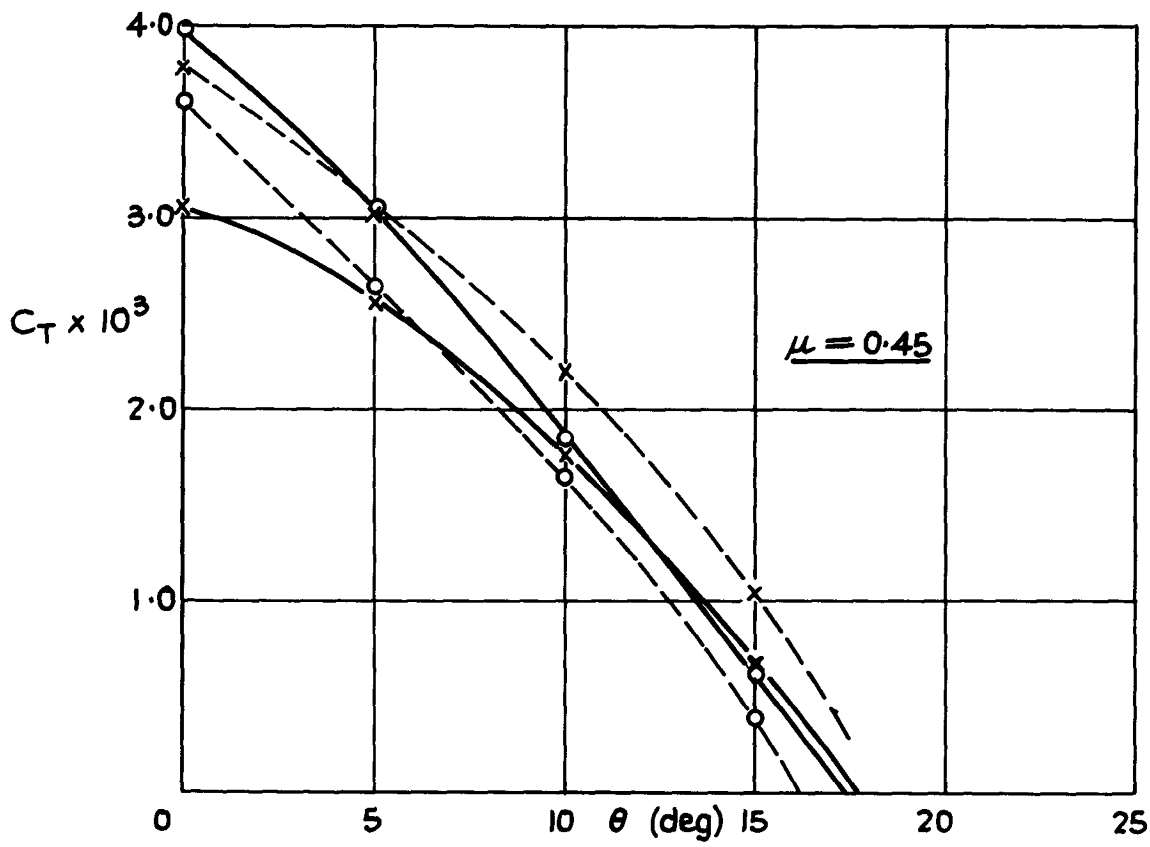

Division of thrust between rotors.
$L_2\ H_2\ A_{-4\cdot4^\circ} \quad \theta_0 = 8^\circ$

FIG. 18a

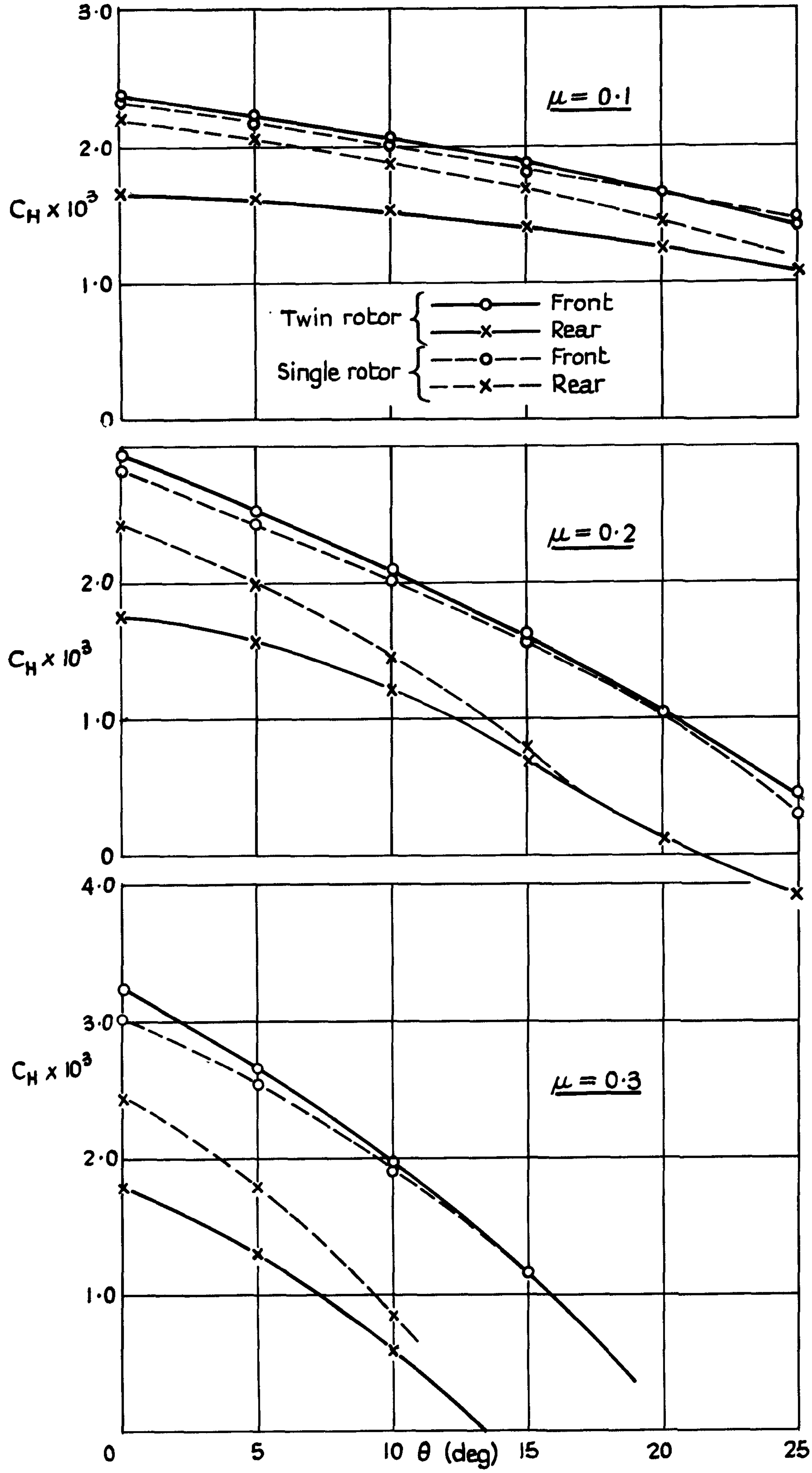

Division of thrust between rotors

$L_2\ H_2\ A_{4°}$ $\theta_0 = 8°$

FIG. 18 b

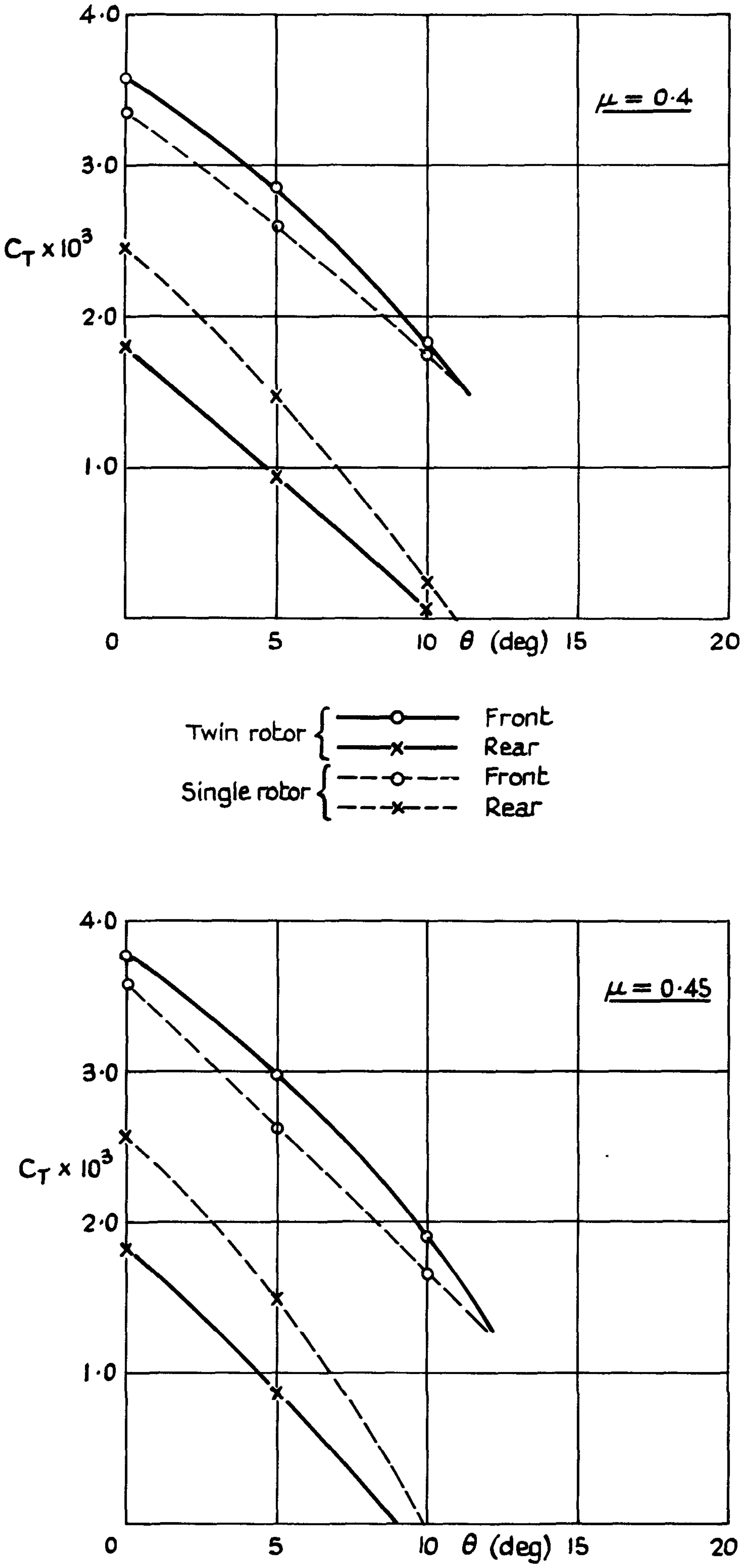

Division of thrust between rotors.

$L_2 \; H_2 \; A_{4^\circ} \qquad \theta_0 = 8^\circ$

FIG. 19a

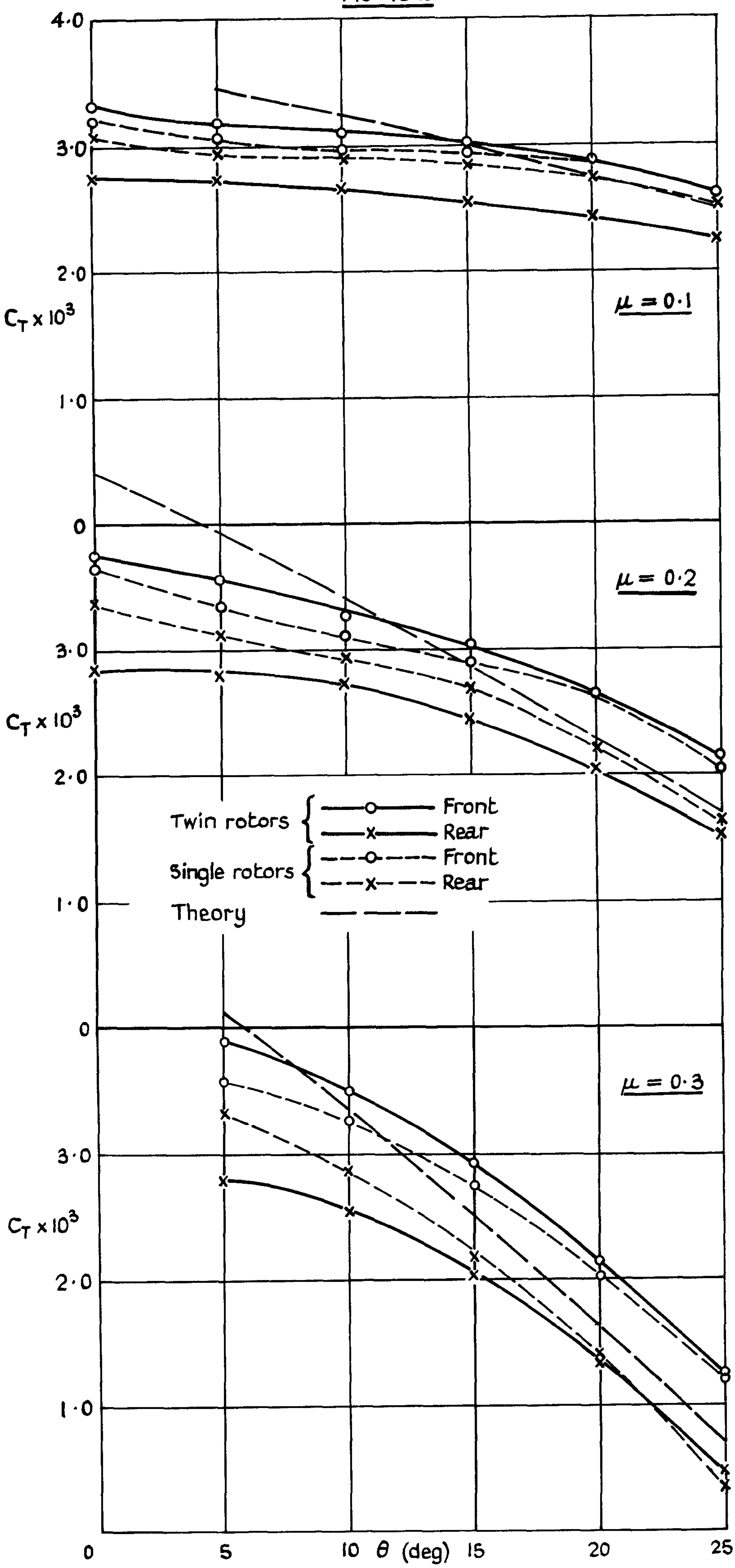

Division of thrust between rotors. $L_2 H_2 A_0$ $\theta_0 = 12°$.

FIG. 19 b

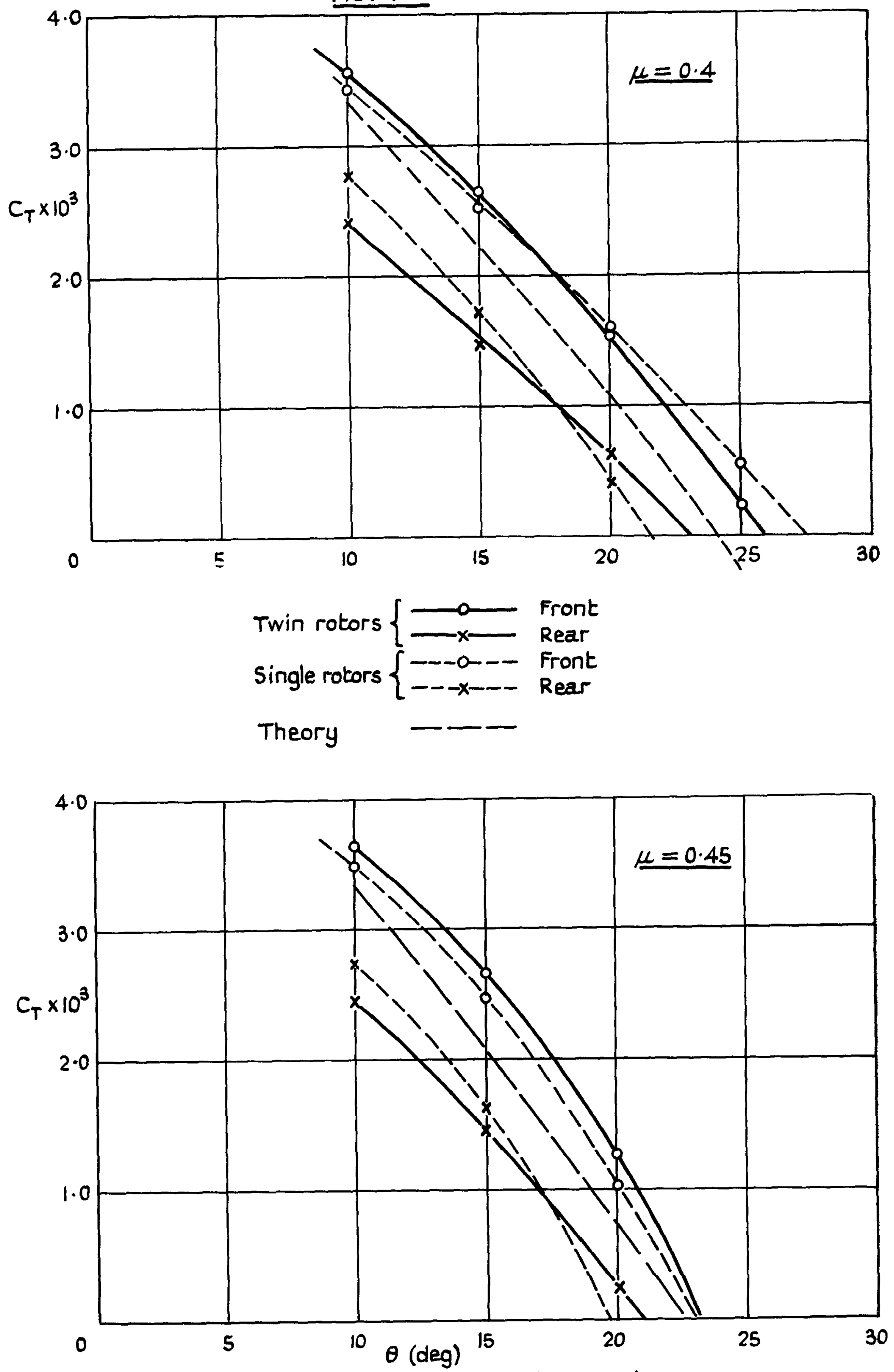

Division of thrust between rotors

$L_2\ H_2\ A_0 \qquad \theta_0 = 12°$

FIG. 20a.

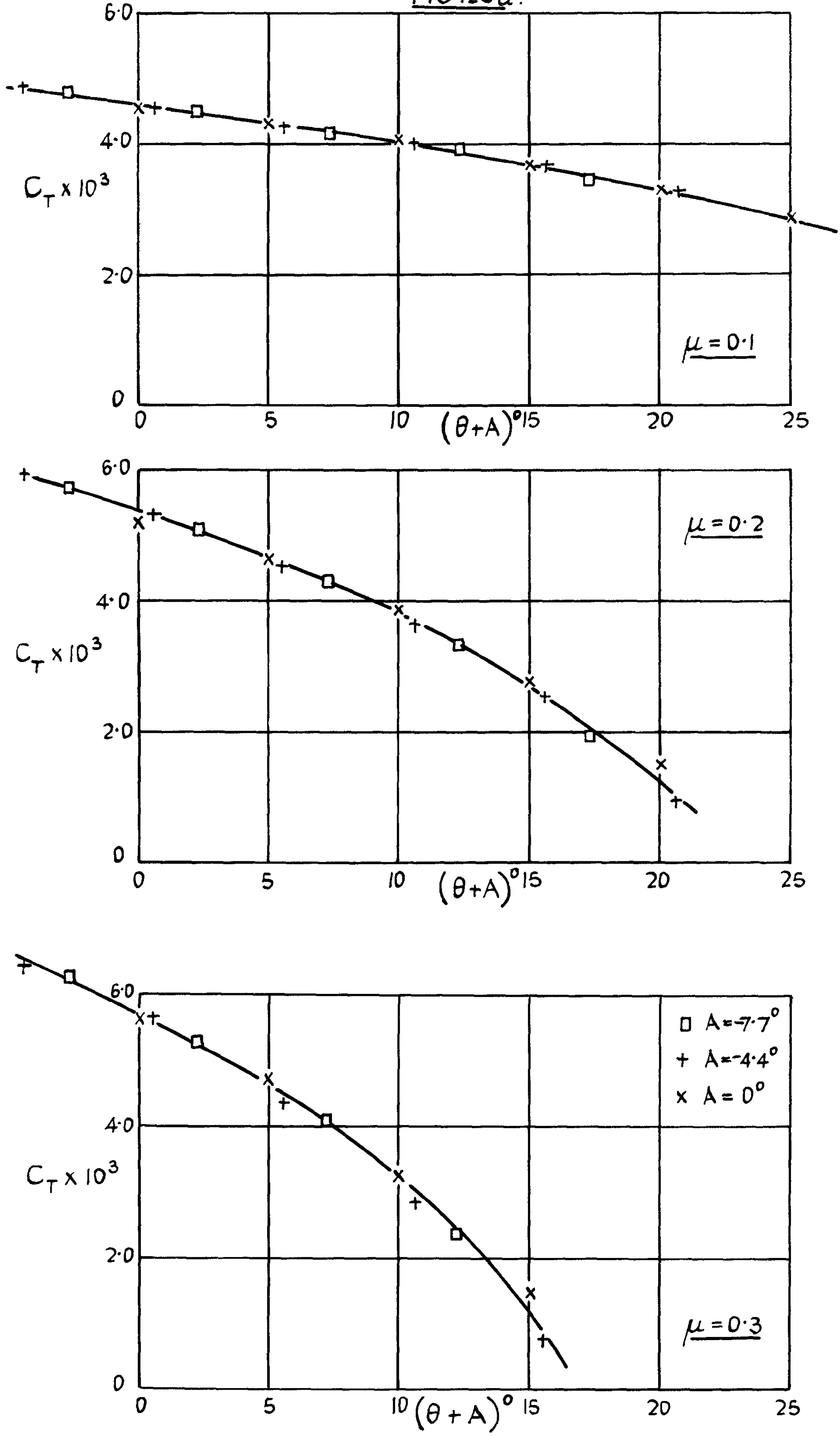

Rear rotor only.

L_2H_2A $\theta_0 = 8^\circ$

FIG. 22

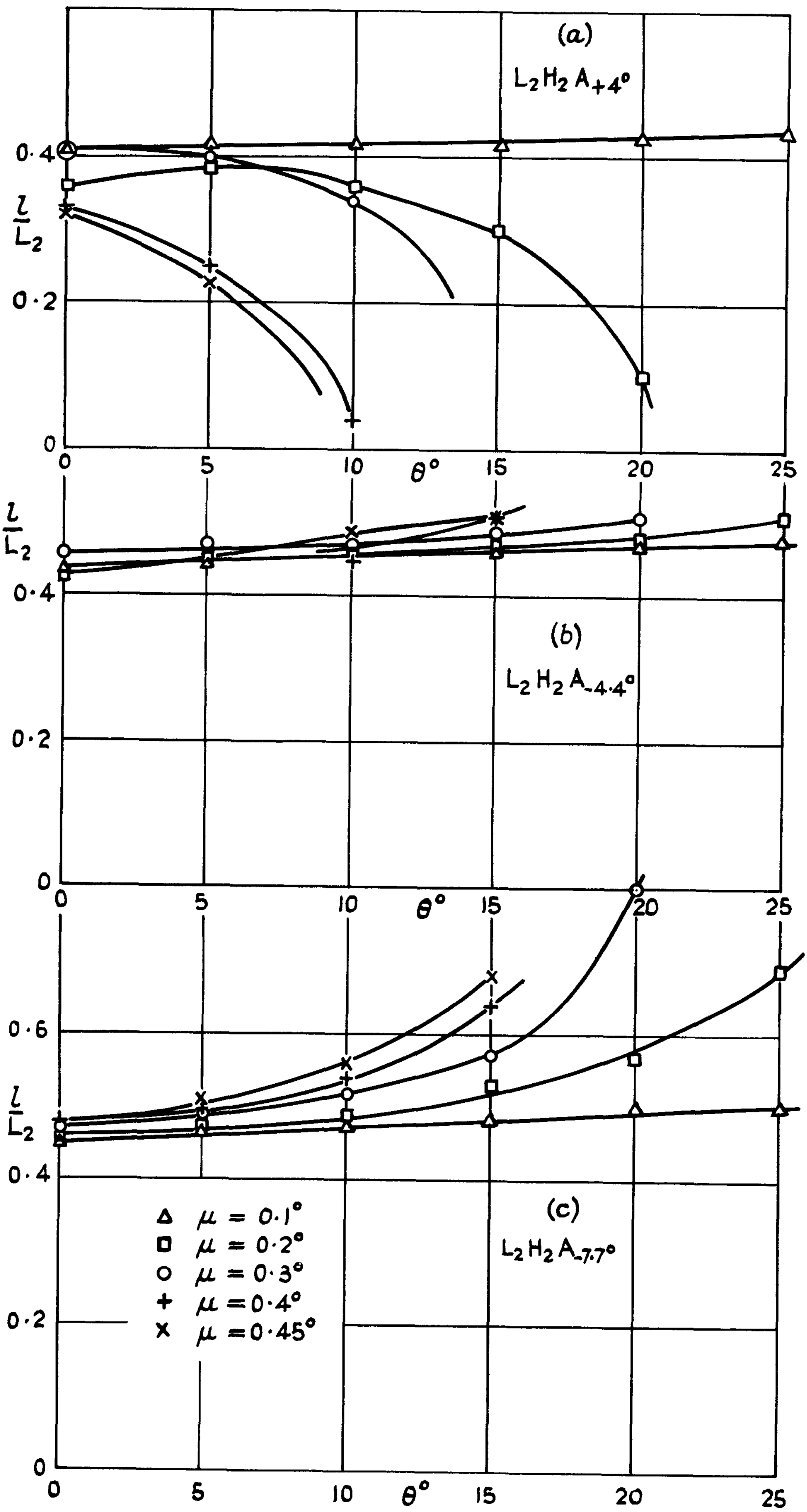

Centres of rotor thrust for $\theta_0 = 8°$

FIG. 23.

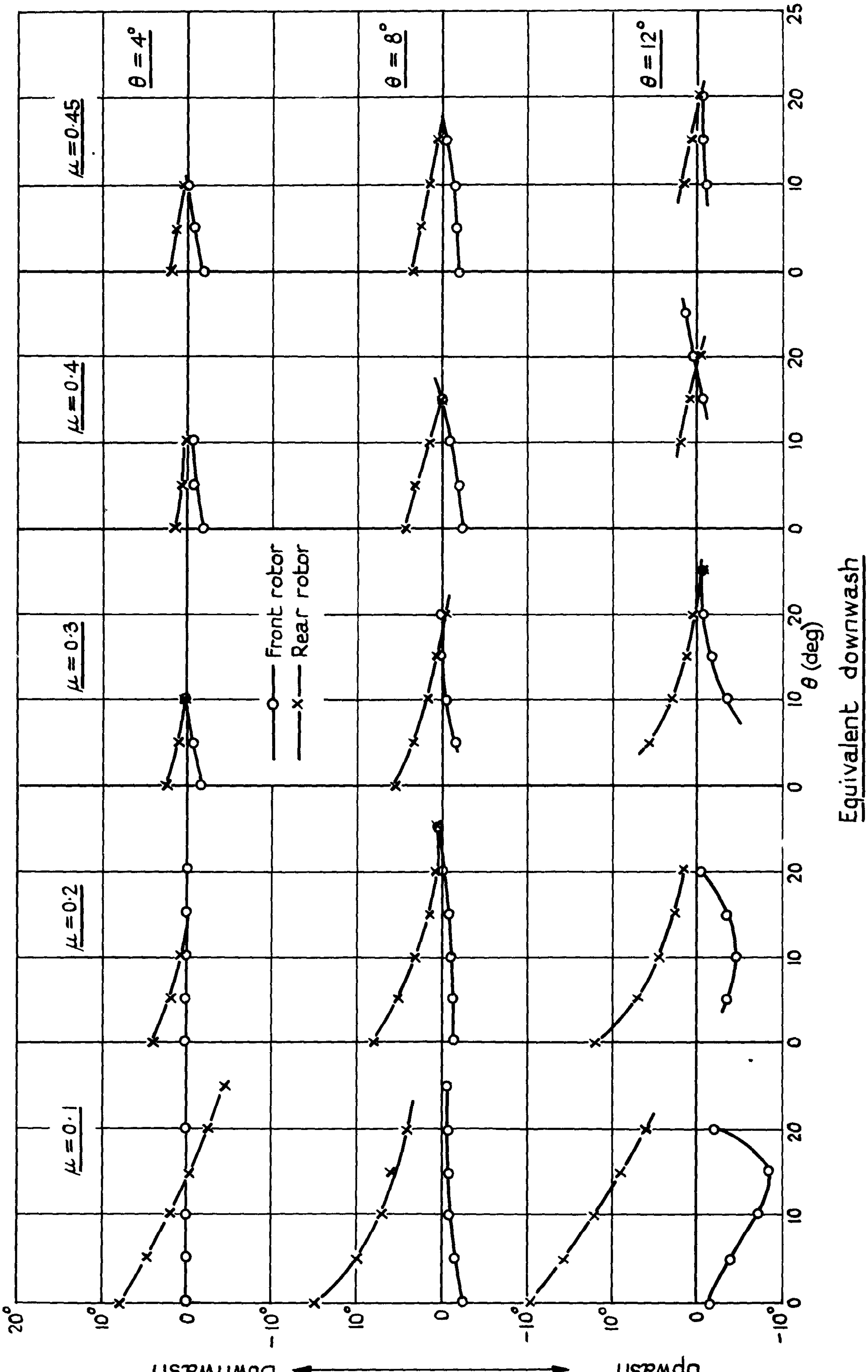

μ = 0·1
μ = 0·2
μ = 0·3
μ = 0·4
μ = 0·45
θ = 4°
θ = 8°
θ = 12°
Front rotor
Rear rotor
θ (deg)
Equivalent downwash
Downwash
Upwash

FIG. 24.

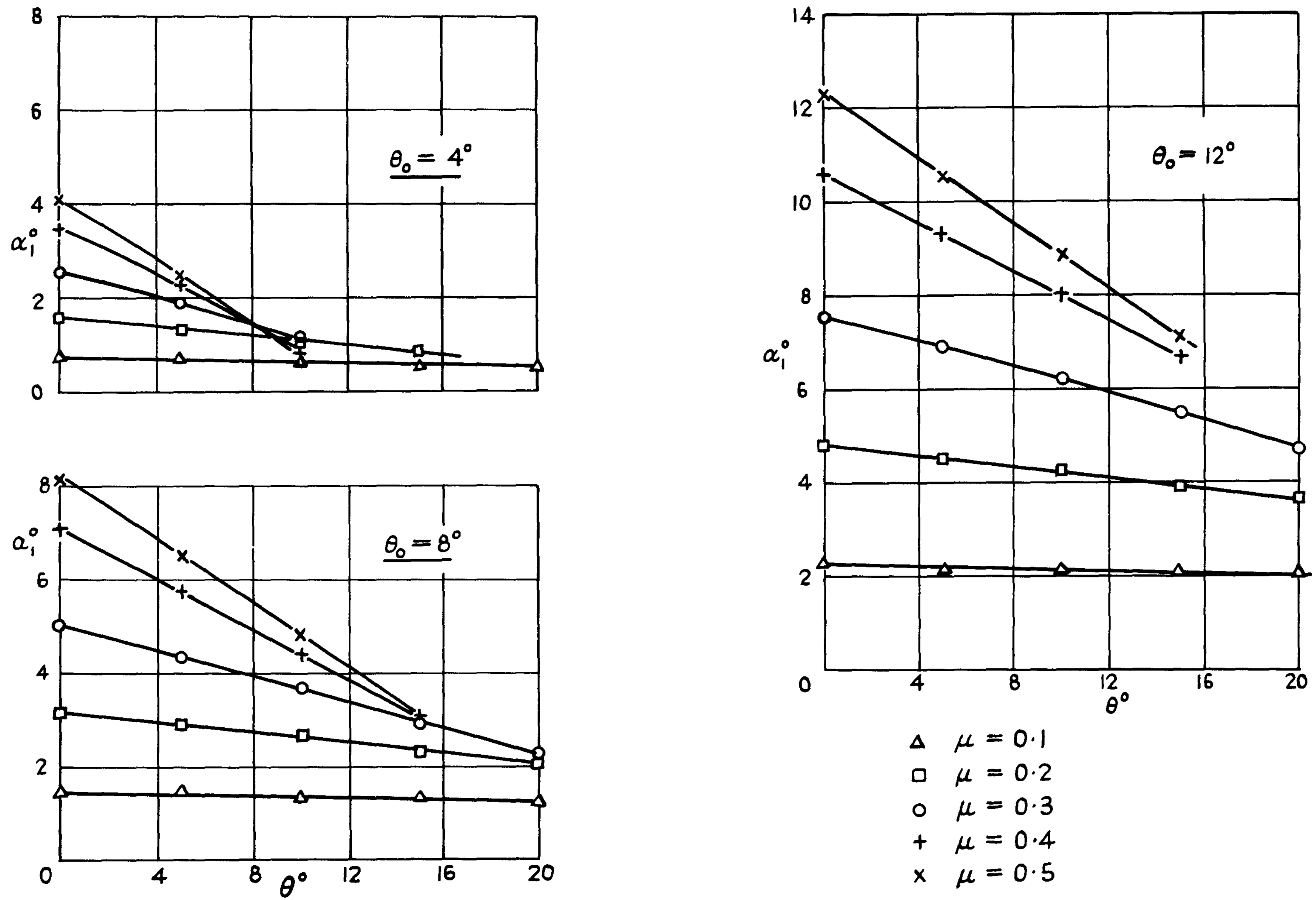

Theoretical flapping angles (With offset)

FIG. 25

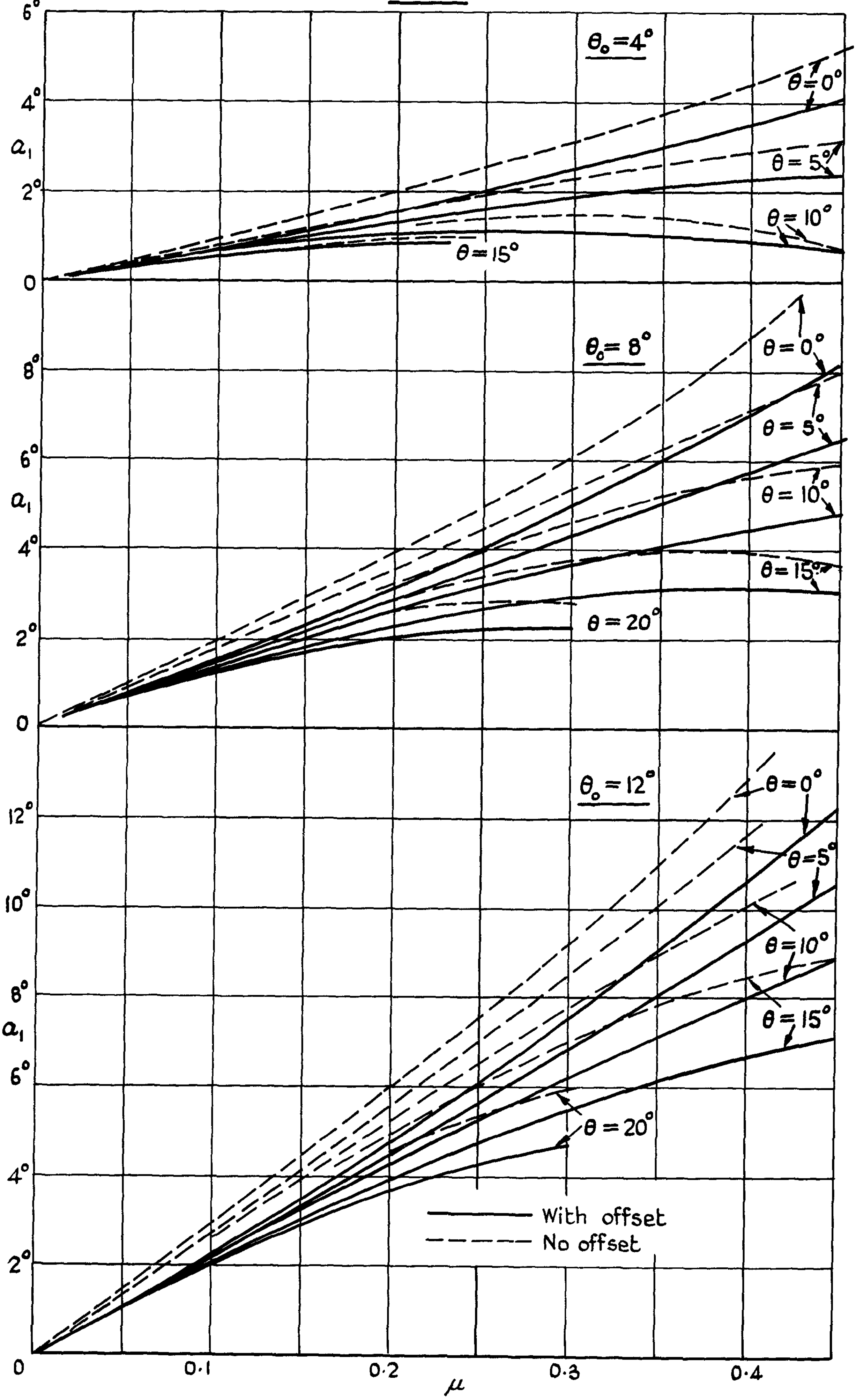

Theoretical flapping angles (with and without offset)

FIG. 26.

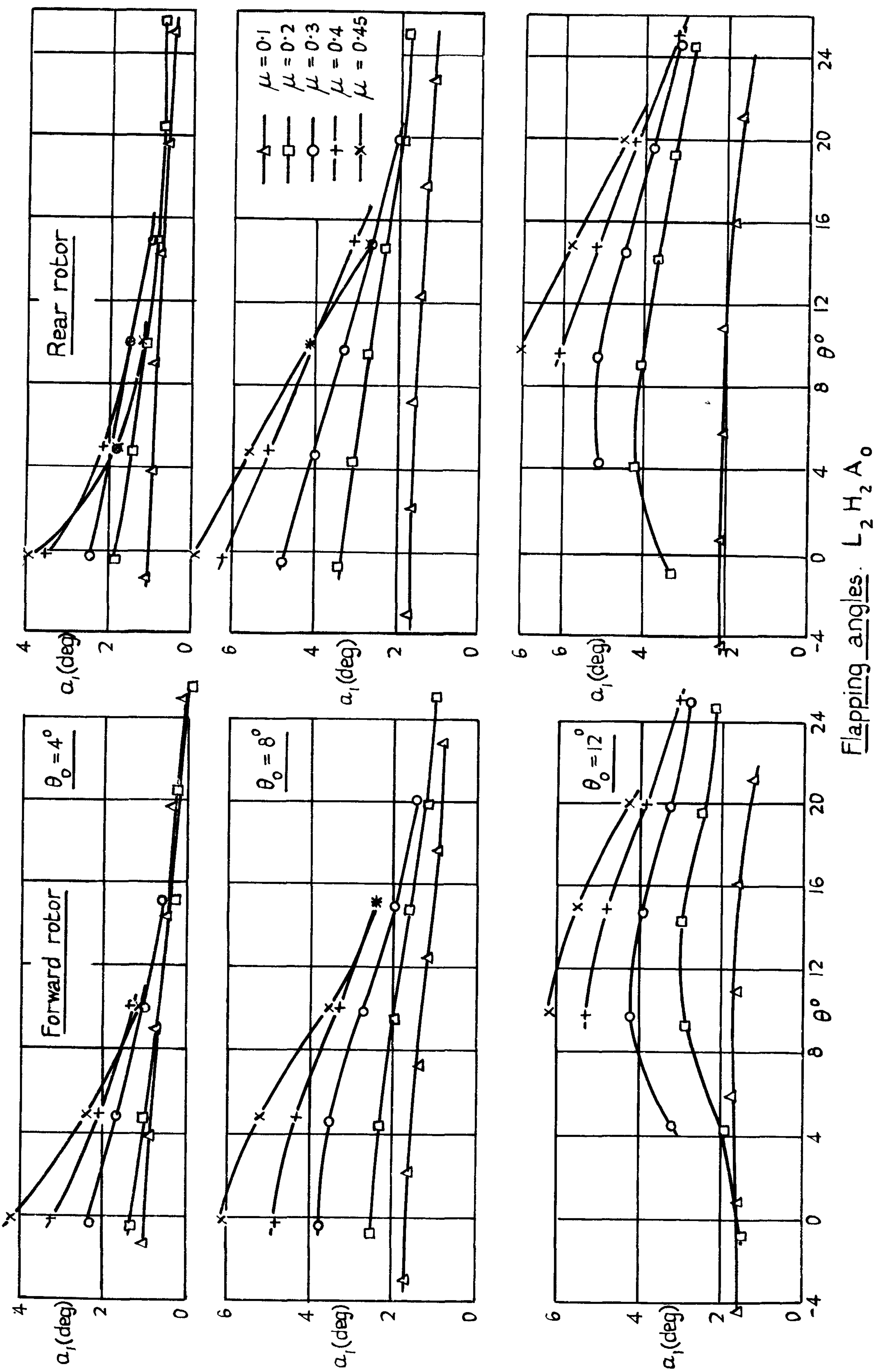

Flapping angles. $L_2 H_2 A_o$

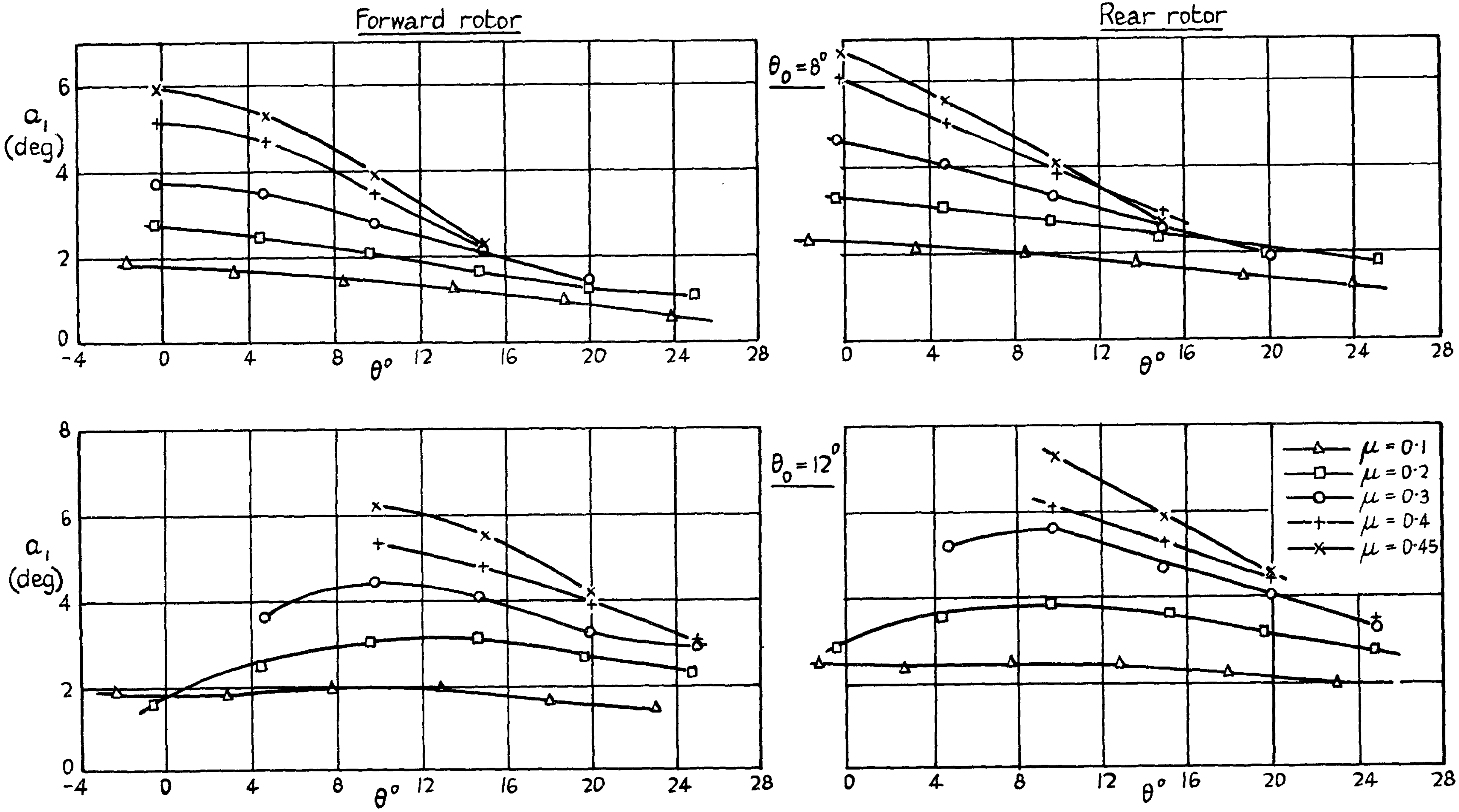

FIG. 27

Flapping angles. Single rotors.
$L_2 H_2 A_0$

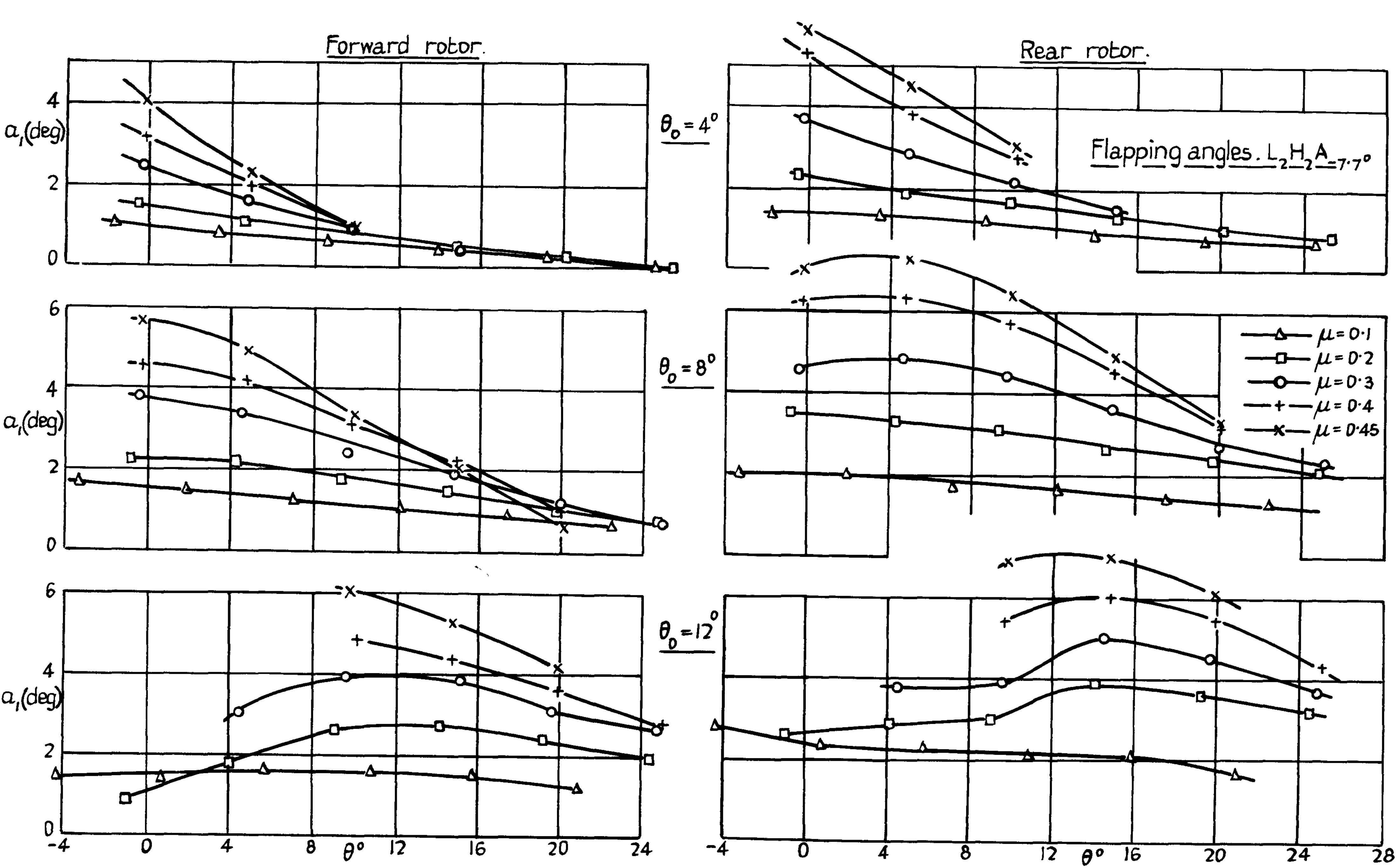

Forward rotor.
Rear rotor.
Flapping angles. L2H2A=7.7°
$\theta_0 = 4^\circ$
$\theta_0 = 8^\circ$
$\theta_0 = 12^\circ$
$\mu = 0.1$
$\mu = 0.2$
$\mu = 0.3$
$\mu = 0.4$
$\mu = 0.45$
a_1(deg)
θ°

FIG. 28

Flapping angles

$L_2 H_2 A_{-4\cdot4^o}$

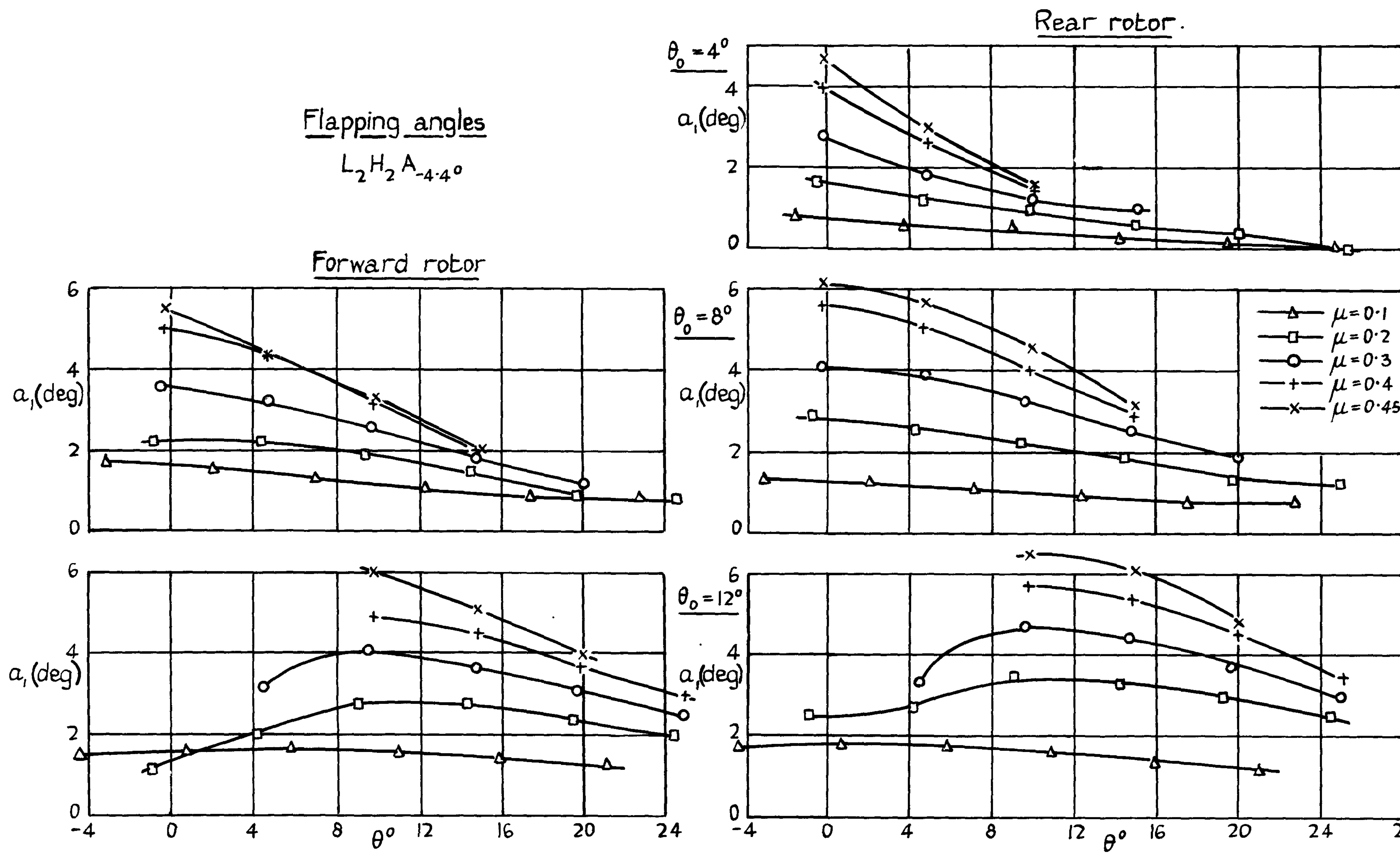

FIG. 29

Flapping angles.

$L_2 H_2 A_{+4°}$

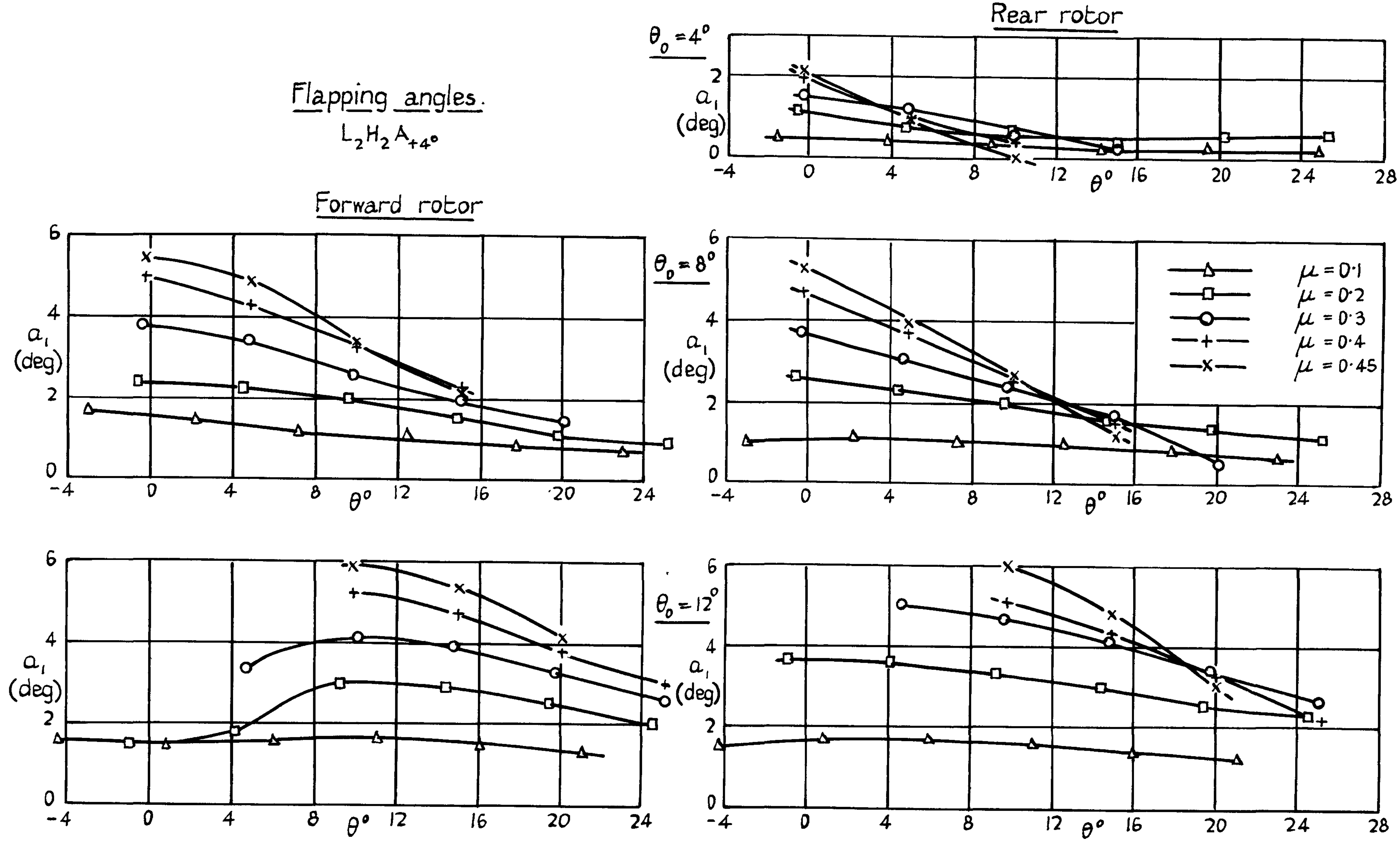

FIG. 30

FIG. 31

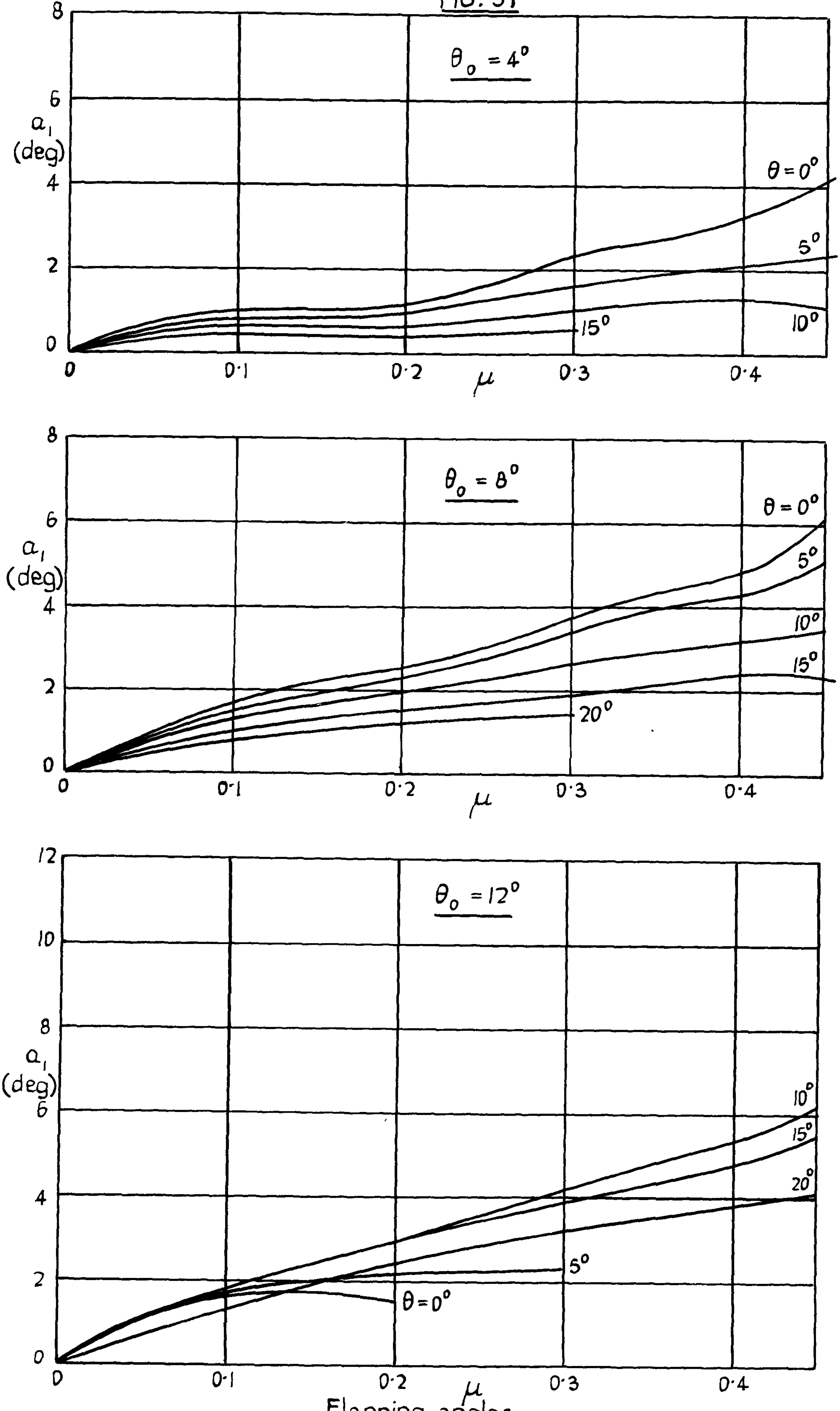

Flapping angles.

Twin rotors. Forward rotor. $L_2 H_2 A_0$

FIG. 32

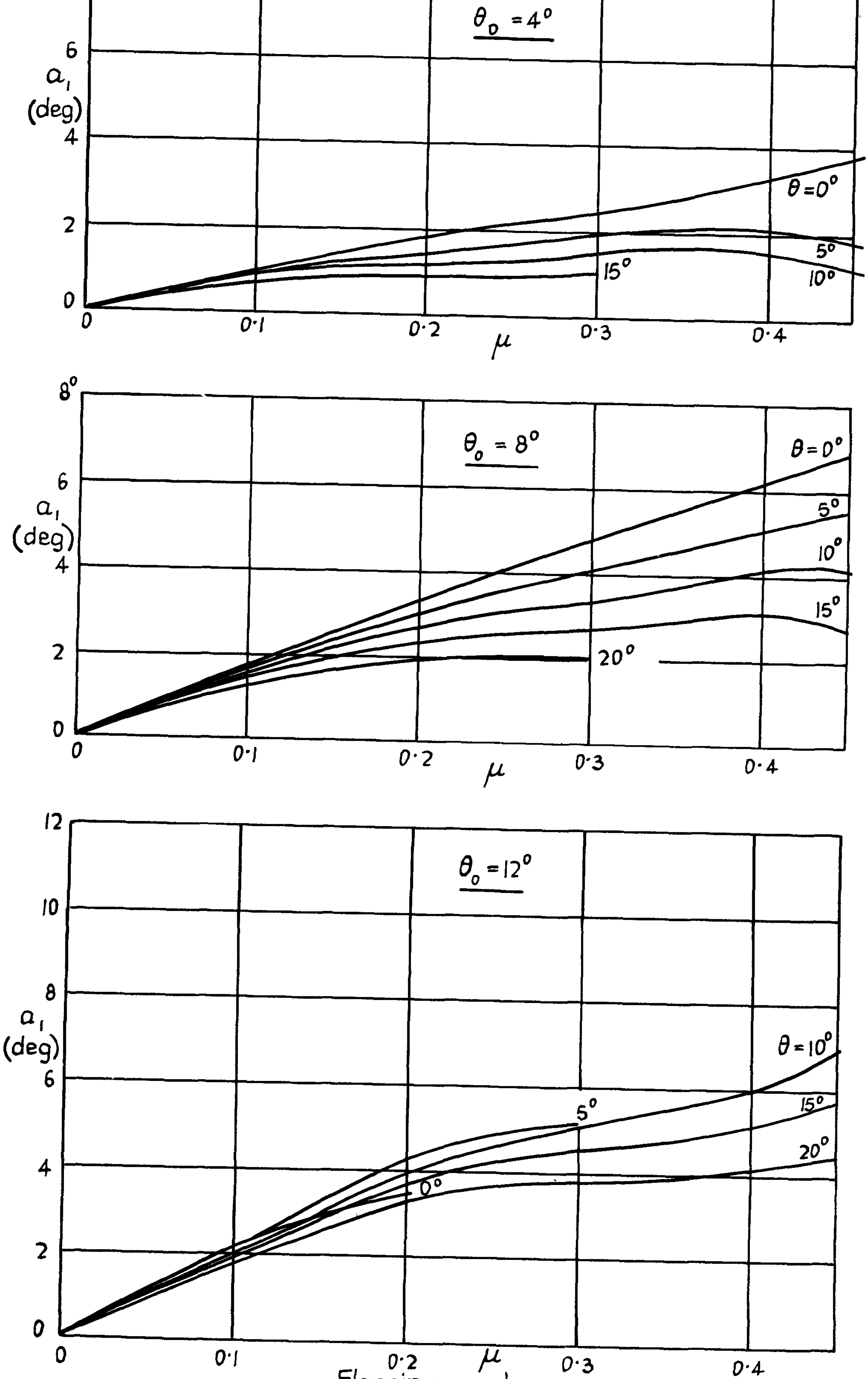

Flapping angles.
Twin rotors. Rear rotor. $L_2H_2A_0$.

FIG. 33

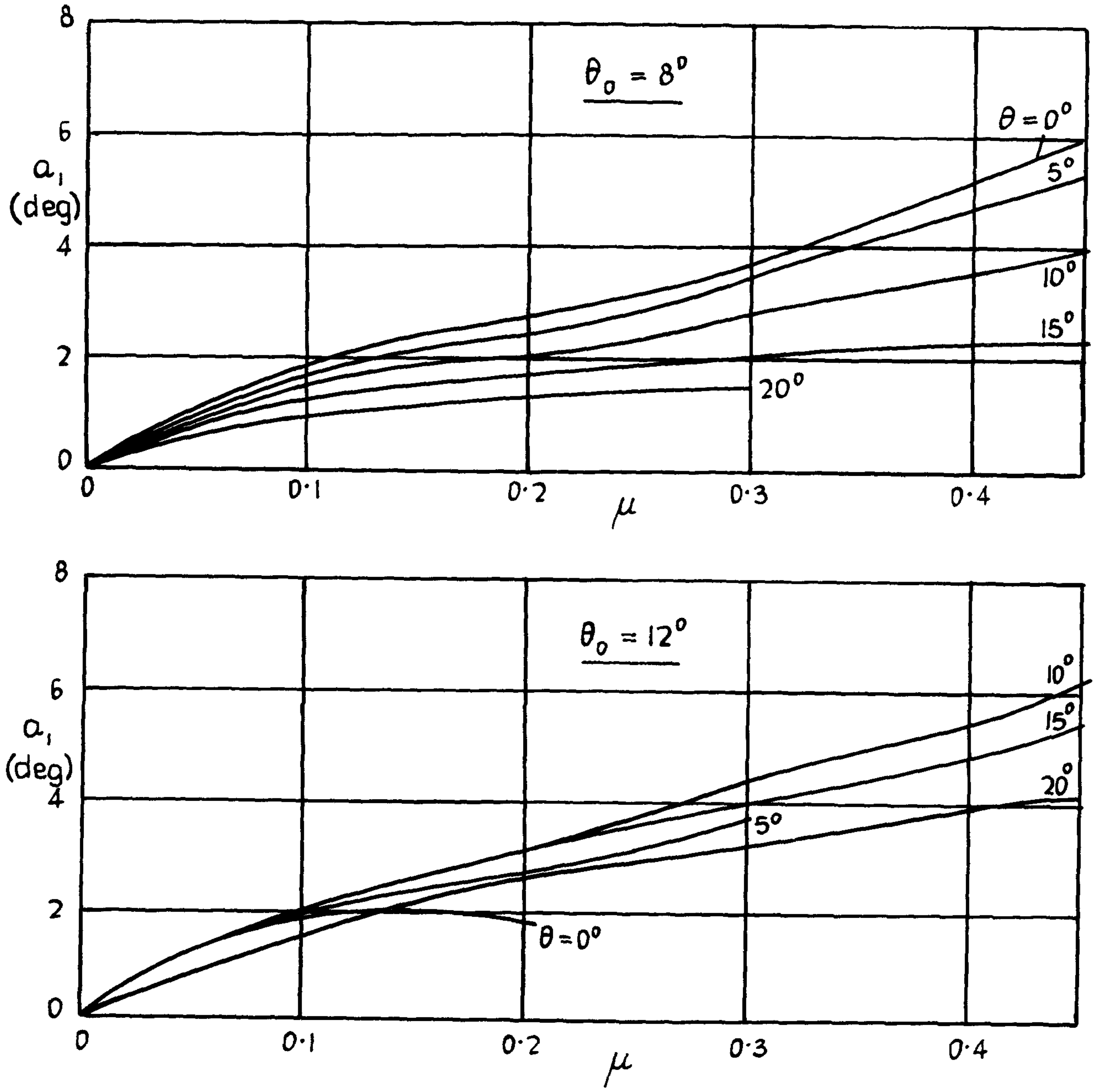

Flapping angles.
Forward rotor only. $L_2 H_2 A_0$

FIG. 34

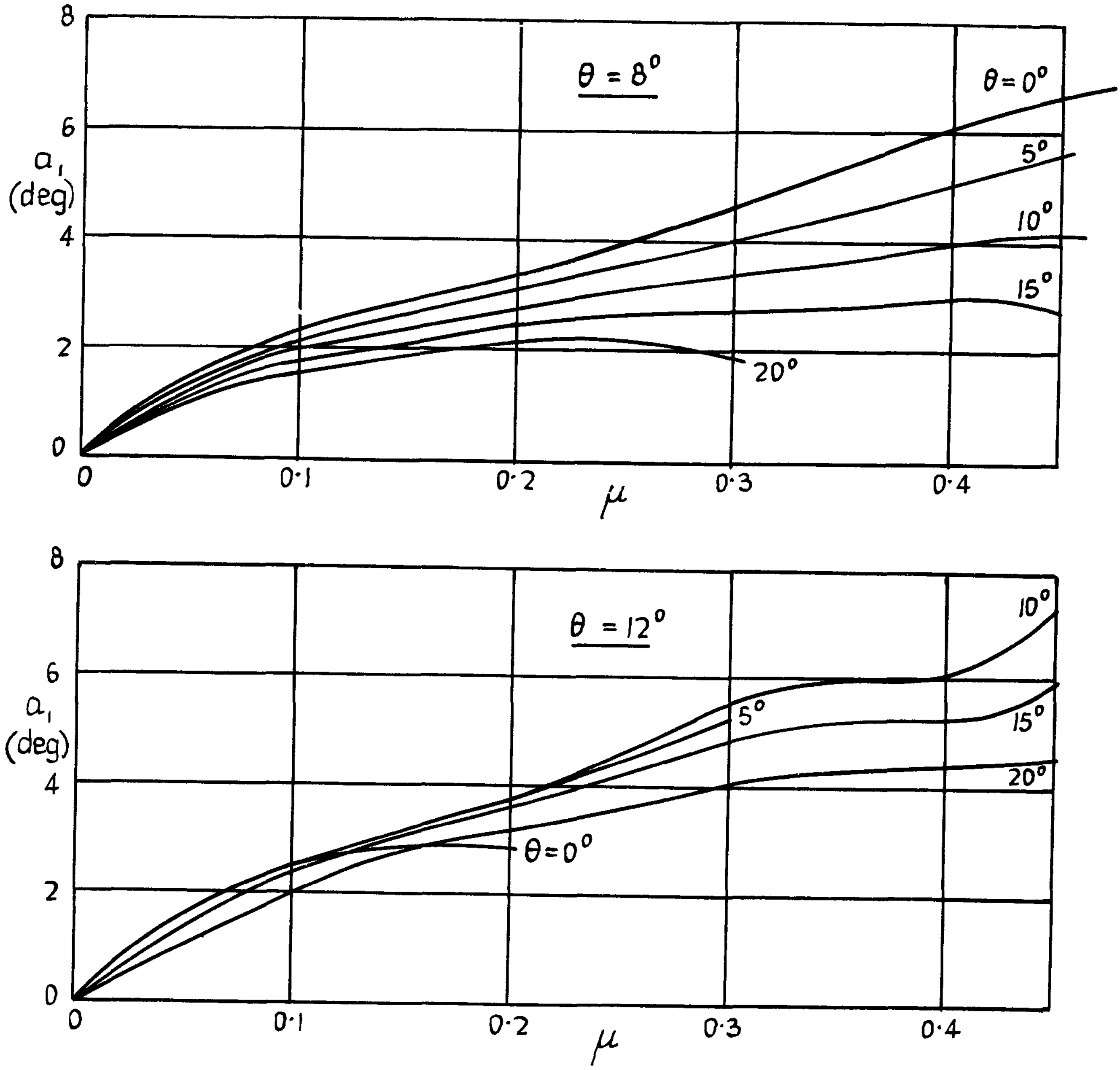

Flapping angles.
Rear rotor only. $L_2 H_2 A_0$

DS 82387/1 Wt 60 K4 11/60 CL

C.P. No. 517
(22,103)
A.R.C. Technical Report

© *Crown copyright* 1960

Printed and published by
HER MAJESTY'S STATIONERY OFFICE

To be purchased from
York House, Kingsway, London W.C.2
423 Oxford Street, London W.1
13A Castle Street, Edinburgh 2
109 St. Mary Street, Cardiff
39 King Street, Manchester 2
50 Fairfax Street, Bristol 1
2 Edmund Street, Birmingham 3
80 Chichester Street, Belfast 1
or through any bookseller

Printed in England

S.O. Code No. 23-9012-17

C.P. No. 517